

Flexible Runway Scheduling for Complex Runway Systems

A Multi-Objective Optimization for Fuel
Use and Noise Disturbance at Amsterdam
Airport Schiphol

A.W. Abbenhuis



Disclaimer

The cover image is taken by Mike Kelly ©,
Runway operations on RWY24 at Amsterdam Airport in 2016

Flexible Runway Scheduling for Complex Runway Systems

A Multi-Objective Optimization for Fuel
Use and Noise Disturbance at Amsterdam
Airport Schiphol

by

A.W. Abbenhuis

to obtain the degree of Master of Science in Aerospace Engineering
at the Delft University of Technology,
to be defended publicly on Thursday April 1, 2021.

Student number:	4367510	
Project duration:	August 15, 2020 – April 1, 2021	
Thesis committee:	Prof.dr.ir. J.M. Hoekstra,	TU Delft, Chairman
	Ir. P.C. Roling,	TU Delft, Daily Supervisor
	Ir. A. Bombelli,	TU Delft, Supervisor

An electronic version of this thesis is available at <http://repository.tudelft.nl/>.

Acknowledgements

More than 10 years ago my interest in aviation was aroused after a visit to the Smithsonian National Air and Space Museum in Washington D.C. and has grown ever since. After a graduation project in high school related to sustainable aviation, the next step at the faculty of Aerospace Engineering was one of the best decisions I have made so far. The completion of my MSc thesis is not as I imagined it to be a year ago. A completely remote thesis with practically no interaction at the faculty, contact with students or supervisors and presentations through virtual calls is the result of the ongoing Corona pandemic. Nevertheless, I am proud of the result presented in this thesis report.

I would like to express a deep gratitude to ir. Paul Roling for his continuous support throughout the entire project. You were always available to help me when I was stuck and the brainstorm sessions we've had led to significant improvements in the work. Furthermore, I would like to thank ir. Alessandro Bombelli for his support throughout various milestone meetings. Your feedback and ideas helped the research to a higher level. Finally, I would like to thank Prof. dr. ir. Jacco Hoekstra for his role as chairman of the thesis committee.

I also want to take this opportunity to thank family and friends. Bart Jacobson, our friendship developed with the start of Design Synthesis Exercise and since then we've been on the same page on almost all subjects. During this thesis period you were always available for a quick chat, a piece of advise or an extra set of eyes on my work and I am grateful for that. A special thanks to the boys at home who were always available to offer a listening ear. Finally, to my mom, dad, brother and especially my sister. You've always been there during my entire education and are my most loyal and critical supporters which helped my achieve the level of where I am today.

Anthonie W. Abbenhuis
Delft, March 2021

Contents

List of Figures	vii
List of Tables	ix
Nomenclature	xv
1 Introduction	1
1.1 Introduction	1
1.2 Problem Statement	1
1.2.1 Motivation	1
1.2.2 Thesis Objective	2
1.2.3 Scope	2
1.2.4 Research Question	2
1.3 Thesis Outline	2
I Scientific Paper	3
II Literature Study	19
2 Airport Capacity Modeling	21
2.1 Airport Capacity Definitions	21
2.2 Runway Capacity Factors	22
2.2.1 Geometry of the Runway	22
2.2.2 Runway Configurations	23
2.2.3 Air Traffic Management Constraints	24
2.2.4 Aircraft Mix & Sequencing	26
2.2.5 Meteorological Conditions	26
2.3 RECAT-EU Separation	27
2.4 Capacity Modeling & Calculation	28
2.4.1 Inter-Arrival Time	28
2.4.2 Inter-Departure Time	28
2.4.3 Maximum Throughput	29
2.5 Research on Runway Capacity Modeling	29
2.5.1 Macroscopic Models	29
2.5.2 Mesoscopic Models	30
2.5.3 Microscopic Models	31
2.5.4 Decision Support Tools	32
3 Noise Modeling	33
3.1 Aircraft Noise	33
3.1.1 Engine Noise	33
3.1.2 Airframe Noise	34
3.2 Noise Metrics	34
3.2.1 Noise Levels	34
3.2.2 Effect of Exposure	35
3.2.3 Noise Annoyance	37
3.3 Noise Mitigation & Regulation	37
3.3.1 Reduction of Noise at the Source	37
3.3.2 Land-Use Planning and Management	38
3.3.3 Noise Abatement Operational Procedures	38
3.3.4 Operating Restrictions	39

3.4	Noise Visualization	39
3.4.1	Noise Contour	39
3.4.2	Noise Grid	39
3.5	Research on Noise Modeling	40
3.5.1	The Integrated Noise Model (INM)	40
3.5.2	The Aviation Environmental Design Tool (AEDT)	41
3.5.3	The Dutch Aircraft Noise Model (NRM)	41
4	Fuel Burn Modeling	43
4.1	Airline Cost Structure	43
4.2	Fuel Trend	44
4.3	Fuel Burn Modeling	44
4.4	Base of Aircraft Data (BADA)	45
III	Supporting Work	47
5	Previous Work	49
5.1	Flexible Runway Allocation Model	49
5.1.1	Objective Function	49
5.1.2	Constraints	50
5.1.3	Improvement Areas	50
5.2	Runway Dependencies for Complex Runways	50
5.2.1	Converging & Diverging Runways	51
5.2.2	Intersecting Runways	52
5.2.3	Parallel Runways	53
5.2.4	Opposite Direction Operations	53
6	Flexible Runway Scheduling Model	55
6.1	Model Architecture	55
6.2	Pre-processors	57
6.2.1	Fuel Pre-processor	57
6.2.2	Noise Pre-processor	57
6.2.3	Separation Pre-processor	57
6.3	IBM ILOG CPLEX	58
7	Amsterdam Airport Schiphol Results	61
7.1	Aircraft Mix & O/D Data	61
7.2	Runway Dependencies for EHAM	61
7.2.1	Arrival - Arrival	62
7.2.2	Departure - Departure	64
7.2.3	Departure - Arrival	64
7.2.4	Arrival - Departure	65
7.3	Timetable	66
7.4	Delay	67
IV	Appendices	69
A	Amsterdam Airport Schiphol Data	71
B	Noise Grids and Runway Allocation	75
	Bibliography	81

List of Figures

2.1	Converging or diverging runways and dependencies [49]	24
2.2	Dutch airspace around Amsterdam Airport Schiphol (EHAM)[29]	25
2.3	Situation for calculation of runway capacity in arrival mode[39]	28
3.1	Different sources of engine noise [31]	33
3.2	Different sources of airframe noise [31]	34
3.3	Equal loudness contours and corresponding phon and sone values [13]	35
3.4	Equal noisiness contours in terms of frequency and pressure band [13]	36
3.5	A-, B-, C- and D-weighting functions [13]	36
3.6	Four principal elements of the ICAO's Balanced Approach to Aircraft Noise Management [26]	37
3.7	Progression of ICAO noise standards [26]	38
3.8	Noise certification for Boeing 747-400 and Boeing 777-200 [13]	38
3.9	Noise contour of single aircraft take-off	40
3.10	Noise contour Amsterdam Airport Schiphol for different L_{DEN} values	40
3.11	Noise grid of AAS [12]	40
4.1	Airline cost breakdown [50]	43
4.2	Fuel prices 1990-2019 [42]	44
5.1	Jet blast and wake turbulence between two departures on diverging runways [49]	51
5.2	Jet blast and wake turbulence between a departure and arrival on converging/diverging runways [49]	52
5.3	Missed approach path intersects with departure path [49]	52
5.4	Intersecting Missed Approach Paths of two arrivals [49]	53
5.5	Opposite Direction Operations on the same runway [50]. The order of operation is indicated with numbers.	54
6.1	Architecture of the Flexible Runway Scheduling Model	56
7.1	Aircraft Composition Scenario 1: Outbound Peak	62
7.2	Aircraft Composition Scenario 2: Inbound Peak	62
7.3	Aircraft Composition Scenario 3: 2 + 2	62
7.4	Departing directions for Scenario 1	62
7.5	Origins of arrivals in Scenario 1	62
7.6	Departing directions Scenario 2	63
7.7	Origins of arrivals in Scenario 2	63
7.8	Departing directions Scenario 3	63
7.9	Origins of arrivals in Scenario 3	63
7.10	Runway System for Amsterdam Airport Schiphol (AAS/EHAM) [5]	64
7.11	Runway Allocation in timetable for Scenario 1 with $\alpha = 0.4$	66
7.12	Runway Allocation in timetable for Scenario 2 with $\alpha = 0.2$	66
7.13	Runway Allocation in timetable for Scenario 3 with $\alpha = 0.65$	67
7.14	Assigned Delay for Scenario 1 with $\alpha = 0.4$	67
7.15	Assigned Delay for Scenario 2 with $\alpha = 0.2$	67
7.16	Assigned Delay for Scenario 3 with $\alpha = 0.65$	67
B.1	Noise Grid Scenario 1: Noise optimized	75
B.2	Noise Grid Scenario 1: Multi-objective optimized	75
B.3	Noise Grid Scenario 1: Fuel optimized	75
B.4	Noise Grid Scenario 1: Reference Scenario	75

B.5	Runway Allocation Scenario 1: Noise optimized	76
B.6	Runway Allocation Scenario 1: Multi-objective optimized	76
B.7	Runway Allocation Scenario 1: Fuel optimized	76
B.8	Runway Allocation Scenario 1: Reference Scenario	76
B.9	Noise Grid Scenario 2: Noise optimized	76
B.10	Noise Grid Scenario 2: Multi-objective optimized	76
B.11	Noise Grid Scenario 2: Fuel optimized	77
B.12	Noise Grid Scenario 2: Reference Scenario	77
B.13	Runway Allocation Scenario 2: Noise optimized	77
B.14	Runway Allocation Scenario 2: Multi-objective optimized	77
B.15	Runway Allocation Scenario 2: Fuel optimized	77
B.16	Runway Allocation Scenario 2: Reference Scenario	77
B.17	Noise Grid Scenario 3: Noise optimized	78
B.18	Noise Grid Scenario 3: Multi-objective optimized	78
B.19	Noise Grid Scenario 3: Fuel optimized	78
B.20	Noise Grid Scenario 3: Reference Scenario	78
B.21	Runway Allocation Scenario 3: Noise optimized	78
B.22	Runway Allocation Scenario 3: Multi-objective optimized	78
B.23	Runway Allocation Scenario 3: Fuel optimized	79
B.24	Runway Allocation Scenario 3: Reference Scenario	79

List of Tables

2.1	Parallel runway separations [37]	23
2.2	Wake Turbulence Categories defined by ICAO [23]	25
2.3	Distance-based separation minima in nmi [23]	26
2.4	Time-based separation minima in seconds [23]	26
2.5	Distance-based separation minima in nmi based on RECAT-EU [43]	27
2.6	Time-based separation minima in seconds based on RECAT-EU [43]	27
2.7	Runway occupancy times in seconds based on weight category [43]	27
7.1	Staggering distances in nmi between two consecutive arrivals on EHAM	63
7.2	Percentage of the DROT for two consecutive departures on EHAM	65
7.3	Staggering distances in nmi for aircraft arriving after a departure on EHAM	65
7.4	Percentage of the AROT for aircraft departing after an arrival on EHAM	65
A.1	Part of the flight schedule for EHAM on August 8th, 2019. Used for analysis of scenario 3.	71
A.2	Taxi-in distances at EHAM for operations from the runway to the pier. All values are expressed in meters. Runways without distances are not open for arrival.	73
A.3	Taxi-out distances at EHAM for operations from the pier to the runway. All values are expressed in meters. Runways without distances are not open for departures.	73
A.4	Departure distances at EHAM for departing operations from the runway to the first waypoint indicator on the Standard Instrument Departure. All values are expressed in nautical miles.	74
A.5	Arrival distances at EHAM for arriving operations from the Initial Approach Fix to the runway threshold. All values are expressed in nautical miles.	74

Nomenclature

Abbreviations

AAS	Amsterdam Airport Schiphol
ABS	Airport Business Suite
AC	Aircraft Type
ADV	Auxiliary Decision Variable
AEDT	Aviation Environmental Design Tool
AEL	Acoustic Energy Level
AMAN	Arrival Manager
AND	Approximate Network Delays
ANSP	Air Navigation Service Provider
AROT	Arrival Runway Occupancy Time
ASE	Airport Strategic Exploration
ATC	Air Traffic Control
ATCo	Air Traffic Controller
ATM	Air Traffic Management
BADA	Base of Aircraft Data
BAS	Bewoners Aanspreekpunt Schiphol
CADM	Complete Arrival Departure Manager
CAGR	Compound Annual Growth Rate
CDA	Continuous Descent Approach
CDM	Collaborative Decision Making
CSPR	Closely Spaced Parallel Runways
CTA	Control Areas
CTR	Control Zone
DLR	German Aerospace Center
DM	Decision Maker
DMAN	Departure Manager
DOC	Direct Operating Cost
DROT	Departure Runway Occupancy Time
DSS	Decision Support System
DUT	Delft University of Technology
DV	Decision Variable
EDMS	Emissions and Dispersion Modeling System
ETA	Expected Time of Arrival
ETD	Expected Time of Departure
FAA	Federal Aviation Administration
FAA-ACM	Federal Aviation Administration Airport Capacity Model

FAF	Final Approach Fix
FCFS	First Come, First Serve
FDOC	Fixed Direct Operating Cost
FIR	Flight Information Region
FRAM	Flexible Runway Allocation Model
FRSM	Flexible Runway Scheduling Model
HERMES	Heuristic Runway Movement Event Simulation
IAF	Initial Approach Fix
IATA	International Air Transport Association
ICAO	International Civil Aviation Organization
IFR	Instrument Flight Rules
IMC	Instrument Meteorological Conditions
INM	Integrated Noise Model
IOC	Indirect Operating Cost
IPR	Independent Parallel Runways
LCC	Low-Cost Carriers
LH	Lower Heavy RECAT-EU Category
LIFR	Low Instrument Flight Rules
LM	Lower Medium RECAT-EU Category
LOS	Level-Of-Service
MACAD	MANTEA Capacity and Delay Model
MAP	Missed Approach Path
MILP	Mixed Integer Linear Programming
MIT	Massachusetts Institute of Technology
MSPR	Medium Spaced Parallel Runways
MTC	Maximum Throughput Capacity
MTOW	Maximum Take-Off Weight
MUAC	Maastricht Upper Area Control
MVA	Minimum Vectoring Altitude
MVFR	Marginal Visual Flight Rules
NADP	Noise Abatement Departure Procedures
NATS	UK National Air Traffic Service
NNC	Non-Noise Certificated
NOC	Non-Operating Cost
NPR	Noise Preferential Routes
NRM	Dutch Aircraft Noise Model
OD	Origin or Destination
PHCAP	Practical Hourly Capacity
R	Runway
ROC	Rate Of Climb
ROD	Rate Of Descent
ROT	Runway Occupancy Time
RPK	Revenue Passenger Kilometer

RWY	Runway
SARP	Standards and Recommended Practices
SEL	Sound Exposure Level
SID	Standard Instrument Departure
SMAN	Surface Manager
SPL	Sound Pressure Level
STAR	Standard Terminal Arrival Route
SVFR	Special Visual Flight Rules
TAAM	Total Airspace & Airport Modeller
TAM	Total Airport Management
TBS	Time-Based Separation
TC	Total Cost
TFB	Total Fuel Burn
TFU	Total Fuel Used
TMA	Terminal Control Area
TMAN	Turnaround Manager
TOC	Total Operating Cost
UH	Upper Heavy RECAT-EU Category
UM	Upper Medium RECAT-EU Category
UTA	Upper Airspace
VDOC	Variable Direct Operating Cost
VFR	Visual Flight Rules
VMC	Visual Meteorological Conditions
WC	Weight Class
WHO	World Health Organization
WTC	Wake Turbulence Category

Symbols

\bar{c}	Communication buffer between pilots and ATC	sec
ΔL_A	Corrective factor A-weighting	dB(A)
\dot{m}_f	Mass fuel flow of aircraft	$\frac{kg}{s}$
c_d	Delay cost for flight f	$\frac{kg}{s}$
C_{f1}	Aircraft specific fuel coefficient	$\frac{kg}{min \cdot kN}$
C_{f2}	Aircraft specific fuel coefficient	knots
c_f^r	Fuel cost of assigning flight f to runway r	kg
c_{opt}	Optimization cost for model performance	-
$C_{Tc,1}$	Aircraft specific maximum climb thrust coefficient	N
$C_{Tc,2}$	Aircraft specific maximum climb thrust coefficient	ft
$C_{Tc,3}$	Aircraft specific maximum climb thrust coefficient	$\frac{1}{ft^2}$
C_T	Thrust specific fuel consumption	$\frac{kg}{min \cdot N}$
c_{xy}	Noise cost for gridpoint xy	people
D	Distance of flight segment	nmi

D_f	Delay assigned to flight f	sec
D_{max}	Maximum assigned delay	sec
D_{min}	Minimum distance between aircraft and runway threshold	nmi
D_{st}	Staggering distance for arriving aircraft	nmi
$E[T]$	Expected service time	sec
E_0	Reference sound exposure	dba
E_n	Acoustic energy level of sound	dba
F	Set of flights	-
g_{xy}	Binary decision variable indicating grid measurement points	-
H_p	Geopotential altitude	ft
HA	Percentage of highly annoyed people	%
i	Leading aircraft when comparing with other aircraft	-
j	Trailing aircraft when comparing with other aircraft	-
$L_{Aeq,T}$	Equivalent A-weighted sound level	dba
L_{AE}	Sound Exposure Level	dba
L_A	A-weighted sound pressure level	dba
L_{DEN}	Day-Evening-Night average level	dba
M	Big-M method variable	-
n	Common approach path	nmi
n_f	Normalization parameter for fuel burn objective	-
n_n	Normalization parameter for noise emission objective	-
OR	Number of order changes from FCFS sequence	-
P	Set of gridpoints	-
p_{e0}	Reference sound pressure level	Pa
p_e	Absolute pressure level	Pa
$p_{i,j}$	Probability of occurrence for specific aircraft combination	-
R	Set of runways	-
$R_{A,com}$	ROT for arriving aircraft to complete (part of) the landing	sec
$R_{A,int}$	ROT for arriving aircraft until intersection point with other runway	sec
$R_{D,cl}$	ROT for departing aircraft until clearance of intersection with other runway	sec
$R_{D,int}$	ROT for departing aircraft until intersection point with other runway	sec
R_r	Set of closed runways	-
$s_{i,j}$	Minimum required longitudinal separation between flight i and j	nmi
SW	Specified window where flights can switch order	sec
T_1	1 second integration time	sec
$t_{D,lu}$	Line-up time for departing aircraft	sec
T_f	Time of operation of flight f	sec
T_{hr}	Thrust of aircraft	kN
$T_{i,j}$	Minimum separation time between flight i and j	sec
T_{max}	Time of latest assigned flight	sec
T_{ref}	Reference time for the period in which noise events take place	sec
TS_f	Scheduled time of flight f	sec
V_{A_j}	Final approach speed of approaching aircraft	kts

V_i	Final approach speed of leading aircraft	kts
V_j	Final approach speed of trailing aircraft	kts
V_{TAS}	True Airspeed	$\frac{m}{s}$
w	Penalty factor for noise events	dBa
W_q	Expected time in queue per user	sec
x_f^r	Binary decision variable indicating flights to runways	-
$x_{i,j}$	Binary decision variable indicating operating order	-

Greek Symbols

α	Weight parameter applied to fuel burn objective	-
β	Weight parameter applied to noise emission objective	-
λ	Demand rate	$\frac{1}{hr}$
μ	Service rate or capacity	$\frac{1}{hr}$
ρ	Utilization ratio	$\frac{1}{hr}$
σ_T	Variance of service time	sec

1

Introduction

1.1. Introduction

With an increasing demand for flight, the airspace is becoming more crowded and with this airport capacity is becoming a limiting factor in air operations. As airport capacity is mainly driven by the runway system, airports investigate possibilities to expand their runway system. The most effective method is to build a new runway in the vicinity. However, for airports located in densely populated areas this is most often not possible. Even more, the airport capacity is further limited for these airports due to noise regulations by the local government. Airports are allowed to only use a part of their runway system depending on wind conditions and noise limits or are constrained in their total movements per year. Besides noise regulation, the discussion about fuel emissions is becoming more apparent as climate agreements call for a more sustainable aviation sector. Not only the development of more sustainable aircraft is explored, but more efficient operations can have an advantageous effect as well.

1.2. Problem Statement

To analyse airport capacity multiple models are constructed over the years and with the development of computing power those models became more accurate. Current models are able to analyse to a great extent the airport capacity and the influence of different operating strategies. Besides airport capacity research, research is also performed to model noise profiles for arriving and departing aircraft. Such models as developed by the FAA are able to provide extensive information about noise contours and provide insights in disturbances. The final field of research considered is fuel burn modeling. EUROCONTROL developed a database where accurate information is gathered for all aircraft types currently in operation. In this database information about engines and fuel burn is accessible and fuel burn profiles can be constructed.

A model which is able to incorporate both objectives, fuel burn and noise disturbance, while respecting the airport capacity has only recently been developed by Delsen [12]. A flexible allocation model was developed which optimizes the operation based on both objectives instead of the preference list used by airports. This model was further refined by Van Der Meijden [50] to incorporate more detail in the operations. However, the current model has shortcomings in delay allocation and separation modeling for complex runway systems.

1.2.1. Motivation

Previous research at Delft University of Technology (DUT), performed by Delsen [12] investigated the advantages of flexible runway allocation instead of the preference list used at airports constrained by noise regulations. A model where a trade-off between fuel burn and noise disturbance could be made was proposed and proved to be a promising method. Further refinement of the model was done by Van Der Meijden [50]. Incorporation of pair-wise separation was implemented and the level of detail of the model was increased. At the same time at DUT another model was proposed to calculate the runway capacity for a complex runway system based on every occurring dependency between runways. This model, researched by Van Der Klugt [49] proved to be an accurate model.

To this day, the current flexible runway allocation model could be improved with the incorporation of the dependencies for complex runway systems and with possibilities to assign continuous delays in order to optimize the airport capacity. These improvements would open up possibilities to investigate the effect of flexible

runway scheduling on complex runway systems and would provide further arguments for a new operation method for airports constrained in their current-day operation.

1.2.2. Thesis Objective

The objective of this thesis research is to develop a new flexible runway scheduling model. By changing the modeling method from an allocation model to a scheduling model it will be possible to assign continuous delays to the aircraft, enhancing the runway capacity. Furthermore, a new method for separation will be proposed such that the model can be used for every airport and runway system. This new model will offer new insights in the possibilities for airports to expand their operations while complying with noise regulations. As current day operations are solely based on noise disturbance, the model will also provide insights into the possibilities of fuel savings while complying with those noise regulations.

1.2.3. Scope

The scope of this research is focused on two aspects. The first aspect is to develop a new type of model for flexible runway operations such that flights are scheduled instead of allocated. The second aspect is to incorporate a new strategy for separation modeling to capture the dependencies in a complex runway system. The scope of this research does not include the operational restrictions in the taxi system. It also does not include the uncertainty of operation. This means that flights are expected at their scheduled time and that external factors causing delays or early arrivals are not incorporated. The research scope furthermore does not consider the effect of flexible runway scheduling on Air Traffic Control. As flexible scheduling will increase the workload for ATC, research can be directed in a later stage to analyse the effects of this newly proposed method.

1.2.4. Research Question

Based on the problem statement, motivation, objective and scope a research question can be constructed for this thesis. The goal is to improve the current model by changing the method of modeling and by implementing a new separation strategy. The research question is as follows.

"Can the performance of the flexible runway allocation model be further improved by changing the optimization method to a flexible scheduling model and by implementing a method to calculate dependencies for a complex runway system while considering noise annoyance, fuel burn and runway capacity based on a specific demand of flights at a specific airport?"

This research question can be split into several sub-questions to specify the different areas where this research is performed. Together they will answer the research question.

1. How can a scheduling method be used to model airport operations and how does it differ from an allocation model?
2. How does the separation constraint need to be structured such that it can incorporate dependencies within a complex runway system?
3. What models and databases are available for the calculation of noise profiles and fuel burn schemes and how can they be incorporated into the scheduling model?

1.3. Thesis Outline

This thesis report is organised as follows. In Part I, the scientific paper is presented and can be viewed as a stand-alone document. In Part II the Literature Study is presented. The Literature Study is already presented and graded in an earlier stage and provides the background for which this model is constructed. Finally, in Part III additional information is provided. This information is about earlier models, algorithms used in the Flexible Runway Scheduling Model and supporting results for some of the statements made in the paper. Finally, Part IV contains the appendices related to additional information about Amsterdam Airport Schiphol.

I

Scientific Paper

Flexible Runway Scheduling for Complex Runway Systems: Using a Multi-Objective Optimization

A.W. Abbenhuis,
Delft University of Technology
Aerospace Engineering, Air Transport & Operations
Delft, The Netherlands

Abstract

Runway usage at complex airports is currently prescribed by a preference list focusing on minimizing noise and providing a manageable flow for ATC. However, fuel burn and the demand of flight is not considered. This study proposes a flexible runway scheduling model and is an improvement of the current flexible runway allocation model. The model is able to assign continuous delay to the scheduled flights and by changing the decision variables a new separation constraint is proposed to accurately model complex runway dependencies. A multi-objective optimization is performed for fuel burn and noise disturbance using Mixed-Integer Linear Programming (MILP). The model is tested on Amsterdam Airport Schiphol (AAS) for different scenarios. A fuel reduction of up to 7% is possible depending on the operational peak and O/D data. At the same time, noise violations are limited in the vicinity of the airport. This provides the opportunity to expand operations while complying with local noise regulations. Furthermore, the model can be used to explore operating strategies for different objectives for every runway configuration.

Index Terms - Runway Capacity, MILP, Noise, Fuel, Schiphol

I Introduction

In 2020 the aviation sector was brought to a standstill due to the Corona virus. However, the growth as seen in the previous years is expected to recover [1]. Data provided by the International Air Transport Association (IATA) [11] states that in 2018 over 8.3 trillion Revenue Passenger-Kilometers (RPK) were flown and estimates provided by the International Civil Aviation Organization (ICAO) expect a growth of 4.3 per cent per year for the period 2015-2035 in terms of RPK [12].

The growth of the aviation sector has a direct influence on the operations of airports. As the demand for flying increases, the number of operations performed at an airport increases with it. To cope with the increasing operations, several factors and expansion possibilities

can be considered while ensuring capacity, safety and regulations.

As physical growth of the airport is often not possible due to local restrictions, airports turn to other possibilities to optimise their operations given the current infrastructure. One of the biggest contributors to airport capacity is the runway capacity which is defined by Neufville as: *"the expected number of movements in a time period on a runway system without violating Air Traffic Management (ATM) rules, assuming continuous demand"* [18]. To improve runway capacity, several studies in different research areas have been performed. The RECAT-EU scheme is one of those results and is a revised separation scheme described by Rooseleer and Treve [20] and validated by Hu et al. [10].

Noise disturbance has become a topic of discussion in the expansion of airport operations [4]. Airports operating under noise restrictions often follow a preferred runway list according to regulations and agreements with (local) governments. These preferred sequences together with ICAO noise abatement procedures ensure noise disturbance is limited but not negligible [2][13].

In recent years the call to make aviation more sustainable has become louder and more efficient fuel burn profiles can have a significant impact on the emissions from aircraft.

In order to analyse the effect of infrastructural changes, operational changes or other new techniques, computer models can be constructed. Over the years, several models have been constructed to calculate and predict the airport capacity. Blumstein [3] was the first to calculate the runway capacity for a single runway operating in arrival mode. Extensions were made by Harris [8], Hockaday and Kanafani [9] and Gilbo [7] who made developments by incorporating random variables, implementing sequencing strategies and varying operating conditions, respectively. The FAA constructed its own model which serves as the basis of a lot of today's models [23]. Another analytical model is the Mantea Capacity and Delay Model described by Stamatopoulos [22], which serves as a tool for decision makers to provide a quick overview of system changes.

As computer performance improved, microscopic models emerged with it. These simulation models are able to provide more accurate estimations, but with the dis-

advantage of large computing times. In a research performed by Odoni et al. several models are described [19]. The Airport Machine and SIMMOD are node-link models which are able to calculate the capacity of the whole airfield. TAAM [16] is a model which can be used for different ATM concepts. The Airport Business Suite (ABS) is a model which can be used for strategic exploration [27]. In recent years a runway allocation model was incorporated in the ABS which was able to capture the complex dependencies between various runway configurations and resulted in a more accurate estimation of the runway capacity [25].

The urgency for a higher airport capacity in combination with less noise disturbances and more fuel savings led to the development of a new model. A flexible runway allocation method was proposed by Delsen [5] and proved to be an effective model for optimisation in fuel burn and noise emission while removing the need for a preference list. Further improvements of the model proposed by Van Der Meijden led to a more accurate representation of the aircraft in the model as no longer two types of aircraft were considered and the fact that pair-wise separation was implemented [26]. However, the current model uses a discrete representation for flight scheduling which negatively impacts the capacity. Furthermore, the separation modeling is performed such that dependencies between runways are not captured effectively which makes the use of the model limited.

This research is focused at improving the flexible allocation model. By changing the model to a scheduling method instead of an allocation method it is possible to assign continuous delays as opposed to discrete delays. Furthermore, by changing decision variables and assigning auxiliary decision variables, the scheduling model will be more suitable to capture dependencies for complex runway systems. The model constructed by Van Der Klugt [25] can then serve as a basis for the dependency calculations. Furthermore, the implementation of more accurate noise estimations based on the new Aviation Environmental Design Tool (AEDT) [24] will lead to a model which will represent the actual situation more accurate.

The structure of this paper is as follows. The theory behind capacity models and the methods for noise and fuel calculations are presented in Section II. In Section III the mathematical model is presented. To analyse the effect of the method a scenario at Amsterdam Airport Schiphol (AAS) is evaluated and the results are presented in Section IV. This will be discussed in Section V together with further recommendations. Finally, this research is concluded in Section VI.

II Theory

This section explains the theory used for the construction of the model. The separation calculations used to determine the minimum time separation between flights is discussed in Section II-A. The method to calculate fuel burn profiles for different flight segments is

explained in Section II-B. Finally, in Section II-C the calculation for noise emission is presented.

II-A Separation Modeling

The most dominant factor influencing runway capacity is the minimum separation requirement between operations [3]. The minimum separation time is dependent on several parameters such as i) operation type, ii) weight class and iii) runway use. The model builds further upon the pair-wise separation method as proposed by Van Der Meijden [26].

The first type of minimum separation requirements arises when single runway use is considered. If two consecutive arrivals are performed at the same runway end the minimum separation time, $T_{i,j}$, between the first flight i and second flight j is given by (1) and (2). It is defined as the maximum of the required longitudinal separation and the arrival runway occupancy time $AROT_i$. Equation (1) is applied if the approach speed of i is larger than j and (2) when vice versa [18]. Furthermore, the common approach path, n , is dependent on the runway while the required longitudinal separation, $s_{i,j}$, is determined by the RECAT-EU scheme and the weight classes of both aircraft [20].

$$T_{i,j} = \max \left[\frac{n + s_{i,j}}{V_j} - \frac{n}{V_i}, AROT_i \right] \quad (1)$$

$$T_{i,j} = \max \left[\frac{s_{i,j}}{V_j}, AROT_i \right] \quad (2)$$

The minimum separation for two consecutive departures or a departure followed by an arrival is given by (3). Where $TBS_{i,j}$ is the time based separation given by RECAT-EU [20] and $DROT_i$ is the departure runway occupancy time. When an arrival is followed by a departure the minimum separation is only based on the arrival runway occupancy time, $AROT_i$, as shown in (4).

$$T_{i,j} = \max [TBS_{i,j}, DROT_i] \quad (3)$$

$$T_{i,j} = [AROT_i] \quad (4)$$

The second type of minimum separation requirements originates when two consecutive flights are in the opposite direction from each other on the same runway [26]. When consecutive arrivals are performed the minimum required separation between them is determined by the minimum vectoring altitude (MVA) and the rate of descent (ROD) together with a communication buffer (\bar{c}) as shown in (5).

$$T_{i,j} = \frac{MVA}{ROD} + \bar{c} \quad (5)$$

If two consecutive departures take place or when an arrival is followed by a departure, the minimum time separation is based on the runway occupancy time of the first aircraft as shown in (6) and (7), respectively.

$$T_{i,j} = DROT_i \quad (6)$$

$$T_{i,j} = AROT_i \quad (7)$$

The last operation mode is a departure followed by an arrival on opposite runway ends. The minimum

separation requirement depends on both the rate of descent of the arriving aircraft as well as the rate of climb (ROC) of the departing aircraft. The minimum separation is given in (8).

$$T_{i,j} = \frac{MVA}{ROD} + DROT_i + \frac{MVA}{ROC} \quad (8)$$

When runways are closely located to each other or when their arriving or departing flight trajectories intersect dependencies arise between those runways. This is the third type of separation requirements. In the research performed by Van Der Klugt [25] accurate equations are provided to calculate minimum separation times for all dependencies which can arise in a complex runway system. In this paper an overview is provided, but for a detailed analysis the reader is referred to [25].

When two aircraft approach different runways and their projected missed approach paths (MAP) coincide, extra separation is necessary. This is done by applying a staggering distance, D_{st} , to the trailing aircraft. The minimum separation time is given in (9). Note that this distance is dependent on the specific situation of the runways, but that a minimum distance of 1.5 *nmi* is taken in this research.

$$T_{i,j} = \frac{D_{st}}{V_{A_j}} \quad (9)$$

For two departures there are two things to consider: i) the wake turbulence or ii) the jet blast on another runway caused by a departing aircraft. The equations are given in (10) and (11), respectively. The time until intersection, $R_{D_{int}}$, or until the clearance point, $R_{D_{cl}}$, is determined as a percentage of the $DROT$. Furthermore, the line-up time is dependent on the weight class of the aircraft.

$$T_{i,j} = R_{D_{int}} + t_{D_{lu}} + \bar{c} \quad (10)$$

$$T_{i,j} = R_{D_{cl}} + \bar{c} \quad (11)$$

When an arrival is followed by a departure on two different runways the jet blast and MAP have to be considered. The first is given in (12) where the time until intersection, $R_{A_{int}}$, is determined as a percentage of the $AROT_i$. A clearance for departure is given after it is certain that the arriving aircraft has completed the landing (or part of it). This is shown in (13) where the completion time, $R_{A_{com}}$, can be as small as 10 seconds.

$$T_{i,j} = R_{A_{int}} + t_{D_{lu}} + \bar{c} \quad (12)$$

$$T_{i,j} = R_{A_{com}} + \bar{c}_D \quad (13)$$

When the operation sequence is reversed, the minimum separation time between a departure and arrival is dependent on a minimum distance the arrival should be from the runway threshold, D_{min} . This is shown in (14).

$$T_{i,j} = \frac{D_{min}}{V_{A_j}} - \bar{c} \quad (14)$$

The final dependency which should be taken into account are operations on parallel runways. The occurrence of this dependency is determined by the distance

between the centerlines of both runways. When this distance is below 762 *m* the runways need to be operated as a single runway with exception of the arrival-departure scenario. For a distance greater than 762 *m* but smaller than 1300 *m* an extra, direct, separation of 1.5 *nmi* must be applied between two arriving aircraft. If the distance is greater than 1300 *m* the runways can be considered to be independent for all operations.

II-B Fuel Burn Modeling

As the model will make a trade-off between fuel burn and noise disturbance, accurate modeling of both is important. In this research a method is proposed for the fuel burn calculation which is based on previous research performed by Delsen [5] and parameters obtained from the Base of Aircraft Data (BADA) [6]. To calculate the fuel burn of a flight the flight path is divided into several stages for which the individual fuel burn is calculated. The total fuel burn calculation is given in (15) and is expressed in kilograms of kerosene. The fuel burn per segment is then calculated using (16).

$$TFB = \sum_{s \in S} TFB_s \quad (15)$$

$$TFB_s = \frac{D \cdot \dot{m}_f}{V_{TAS}} \quad (16)$$

The distance per segment (D) can be obtained from Aeronautical Information Packages [15] which are provided per airport. The fuel flow (\dot{m}_f) in [$\frac{kg}{s}$] is obtained from BADA. This database provides coefficients of all types of aircraft which are currently in use. The fuel flow is thrust dependent and can be obtained through (17).

$$\dot{m}_f = C_T \cdot T_{hr} \quad (17)$$

The thrust specific fuel consumption, C_T , is specified as a function of airspeed (V_{TAS}) and the calculation differs for jet engines and turboprop engines. The coefficients C_{f1} and C_{f2} are obtained from BADA [6]. The calculations are shown in (18) and (19) for jet engines and turboprop engines, respectively.

$$C_T = C_{f1} \cdot \left(1 + \frac{V_{TAS}}{C_{f2}}\right) \quad (18)$$

$$C_T = C_{f1} \cdot \left(1 - \frac{V_{TAS}}{C_{f2}}\right) \cdot \frac{V_{TAS}}{1000} \quad (19)$$

Maximum thrust is calculated for climb conditions at different altitudes which are then multiplied by a coefficient for different configurations, e.g. landing, approach or taxiing. The maximum thrust calculation for a jet aircraft is shown in (20) where the coefficients are obtained from BADA [6] and the geopotential altitude is indicated by H_P .

$$T_{hr,max} = C_{Tc,1} \cdot \left(1 - \frac{H_P}{C_{Tc,2}} + C_{Tc,3} \cdot H_P^2\right) \quad (20)$$

In this research the segments for arriving aircraft are divided into three parts: i) the segment from the Initial Approach Fix (IAF) to the Final Approach Fix (FAF),

ii) the segment from the FAF to the runway and iii) the segment from the runway to the pier. For departing aircraft the segments are divided in two parts: i) the segment from the pier to the runway and ii) from the runway to the first waypoint on the Standard Instrument Departure (SID).

The model is able to assign delays to aircraft if necessary. This delay comes at the cost of additional fuel consumption and has to be incorporated in the model as well. For arriving aircraft it is assumed that the delay takes place at the IAF. The fuel flow at that stage is taken as the cost per second of delay for arriving aircraft. For departing aircraft it is assumed that the fuel burn during the taxi phase is extended. In the model, taxi thrust is assumed to be 7% of total thrust [14] from which the fuel flow can be calculated with previous equations.

II-C Noise Modeling

The second objective for which the model will optimize is noise disturbance. As fly-over noise is a non-stationary signal, the duration of the sound has to be taken into account. For this, the Sound Exposure Level (SEL or L_{AE}) can be used as shown in (21). The overall A-weighted sound pressure level is indicated by L_A . The integration time is removed and replaced with a constant of $T_1 = 1s$.

$$L_{AE} = 10 \log \left[\frac{1}{T_1} \int_0^T 10^{\frac{L_A(t)}{10}} dt \right] \quad (21)$$

For regulatory purposes the Day-Evening-Night average Level, L_{DEN} , is introduced. This value quantifies the noise disturbance in a 24-hour period and can be used to evaluate noise disturbance in a community. In the calculation for L_{DEN} penalty factors are applied for noise events occurring in the evening ($w = 3.167$) and the night ($w = 10$). To calculate L_{DEN} Equation (22) is used.

$$L_{DEN} = 10 \log \left[\sum_{n=1}^{n_{flights}} w_n 10^{\frac{SEL_n}{10}} \right] - 10 \log \left[\frac{T_{ref}}{T_0} \right] \quad (22)$$

To use the equation in a linear optimization problem, the logarithmic parts of the equation have to be adjusted. For this, the Acoustic Energy Level can be used which is defined in (23). In (23), E_0 is the reference sound exposure. Implementing this in (22) leads to the equation presented in (24).

$$AEL = \frac{E_n}{E_0} = 10^{\frac{SEL_n}{10}} \quad (23)$$

$$L_{DEN} = 10 \log \left[\sum_{n=1}^{n_{flights}} w_n \frac{E_n}{E_0} \right] - 10 \log \left[\frac{T_{ref}}{T_0} \right] \quad (24)$$

When the L_{DEN} is exceeded by a user-defined limit the cost of this violation is given by the number of people living at that gridpoint.

To calculate the SEL for an aircraft operation a noise modeling program is used. In this research use is made of the novel Aviation Environmental Design Tool

(AEDT) designed by the FAA [24]. To use the program the user has to define the Standard Terminal Arrival Routes (STARs) and Standard Instrument Departures (SIDs) for an airport of choice. By defining a grid with measurement points the value for a single operation on a specific STAR or SID can be modeled for all gridpoints. By defining the group of aircraft of interest, a set of measurements can be obtained for every combination of runway, aircraft and STAR/SID for each individual gridpoint. For the exact calculations of the AEDT the reader is referred to the manual [24]. In this research it is assumed that the assigned delay does not imply extra noise disturbance. Delay is assigned at the IAFs or at the ground, not adding noise to the defined noise grid.

III Model

In this section the mathematical model is presented together with the top-level architecture of the computer program. To solve for both fuel consumption and noise emission the objective function is constructed accordingly as discussed in Section III-A. For the model to work according to regulations, different constraints are put in place which are presented in Section III-B. Finally, to give an overview of the whole linear program a flow diagram is presented in Section III-C.

III-A Objective Function

The model is formulated as a Mixed Integer Linear Program (MILP) where variables can be either integer or binary. The sets for the model are presented in Table I.

Table I: Sets for the model

Set	Description
F	Number of flights
R	Number of runway ends
R_r	Runway ends closed for operation
P	Number of gridpoints

The decision variables (DV) and auxiliary decision variables (ADV) are summarized in Table II. The condition for which a binary variable is one is given as description, otherwise the variable is zero. An auxiliary decision variable is not directly in the objective function, but a combination of them can be used in the optimization process to enhance the performance.

The objective function is given in (25) and consist of three parts. It should be noted that the objective is a minimization problem.

$$\begin{aligned} \min \quad Z = & \alpha \cdot n_f \sum_{f \in F} \left[\left(\sum_{r \in R} c_f^r x_f^r \right) + c_d D_f \right] \\ & + \beta \cdot n_n \sum_{xy \in P} c_{xy} g_{xy} \\ & + c_{opt} (OR + D_{max} + T_{max}) \end{aligned} \quad (25)$$

Table II: Decision and Auxiliary Decision Variables

Variable	Description
x_f^r	1 if flight \mathbf{f} is assigned to runway \mathbf{r}
g_{xy}	1 if noise limit is exceeded at point \mathbf{xy}
D_f	Delay for flight \mathbf{f} in [sec]
T_f	Operation time for flight \mathbf{f} in [sec]
$x_{i,j}$	1 if flight \mathbf{i} is before flight \mathbf{j}

The objective for fuel consumption is a minimization of the combination of the fuel cost of assigning flight f to runway r indicated by the cost variable c_f^r and the assigned delay in seconds with a cost indicated by c_d in $[\frac{kg}{s}]$.

If the noise limit is violated at a gridpoint, indicated by g_{xy} , than the cost of that disturbance is given by the number of people, c_{xy} , living at that location.

The third part of the objective function are parameters which enhance the performance of the optimization process and have a small penalty, c_{opt} . The model has the option to switch the order of scheduled flights if this favors the overall objective, but endless order changes (OR) are not desired. Furthermore, the model has a penalty for the maximum delay, D_{max} , as this prevents delaying one aircraft endlessly in favor of others. The final parameter, T_{max} , ensures that the flights are handled as quickly as possible.

As fuel use and people affected by noise disturbance do not have the same order of magnitude a normalization has to be applied. The normalization for fuel is shown in (26) and the same method applies for noise.

$$n_f = \frac{1}{\max\left(f_{fuel}^{noise_{opt}}\right) - \min\left(f_{fuel}^{fuel_{opt}}\right)} \quad (26)$$

As the problem is a multi-objective problem, weights are applied to noise disturbance and fuel burn to analyse the behavior of the optimal solution when the emphasis of the objective is varied. The relation between the weights is given in (27). By varying the weights for α from 0 to 1 a Pareto front can be constructed from which ideal solutions can be obtained.

$$\beta = 1 - \alpha \quad (27)$$

III-B Constraints

To create a model that is an accurate representation of the actual situation, several constraints are implemented. To determine the operating time and assigned delay, constraint (28) is used where TS_f is the scheduled time of flight f .

$$T_f - D_f = TS_f \quad , \forall f \in F \quad (28)$$

Each flight has to be assigned to one runway and one runway only. Constraint (29) ensures this. If runways are closed for operation, for instance because of maintenance or because a certain operation is not allowed at that runway end, constraint (30) is used.

$$\sum_{r=1}^R x_f^r = 1 \quad , \forall f \in F \quad (29)$$

$$\sum_{f=1}^F x_f^r = 0 \quad , \forall r \in R_r \quad (30)$$

Flights are allowed to switch order if they are within a specified window (SW) of each other, which is shown in (31). To ensure that order changes outside this window are prohibited two extra constraints are necessary. The first constraint determines the value of the auxiliary decision variable, $x_{i,j}$, which can be used for separation. Notice that if j is smaller than i and not within the SW, this variable is always zero. The second constraint determines the time between the operation and ensures that outside the SW a First-Come, First-Serve principle is used. These constraints are shown in (32) and (33), respectively.

$$x_{i,j} + x_{j,i} = 1 \quad , \forall j \neq i \wedge |TS_i - TS_j| \leq SW \quad (31)$$

$$x_{i,j} = 1 \quad , \forall j > i \wedge |TS_i - TS_j| > SW \quad (32)$$

$$T_j - T_i \geq 0 \quad , \forall j \neq i \wedge TS_j - TS_i > SW \quad (33)$$

$, \forall i \in F$

With the order of flights determined, the separation constraint can be implemented. In (34) it is shown that this constraint is constructed with the big-M method. This makes it possible to only activate constraints when all decision variables are active, otherwise the constraint is inactive. The separation time, $T_{i,j}^{r,q}$, is dependent on the operation of the flights, the aircraft type of both flights including their weight classes and the runways on which they operate. To enhance model performance it is chosen to only consider separation requirements for flights within 2 SW as this would ensure sufficient coverage for all combinations as long as the SW is not smaller than the largest separation requirement.

$$-Mx_{i,j} - Mx_i^r - Mx_j^q + T_j - T_i \geq -3M + T_{i,j}^{r,q} \quad , \forall i \in F, \quad \forall j \in |TS_i - TS_j| \leq 2SW \quad , \forall r, q \in R \quad (34)$$

For noise disturbance an indicator constraint is used. This switches the decision variable to 1 if the noise limit is exceeded and remains 0 otherwise. Note that in (35) the cost coefficient $c_{xy}^{f,r}$ is the AEL value that occurs at a gridpoint when flight f is assigned to runway r .

$$g_{xy} = 1 \leftarrow \sum_{f=1}^F \sum_{r=1}^R c_{xy}^{f,r} x_f^r > L_{limit} \quad \forall xy \in P \quad (35)$$

$$g_{xy} = 0 \leftarrow \sum_{f=1}^F \sum_{r=1}^R c_{xy}^{f,r} x_f^r \leq L_{limit} \quad \forall xy \in P$$

III-C Flow Diagram

To provide a general overview of the structure of the program, a flow diagram is presented in Figure I. The

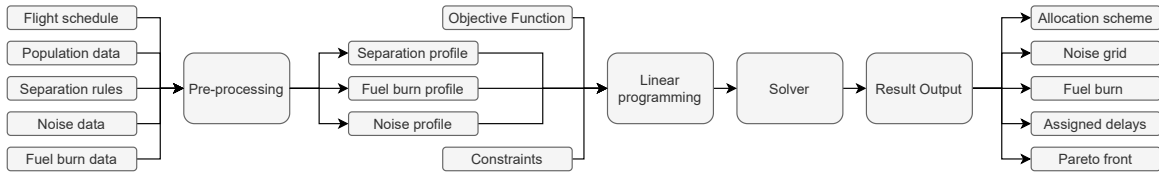


Figure I: Flow diagram

user has to input data which is specific for the airport of interest. A flight schedule is necessary which can be either a full day of operations or only specific hours. Population data is necessary to calculate the cost of noise disturbance in the vicinity of the airport. Separation rules need to be given as well. This consists of both the separation scheme used and the dependencies between runways. Noise data can be obtained through a noise model such as the AEDT. Finally, fuel burn profiles for the aircraft considered are necessary. The pre-processor makes profiles for separation, fuel burn and noise emission and differentiates between different aircraft and runways. The objective function and constraints as discussed in the previous sections are combined in a linear program, which is fed into the solver. In this research use is made of the commercial IBM ILOG CPLEX solver which uses a combination of Branch & Bound and Dynamic Search to obtain the optimal solution.

When varying the weights for fuel and noise the result output processor is able to create a Pareto front where the trade-off between fuel burn and noise disturbance can be visualized. For a combination of weights the result output shows the allocation scheme, noise grid and fuel characteristics for that combination.

IV Results

To evaluate the flexible runway scheduling method a use-case is analysed to investigate the effects on fuel burn and noise disturbance. In Section IV-A different scenarios are explained for operations on Amsterdam Airport Schiphol (AAS) and an example of the computational complexity is provided. To analyse the accuracy of the separation modeling, insights are provided with the reference scenario. This is presented in Section IV-B. In Section IV-C the Pareto fronts for the scenarios are presented. Based on these fronts a combination of weight parameters is chosen and further evaluated in Section IV-D. The fuel savings that can be obtained by switching to the Flexible Runway Scheduling Model (FRSM) are presented in Section IV-E. Finally, in Section IV-F the effect of delay is analysed.

IV-A Airport & Computational Performance

For the analysis of the Flexible Runway Scheduling Model (FRSM) a day of operations at Amsterdam Airport Schiphol (AAS) is analysed. AAS has a complex runway system with 6 runways oriented in different

directions. The *Oostbaan(R04/R22)* is used only for small general aviation and is therefore omitted from this analysis. Because AAS is located in a densely populated area, noise disturbance is an important issue and therefore AAS operates with a preference list. AAS is one of the largest hubs in Europe and is subjected to inbound and outbound waves. During those peaks runways are used in a 2+1 configuration. If the waves overlap AAS can switch to a 2+2 configuration as well [21].

Three peaks at a busy day in August 2019 are evaluated. The FRSM is able to quickly analyse periods of 1-2 hours, but longer periods become increasingly difficult in terms of computing power. As the inbound and outbound waves are the busiest time periods, only those hours are analysed. The details can be found in Table III. To evaluate the effect of the FRSM, reference scenarios are considered as well. The runways in the reference scenario are shown for arriving (A) and departing (D) aircraft.

Table III: Scenarios for AAS

Scenario	Peak	Flights	Reference
1	Outbound	102	A: <i>R18R</i> D: <i>R18L, R24</i>
2	Inbound	159	A: <i>R18R, R18C</i> D: <i>R24</i>
3	2 + 2	123	A: <i>R18R, R18C</i> D: <i>R18L, R24</i>

To provide an overview of the computational complexity additional details are provided and key numbers are shown in Table IV for the first scenario. The number of decision variables is mainly driven by x_f^r . As AAS has 5 runways and thus 10 runway ends the number of combinations between flights and runways is significant. The second biggest contributor is the indicator variable for noise. For AAS a rectangular noise grid with 400 measurement points is considered. The auxiliary decision variable $x_{i,j}$ amounts to the biggest number of variables as every combination between all flights is considered. The first scenario needs approximately 130,000 constraints, mostly separation constraints. The solver has a time limit of 1500 seconds to find a solution; this proved to be sufficient to obtain a gap range within 1% of optimality. However, an increase could be observed as the emphasis is shifted more towards noise.

The model uses a warm start when optimizing for multiple weight parameters. This is done to ensure that

subsequent solutions can only be the same or an improvement with respect to the previous solution and that the solution converges more quickly.

The model reaches a solution which is close to optimal in a short time, but further gap reduction takes a considerable amount of time. As the number of constraints and possible combinations is large, a lot of computing power is needed to explore all combinations and solve the problem.

Table IV: Computational performance indicators for scenario 1

Parameter	Value
Decision Variables	1,624
Auxiliary Decision Variables	10,411
Constraints	~ 130,000
Solving Time	1500 sec
Gap Range	0 - 3%

IV-B Separation

To analyse the accuracy of the separation modeling and to provide insights in the possibilities to change the order of flights, two time periods of different scenarios are examined. A part of the flight schedule is presented in Table V and Table VI with the weight class (WC), aircraft type (AC), scheduled time of operation, the actual operating time and the runway (R).

Table V: Part of the flight schedule in scenario 1

	WC	AC	Sched. Time	Oper. Time	R
1	UH	B744	16:44:00	16:44:00	18L
2	LM	E190	16:44:00	16:46:40	18L
3	UM	E295	16:45:00	16:45:00	24
4	UM	A319	16:45:00	16:45:40	18L

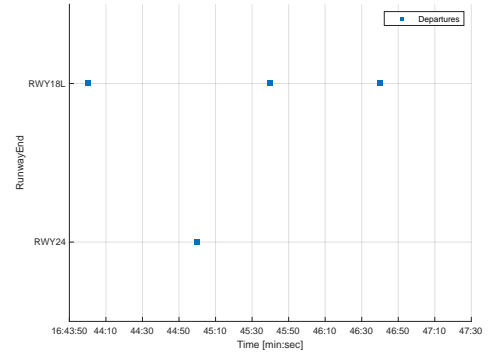
For the first scenario the separation between multiple departures is analysed. Departures performed on *R18L* are dependent on operations on *R24* and vice versa. This means that separation should be applied between those flights while at the same time the separation requirements for consecutive departures on the same runway should be respected. The effect of accurate separation and order changes can be observed from Table V and Figure 2(a). An overview of the separation requirements can be found in the RECAT-EU scheme [20]. It is stated that the pair-wise minimum separation for the flight combination UH-UM is 100 seconds, UH-LM is 120 seconds and UM-LM is 60 seconds. The dependency originating between different runways is due to jet blast and wake turbulence for which (10) and (11) are used. It is calculated that for the combination UH-UM a minimum of 40 seconds of separation is required and after departure on *R24* at least 18 seconds of separation is required

before the next departure on *R18L* can start the take-off roll. Analysing the operating times in Table V it can be found that these separation requirements are respected for every possible combination.

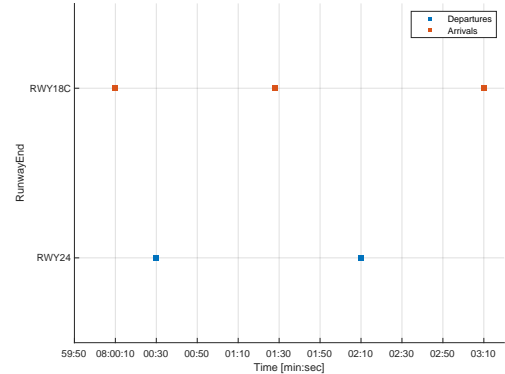
Table VI: Part of the flight schedule in scenario 2

	WC	AC	Sched. Time	Oper. Time	R
1	UM	B737	08:00:00	08:01:18	18C
2	UM	B738	08:00:00	08:00:00	18C
3	UM	A20N	08:00:00	08:00:20	24
4	LM	E175	08:02:00	08:02:00	24
5	UH	A332	08:03:00	08:03:00	18C

In the second scenario a combination of arrivals and departures is analysed for operations on *R24* and *R18C*. For consecutive arrivals the separation requirement for the combination UM-UM and UM-UH is both 78 seconds [20]. A departure at *R24* can start the take-off roll according to (13), which is 20 seconds. The following arrival on *R18C* should be at a minimum distance from the runway threshold, according to (14), which is approximately 40 seconds. The results can be observed in Table VI and Figure 2(b). The aircraft arriving at 08:03 can land immediately at *R18C* as the effects of the previous arrival on that same runway and the previous departure on *R24* are no longer present.



(a) Applied Separation for Reference Scenario 1 between *R18L* and *R24*



(b) Applied Separation for Reference Scenario 2 between *R18C* and *R24*

Figure II: Separation Modeling for Multiple Scenarios

The effect of changing the order between scheduled flights is shown in the first scenario. By delaying certain flights the total separation becomes lower, preferred runways become available or the total fuel use becomes lower.

When the FRSM is active, multiple dependencies arise between runways at AAS. As AAS has intersecting, converging, diverging and parallel runways an extensive set of regulations is implemented for all possible combinations.

IV-C Pareto Front

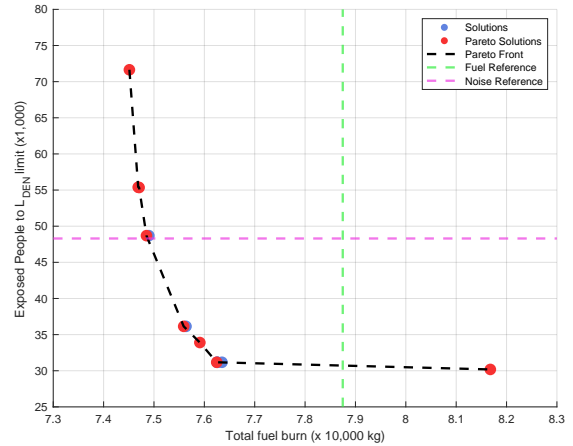
To visualize the effect of varying the weight factors, a Pareto front is plotted for all scenarios as can be seen in Figure III. As this problem is a multi-objective optimization there is not one optimal solution and a Decision Maker (DM) is to decide which solution is deemed *the best*. In the Pareto fronts the values for the reference scenarios are plotted as well. A fuel reference is determined in the reference scenario. An optimization is performed with emphasis placed on fuel only ($\alpha = 1$). For a noise reference a report is used which measures the L_{DEN} violations in a year [17].

It can be noticed that scenario 2 and 3 exhibit a more flattening behavior than the first scenario. This is mostly due to the presence of arriving flights in the scenarios. Arriving flights generally have a lower noise impact further away from the runway as descent is performed with engines idle. Therefore, most noise violations happen at the common approach path which cannot be avoided altogether. This has as a consequence that smaller differences are obtained when changing weights, resulting in more flattened curves.

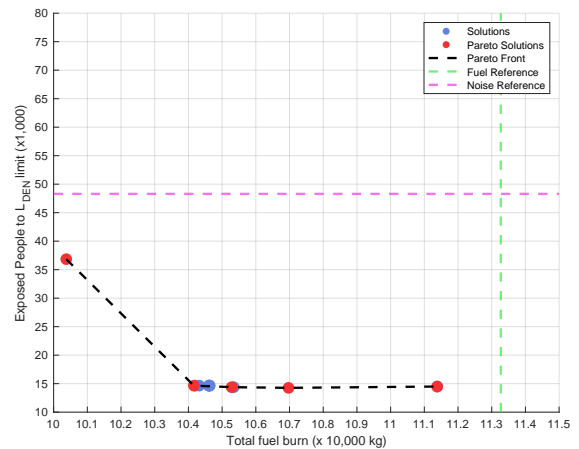
For further analysis a combination of weight parameters is chosen which is located close the left bottom of the Pareto curve to have reductions in both fuel burn and noise disturbance.

IV-D Noise Grid & Runway Allocation

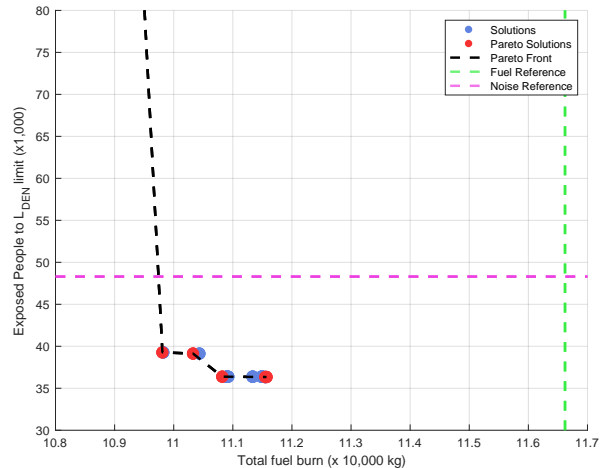
In Figure IV and Figure V the noise grid and runway allocation are shown for a combination of weight parameters for each scenario. In the outbound peak, shown in Figure 4(a) and Figure 5(a), the runways $R18L$ and $R24$ are heavily favored for departing operations. These runways are used in the reference scenario as well. It can be seen that the arrivals in this scenario are spread over all runways and that $R18R$ is used less with respect to the reference scenario. This can be explained for two reasons. The first reason has to do with the fact that operations on $R18R$ require a longer taxi time to the pier and runways located closer are more favorable. The second reason is found when analysing the use of $R24$. The multitude of departing operations on this runway violate the noise limit at the departure trajectory and scheduling extra arrivals on the opposite runway end does not come with extra noise cost. It can be noted that the FRSM in this scenario has a preference of scheduling flights close to the pier to minimize taxi operations. $R18R/R36L$ and



(a) Pareto Front Scenario 1



(b) Pareto Front Scenario 2



(c) Pareto Front Scenario 3

Figure III: Pareto Front for different scenarios

$R18C/R36C$ are then solely used to cope with extra demand if other runways are in use.

The second scenario is an inbound peak and shown in Figure 4(b) and Figure 5(b). In the reference scenario

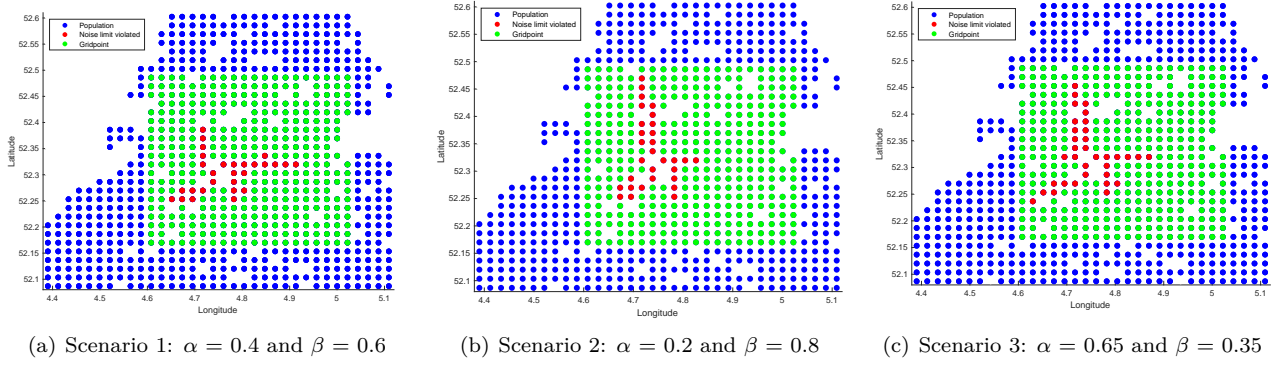


Figure IV: Noise Grids for multiple scenarios

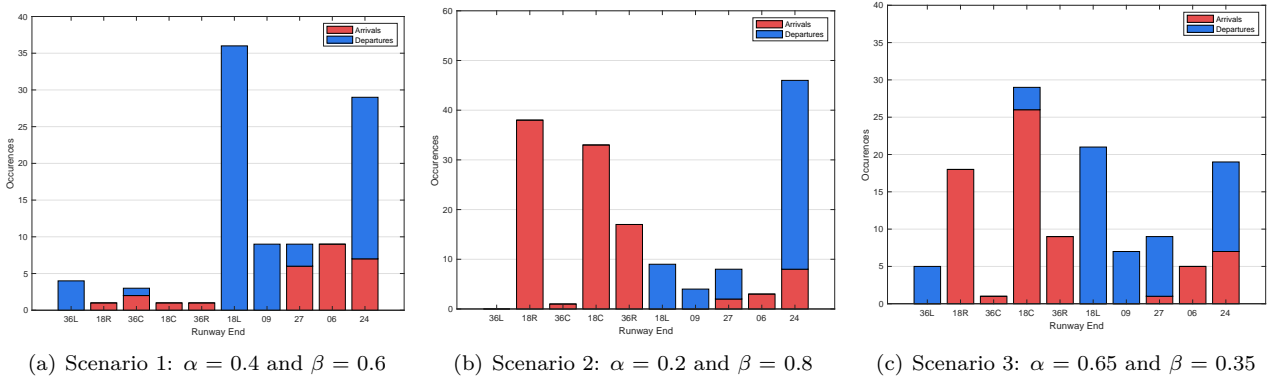


Figure V: Runway Allocation for multiple scenarios

arrival operations are only allowed on $R18R$ and $R18C$, while the FRSM schedules arriving flights on the other runways as well. From the noise grid it can clearly be seen that the operations at $R18R$ and $R18C$ violate the noise limit. The operations on $R18L/R36R$ are noteworthy as the operating runway end is switched multiple times during this period to accommodate for both arriving and departing flights. The fact that $R09/27$ is barely used for operation results in a lower number of violations on gridpoints east of AAS. For the arriving wave the number of people exposed by the noise limit is small. The number of gridpoint violations is in the same order of magnitude as the other scenarios. However, the absence of cities below the final approach fixes of $R18R$ and $R18C$, together with the fact that other violations are only located close to the airport, has as a consequence that the number of people affected by these operations is limited.

The final scenario is shown in Figure 4(c) and Figure 5(c) where the set of flights consist of an equal division between arrivals and departures. With respect to the reference scenario it can be noted that $R24$ is used for both operations. Although $R18C$ and $R18R$ are still the predominant runways for arrivals, it can be noted that some arrivals are also spread to other runways. This gives the possibility to have departing flights on $R36L$ as well. The noise grid for scenario 3 has the most violations with respect to the other scenarios. The fact that this scenario spreads the flights

relatively even over all runways has as a consequence that the departing and arriving routes for all runways are used, resulting in more violations of the noise limit. When comparing the FRSM to reference scenarios it can be concluded that the FRSM spreads the flights over all runways and that this does not lead to an increase in noise violations with respect to the reference scenario. Noise contours as displayed in [17] show matching profiles with the noise grids, indicating that the FRSM does not violate more gridpoints at new locations.

IV-E Fuel saving

To analyse the effect of the new scheduling method on the total fuel burn, a comparison can be made with the reference scenario. In Figure VI the fuel saving is shown for the different scenarios with respect to the reference scenario. The fuel saving can vary from 3.6% for the outbound scenario to 7.1% for the inbound scenario. The mixed operation scenario has a fuel saving of 5.0%. As AAS has, on average, 5 daily inbound and 6 outbound peaks a significant fuel saving can be obtained for a full day of operation.

The difference between fuel saving for the outbound and inbound scenario can be explained when analysing Figure 5(a) and Figure 5(b) and investigating the origin and destination of the flights. The destinations for the departing flights are mostly located south, heav-

ily favoring *R18L* and *R24*. These runways are also used in the reference scenario. This means that most departing flights already operate on their fuel-optimal runway. This reduces the potential for fuel saving. The origin of the arrival flights is spread more evenly and therefore higher fuel saving can be obtained when the flights are spread over the entire runway system.

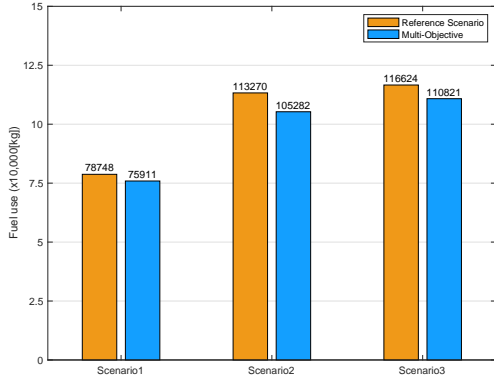


Figure VI: Fuel use for reference scenario and multi-objective scenario

IV-F Delay Distribution

The FRSM has the possibility to delay certain flights for separation requirements or when this favors the overall optimization. Further analysis is done by comparing three optimizations for each scenario. These optimizations consist of a run where emphasis is placed on noise optimization ($\beta = 1$), fuel optimization ($\alpha = 1$) and the multi-objective scenario as obtained from the Pareto front. The total delay is calculated first and then divided by the flights in that scenario to obtain an average delay.

In the first scenario it can be seen that the delay increases as more emphasis is placed on fuel optimization. While this seems counterintuitive at first, it indicates that it can be favorable to delay some aircraft to wait for a vacant preferred runway.

In the second scenario it can be seen that delay decreases when more emphasis is placed on fuel saving. For a noise optimized scenario the model assigns more delay to limit the number of runways used, thereby decreasing the number of gridpoints with a noise limit violation.

The difference in the delay trend can be explained on the basis of the operations performed. In general, the cost of delaying a taxiing aircraft is lower than for an aircraft in the air. As the first scenario consist of mostly departing flights, the cost of waiting for a preferred runway is less than the difference for the second optimal runway. For the arriving scenario, flights are preferred to be on the ground as quickly as possible as this is deemed more efficient than waiting in the air for a preferred runway.

Further analysis also proved the effectiveness of assigning a penalty to the maximum delay as it is not

avored to delay one aircraft endlessly in favor of others. It showed that the maximum assigned delay in the scenarios is about 6-7 minutes, which is deemed acceptable.

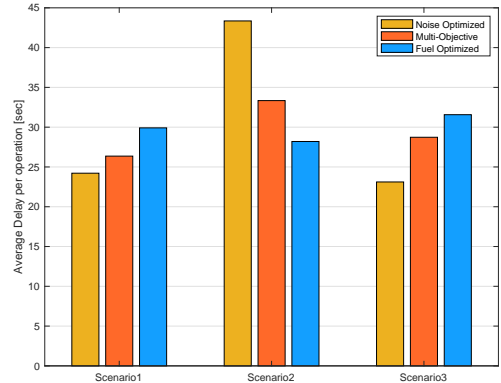


Figure VII: Delay distribution for three optimizations: noise, fuel and multi-objective

V General Discussion

In this paper a model is presented for flexible runway scheduling at airports with a complex runway system. This model is an extension of earlier work with improvements in separation modeling and delay allocation. In this section the results, possibilities and sensitivities are analysed as well as future recommendations for this model. In Section V-A the results will be discussed and their implications. In Section V-B several key trends and the effects of these results on airport operations are presented. Finally, recommendations are presented in Section V-C for future research.

V-A Fuel & Noise

Airports operating in a densely populated area use a preference list for the runway use which is only considering noise disturbances and the current wind conditions. At a time where fuel consumption and specifically fuel saving is becoming a topic of interest, the development of the flexible runway scheduling model (FRSM) proves to be a solution for both. By considering fuel burn and noise disturbance it is shown for Amsterdam Airport Schiphol (AAS) that reductions in both objectives are possible.

For fuel reductions it is found that savings are possible ranging from 3 - 7%. Further analysis of these scenarios showed that the type of operation and the origin or destination of the flights have an impact on the potential fuel reduction with respect to the reference scenarios. For AAS the runways operated in an outbound peak are directed south. In scenario 1 the number of flights having a destination south is more than 50% and so their optimal runway is already operated in the reference scenario. For the inbound reference scenario only runways are used which are oriented

north, while the incoming flights arrive from all directions equally. If flights are scheduled according to the FRSM more optimal flight-runway combinations arise and therefore more fuel reduction is possible. Another source of higher fuel reduction has to do with the taxi times from and to *R18R/R36L*. In the reference scenario, arrival flights are assigned to *R18R* and have to taxi from there to the terminal. Analysis of the airfield shows that the taxi distance from this runway to the terminal can be 2-3 times greater than other runway-terminal combinations. Taxi operations also have a significant impact on fuel burn and therefore reductions are possible by scheduling aircraft closer to the terminal, thereby reducing taxi times.

For noise disturbance the FRSM is compared to the actual noise data from 2016. Based on this data [17] 48,300 people endured noise disturbances above the L_{DEN} limit. The FRSM is able to schedule flights while ensuring this limit is not violated. Further investigation in the number of people that are affected by a noise violation reveals the fact that certain municipalities are located directly under the approach or departure routes of certain runways. The fact that they are located relatively close to a certain runway comes with the consequence that the noise limit is almost always violated if that particular runway is used. When comparing the noise grids for scenario 1 and 2 it can be seen that for the inbound peak more grid-points are violated, but that actually less people are affected by this violation. This is mainly due to the fact that the population located north of *R18C* and *R18R* is sparse. When evaluating scenario 3 it is found that during that operational profile most people are affected by the noise. This is mainly due to the extra noise violation to the left of AAS where also a village is located.

For noise regulations in general a remark should be made. Noise regulations and limits are in agreement with government and are determined on a yearly basis. This means that it is allowed for operational hours to exceed the noise limit as long as this does not affect the yearly average. The scenarios analysed in this research demonstrate that noise limits are indeed violated for a period of time, but it should be taken in mind that this has to be compensated for during operational hours when the demand is lower.

V-B Trends & Possibilities

The results for AAS are further analysed in detail to examine trends and key decisions the model makes. These key decisions could already be used in current day operations without the implementation of the flexible runway scheduling method. First, an analysis is performed for the allocation of weight classes at runways. In scenario 1 a shift can be observed for the allocation of Heavy aircraft ('UH' and 'LH'). When the emphasis of optimization is shifted from noise to fuel, more flights are scheduled on *R18L*, opposed to flights located on *R36L* and *R09*. A similar shift can be observed in scenario 2. For a noise favored opti-

mization ($\beta > 0.5$) most Heavy aircraft are scheduled on *R18C* or *R18R*, while a fuel favored optimization shifts the aircraft allocation towards *R27*.

For every flight there is one runway which amounts to the lowest fuel burn. For every weight class it is examined how many aircraft are assigned to this preferred runway. Overall it is found that with an increasing emphasis on fuel optimization, more flights are placed on their preferred runway. However, some extra trends can be observed. In the first scenario a very high percentage (>65%) of Medium aircraft is assigned to their preferred runway independent of the optimization. In the second scenario the number of Heavy aircraft allocated to their preferred runway increases significantly (3 to 4 times) when the optimization emphasis is placed on fuel ($\alpha > 0.5$).

Besides analysis for weight classes research is also performed for the aircraft types in each scenario. Two general trends can be observed. Some aircraft types are always assigned their preferred runway independent of the optimization. The second trend is that some other aircraft types are always assigned to their preferred runway if fuel optimization becomes dominant. This first trend applies for instance to the A21N, B789 and B763, independent of the scenario. The second trend can be observed for multiple flights, mainly heavy aircraft such as the B744, B77L and B788.

A final trend is observed between runways and waypoints. This is already somewhat discussed in the previous section, but general trends are stated here. In an outbound wave more than 90% of the flights with a destination towards waypoint *IDRID* or *LEKKO* are scheduled on *R24* or *R18L*, respectively, independent of the optimization. For an inbound scenario the same trend is still observed for waypoint *IDRID*. Arriving flights with an origin via waypoint *ARTIP* are placed mostly (>60%) on *R18C* independent of the optimization preference. For a mixed peak, flights with waypoint *IVLUT* are placed almost exclusively on *R18L* independent of the optimization. In this same scenario flights with waypoint *LEKKO* are placed on *R18L* as well as the emphasis is shifted towards fuel.

It is shown that for AAS both fuel and noise can be reduced by changing to a flexible scheduling method. This can have several opportunities in the future. As AAS operates under strict noise regulations, further growth in terms of operations is not allowed in the coming future. Local government and airport management have agreements on the number of operations based on these noise limits and changing to a flexible method could open the conversation for an increase in operations. The flexible scheduling method also has advantages for airlines. Fuel has an important role in the airline cost structure and a reduction can lead to an economic advantage. The third party which benefits from this method are residents in the area. Not only can the flexible scheduling lead to less noise violations, the fact that less fuel is used has a positive effect on the emissions in the vicinity of the airport. Fuel savings have a direct effect on the exhaust emis-

sions produced by aircraft.

For airports operating under less strict noise regulations the flexible scheduling method also provides opportunities. By optimizing more in favor of fuel reduction possibilities could be explored in different operating profiles. Another use could be for airports which operate very close to or over their runway capacity. For different objectives it could be explored which aircraft to delay in favor of others to maximize the runway capacity.

V-C Recommendations

For future research several recommendations are found which can improve the model further. Future research should be directed to the implications on the Air Traffic Management (ATM) system. As flexible operations require a higher awareness, the Air Traffic Controller (ATCo) workload will increase and this should be taken into account.

Another area of future research can be directed to noise disturbance. The current model uses a noise limit to indicate the noise objective. However, once this limit is exceeded there is no extra cost of exceeding this limit more. Resources can be directed to implement an objective that penalizes higher noise violations even more. An additional implementation could be the use of variable noise budgets. As noise limits are determined on a yearly basis a better representation can be accomplished when translating a yearly limit towards an hourly budget.

Another limitation arises when analysing the taxi operations. The FRSM only considers taxi distances, but not the layout of the taxi system. At AAS an example arises where the taxiway has a limiting factor on the operations while this is not considered by the model. For operations from and to *R18R/R36L* only one taxiway is available. This makes it difficult to switch the order of operations as the taxi operation can be a limiting factor. Therefore it is recommended to further analyse the taxi-system and its implications on the model.

Directing resources to model performance would also improve the model. As pairwise separation is used, the amount of constraints to be written by the linear programming tool is very large and takes a considerable amount of time. A proposed research is to implement a sliding time window in the scheduling model. From an ATC perspective scheduling for more than 30 minutes ahead is not feasible as the uncertainty of the operation time becomes too large. By implementing a sliding time window the model assigns flights for the next 30 minutes accurately according to all regulations and for the subsequent 30 minutes only determines a rough runway allocation. A shift in noise modeling will be required, for instance the technique where noise budgets are used as proposed earlier.

Finally, to explore the possibilities and conflicts, the FRSM could be implemented in current-day models to see its effects. As the FRSM is mainly a runway capacity model its collaboration with other airport-

related models could uncover extra hidden features or problem-areas.

VI Conclusion

In this paper an improvement is described for the flexible runway scheduling model to fill an existing gap in the current state of the art. Based on the original model constructed by Delsen [5] and the improvements made by Van Der Meijden [26] the new model is extended with the incorporation of accurate separation strategies for complex runway systems as described by Van Der Klugt [25].

The model is adjusted to a scheduling model instead of an allocation model. By changing the decision variables to no longer incorporate the delay but to assign a continuous variable the model assigns continuous delays to the scheduled flights resulting in more accurate operating times and a more compact flight schedule. It also ensures that an optimization cannot be infeasible as delays are not limited to a maximum. With a new separation constraint is the user able to accurately model complex runway dependencies between runways. With the option to adhere to the First-Come, First-Serve principle the model remains close to the current operating strategies.

The flexible runway scheduling model uses a multi-objective optimization tool which considers both fuel consumption and noise disturbance. For fuel burn characteristics use is made of the Base of Aircraft Data [6] and noise profiles are constructed using the new Aviation Environmental Design Tool [24].

The model is tested for a set of operations at Amsterdam Airport Schiphol as this airport is highly congested, is subject to noise regulations and has a complex runway system. It is found that reductions in both objectives are possible. By creating a Pareto front for different scenarios, a combination of weights can be selected by the user. For the selected outbound peak fuel savings are possible of 3.5% and for the inbound peak this can be up to 7%. For noise disturbance it is found that reductions are possible, but that the location of some households can never be mitigated by the model. It is further shown that it can be beneficial to assign more delay in favor of fuel reduction. Key trends are discovered and analysed which can be implemented in current day operations without many disruptions. These trends relate to the allocation of weight classes on certain runways and combinations between runways and waypoints, which are independent of the optimization emphasis.

The new model should be validated with ATM regulations and the influence of an increased workload for ATC. The new model could be improved by incorporating a taxi scheduling model to explore constraints that arise from flexible runway scheduling. Furthermore, to improve performance research could be directed to solving methods.

With the proposed model, research can be performed to explore the effects of changing the operating stra-

tegy to incorporate both fuel burn and noise disturbance and is applicable to any airport configuration.

References

- [1] B. Pearce. Outlook for Air Transport and the Airline Industry. Technical report, IATA, 2020.
- [2] Bewoners Aanspreekpunt Schiphol. 2019 Jaarrapportage. Technical report, BAS, 2020.
- [3] A. Blumstein. The Landing Capacity of a Runway. *Operations Research*, 7:752–763, 1959.
- [4] D. Halperin. Environmental noise and sleep disturbances: A threat to health? *Sleep Science*, 7:209–212, 2014.
- [5] J. Delsen. Flexible Arrival and Departure Runway Allocation. Master’s thesis, Delft University of Technology, 2016.
- [6] EUROCONTROL. User Manual for The Base of Aircraft Data (BADA). Technical report, Eurocontrol Experimental Centre, 2004.
- [7] E. Gilbo. Airport Capacity: Representation, Estimation, Optimization. *IEEE Transactions on Control Systems Theory*, 1:144–154, 1993.
- [8] R. Harris. Models for Runway Capacity Analysis. Technical report, The MITRE Corporation, 1972.
- [9] S. Hockaday and A. Kanafani. Developments in Airport Capacity Analysis. *Transportation Research*, 8:171 – 180, 1973.
- [10] J. Hu, N. Mirmohammadsadeghi, and A. Trani. Runway Occupancy Time Constraint and Runway Throughput Estimation under Reduced Arrival Wake Separation Rules. *AIAA Aviation 2019 Forum*, 2019.
- [11] International Air Transport Association. WATS World Air Transport Statistics 2019. Technical report, IATA, 2019.
- [12] International Civil Aviation Organization. ICAO Long-Term Traffic Forecasts. Technical report, ICAO, 04 2018.
- [13] International Civil Aviation Organization (ICAO). ICAO Doc 9829, Guidance on the Balanced Approach to Aircraft Noise Management. Technical report, ICAO, 2011.
- [14] H. Khadilkar and H. Balakrishnan. Estimation of Aircraft Taxi-out Fuel Burn using Flight Data Recorder Archives. *AIAA Guidance, Navigation and Control Conference*, 2011.
- [15] Luchtverkeersleiding Nederland (LVNL). Integrated Aeronautical Information Package, 2020.
- [16] M. Bazargan, K. Fleming, P. Subramanian. A SIMULATION STUDY TO INVESTIGATE RUNWAY CAPACITY USING TAAM. *Winter Simulation Conference Proceedings*, 2002.
- [17] Ministerie van Infrastructuur en Milieu. Geluidsbelastingkaarten luchthaven Schiphol voor het gebruiksjaar 2016. Technical report, Ministerie van Infrastructuur en Milieu, 2017.
- [18] R. Neufville and A. Odoni. *Airport Systems: Planning, Design and Management*. McGraw-Hill Education, New York, second edition, 2013.
- [19] A. Odoni et al. Existing and Required Modeling Capabilities for Evaluating ATM Systems and Concepts. Technical report, International Center for Air Transportation MIT, 1997.
- [20] F. Rooseleer and V. Treve. European Wake Turbulence Categorisation and Separation Minima on Approach and Departure. Technical report, EUROCONTROL, 2015.
- [21] Schiphol Group. Gebruiksprognose 2019. Technical report, Schiphol Group, 2018.
- [22] M. Stamatopoulos. A decision support system for airport strategic planning. *Transportation Research Part C*, 12:91–117, 2004.
- [23] W. Swedish. Upgraded FAA Airfield Capacity Model. Volume I Supplemental User’s Guide. *The MITRE Corporation*, FAA-EM-81-1, Volume I and MTR-81W16, Volume I, 1981.
- [24] US DOT Volpe Center. Aviation Environmental Design Tool (AEDT). Technical report, FAA, 2019.
- [25] J. van der Klugt. Calculating capacity of dependent runway configurations. Master’s thesis, Delft University of Technology, 2012.
- [26] S. van der Meijden. Improved Flexible Runway Use Modeling. Master’s thesis, Delft University of Technology, 2017.
- [27] H. Visser and R. Wijnen. THE AIRPORT BUSINESS SUITE: A DECISION SUPPORT SYSTEM FOR AIRPORT STRATEGIC EXPLORATION. *AIAA*, 2003.

II

Literature Study

Note: This part has already been evaluated under the course: AE4020 - 'Literature Study'

2

Airport Capacity Modeling

Runway capacity determines to a great extent the airport capacity, but other factors play a role as well. In this chapter several key objectives are reviewed related to this subject. The structure of this chapter is mainly based on research performed in Chapter 10 of *Airport Systems: Planning, Design and Management* by Neufville and Odoni [37] and multiple different sources are used to substantiate the statements. The structure of this chapter is as follows. In Section 2.1 some general definitions of airport capacity are presented. As runway capacity is the most important driver, in Section 2.2 multiple influencing factors will be analysed. One of these factors is the separation requirements between flights and a recent new scheme is presented in a separate section in Section 2.3. Capacity modeling and the first steps in calculation are presented in Section 2.4. Finally, in Section 2.5 a review is performed of the current state of the art capacity models.

2.1. Airport Capacity Definitions

Airport or runway capacity is defined in several different ways which can often lead to misconceptions. Neufville and Odoni [37] defined four definitions which are explained below.

1. **Maximum Throughput Capacity** - (MTC)

The MTC, sometimes referred to as the saturation capacity, is the maximum number of flights that can operate at a runway system in 1 hour [37]. This is such that Air Traffic Management (ATM) separation regulations are not violated and that the demand of flight is continuous. The MTC is highly dependent on the operational conditions which are defined in the next section.

2. **Practical Hourly Capacity** - (PHCAP)

As the MTC does not consider any delay the PHCAP was defined to consider this as well. The PHCAP is defined as the number of flights in 1 hour with an average delay of 4 minutes per movement. This was proposed by the FAA in 1960s [32]. Usually, the PHCAP is about 80 to 90 percent of the MTC [39].

3. **Sustained Capacity**

The Sustained Capacity is a derivative of the MTC and is defined as the number of movements per hour on a runway system that can be reasonably sustained over a period of several hours [37]. Reasonably sustained refers to the fact that the MTC cannot be operated by air traffic controllers for more than 1 or 2 hours and so the sustained capacity takes the human factor into account. The sustained capacity is about 90 percent of the MTC.

4. **Declared Capacity**

Declared Capacity is linked to airports operating with a "schedule coordination" or "slot allocation". The declared capacity is determined by the airport and is the maximum number of movements per hour at a reasonable Level-of-Service (LOS).

When the runway capacity is exceeded by the demand delays are formed. Neufville & Odoni [37] consider two types of delays. The first is overload delay and occurs when demand is continuously exceeding the capacity for a specific time. The second type is stochastic or probabilistic delay and occurs when the demand

is very close, but lower, than the actual service rate. When the inter-arrival or inter-departure times of the demand differs such that clusters can be formed the capacity could be insufficient making it possible for delays to build up.

Roling [39] states that delays are best represented with the queuing theory. A queuing system consists of three elements: i) a user source, ii) a queue and iii) a service facility with 1+ parallel servers. The long term behavior of the delay is proportional to the utilization ratio, shown in Equation 2.1. The utilization ratio, ρ , is the ratio between the demand rate, λ , and the service rate or capacity, μ , which is given in Equation 2.2. It can be seen that when the utilization ratio approaches 1 the delay increases rapidly.

$$D \sim \frac{1}{1 - \rho} \quad (2.1)$$

$$\rho = \frac{\lambda}{\mu} \quad (2.2)$$

To get information about the expected time a user spends in the queue the Pollaczek-Khinchine formula can be used which is given in Equation 2.4. This assumes a Poisson distributed demand, meaning that the inter-arrival times between the users are independent. Furthermore, a steady-state condition where ρ is smaller than 1 is necessary. In this equation $E[T]$ is the expected service time and can be calculated according to Equation 2.3. Also, σ_T^2 is the variance of the service time. [39]

$$E[T] = \frac{1}{\mu} \quad (2.3)$$

$$W_q = \frac{\rho \left[1 + \frac{\sigma_T^2}{E^2(T)} \right]}{2\mu(1 - \rho)} \quad (2.4)$$

The runway occupancy time (ROT) is the final definition of importance. The ROT has a large influence on the runway capacity as subsequent operations are only possible if the runway is vacant. Pavling [38] did extensive research in ROT and the influence on the overall runway capacity. The main drivers of the ROT are the type of aircraft, landing weight, threshold speed, weather and runway conditions. Also pilot skills play an important role as this has an influence which exit the aircraft can use. EUROCONTROL defines two types of ROT [16].

1. Departure Runway Occupancy Time - (DROT)

The DROT is defined as the time interval between the aircraft crossing the holding stop bar and the main gear lifting off from the runway.

2. Arrival Runway Occupancy Time - (AROT)

The AROT is defined as the time interval between the aircraft crossing the runway threshold and the aircraft tail vacating the runway [38].

2.2. Runway Capacity Factors

Runway capacity from a single runway or runway system is defined by several factors. In this section some of the key elements are described in more detail. First the geometry of runways is discussed. Second the runway configurations are explained extensively. The ATM separation requirements and ATM system in general are analysed thereafter. Fourth, the aircraft mix and sequencing techniques are discussed. Finally, the influence of meteorological conditions is explained.

2.2.1. Geometry of the Runway

The number of runways in the runway system is the main driver for the runway capacity. A distinction must be made between the number of runways and the runways in use at a particular moment, called the runway configuration. Runways can be oriented in many directions and therefore each runway (RWY or R) has its own identifier at an airport. The identifier is a 2 digit number correlating to the true bearing rounded to its nearest ten degrees and then divided by ten. As each runway can be operated in two directions, the identifier always consist of two numbers, which differ by 18 [39]. If two or three runways are parallel, the addition of *L*, *R* or *C* is given to indicate the difference. If more than three runways are parallel, the next runway is given a designator ± 1 with respect to the true bearing [24].

Runway Exits

As the ROT has an influence on the runway capacity it is essential that aircraft are able to vacate the runway as soon as possible after landing. The location and type of exit has a significant influence on the AROT. Trani et al. [3] performed research on reduced ROTs by incorporating high-speed and medium-speed exits along the runway instead of the conventional 90° exits. For a single runway reductions of 15% are possible by implementing super-acute angle exits; exits with a 20 degree turnoff angle with respect to the runway center line.

2.2.2. Runway Configurations

When a runway system consist of multiple runways, dependencies between those runways could occur and can have an important role in the overall capacity. In research performed by Van Der Klugt [49] five different categories were defined for different types of runway dependencies. They are discussed in this part.

Parallel Runways

Parallel runways are those runways whose centerlines are aligned. Dependencies between those runways is mainly driven by the distance between the centerlines of both runways. There are three categories defined by Neufville and Odoni [37] based on that distance. For each category there are four different operational combinations [49]:

1. Arrival - Arrival (A-A)
2. Departure - Departure (D - D)
3. Departure - Arrival (D - A)
4. Arrival - Departure (A - D)

1. Closely Spaced Parallel Runways - (CSPR)

The distance between the centerlines of CSPR is up to 2500 *ft*. For the A-A, D-D and D-A combination the operations should be performed as if it is a single runway. For the A-D combination the departing aircraft is allowed to start its take-off roll the moment the arriving aircraft touches down.

2. Medium Spaced Parallel Runways - (MSPR)

For MSPR the centerlines are between 2500 and 4300 *ft*. For the D-D, D-A and A-D combinations the two runways can be considered to be independent and no extra separation is necessary. For the A-A combination the trailing aircraft has to have a direct 1.5 *nmi* extra separation with respect to the leading aircraft.

3. Independent Parallel Runways - (IPR)

If the centerlines are more than 4300 *ft* apart, the two runways are considered to be IPR. No extra separation is necessary for all operational combinations.

Two additional remarks have to be made. First, for the D-D case the climb path after take-off should be taken into account in determining separation. If this is the same path an extra separation should be applied to ensure safe flight. Second, if runways are staggered the effective distance between centerlines can be reduced. For every 500 *ft* of offset the effective centerline distance can be decreased by 100 *ft* up to a minimum of 1200 *ft*. The different cases are summarized in Table 2.1.

Table 2.1: Parallel runway separations [37]

Separation between centerlines	A-A	D-D	D-A	A-D
≤ 2500 ft	Single Runway	Single Runway	Single Runway	After Touch-Down
2500 - 4300 ft	1.5 <i>nmi</i> separation	Independent	Independent	Independent
≥ 4300 ft	Independent	Independent	Independent	Independent

Converging & Diverging Runways

Converging and diverging runways do not physically cross each other, but their projected centerlines intersect at some point. The separation procedures for these combinations vary for every airport and therefore a standardized set of rules is not applicable. However, the dependencies can be divided into two types and are shown in Figure 2.1 [49].

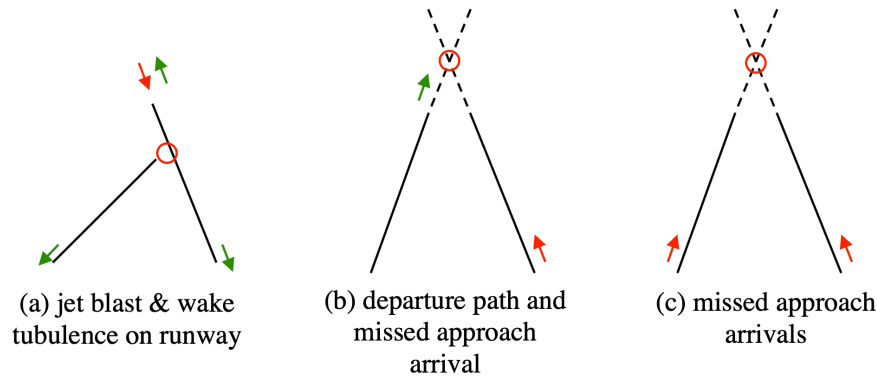


Figure 2.1: Converging or diverging runways and dependencies [49]

- **Jet blast & Wake Turbulence** - Figure 2.1a

An aircraft starting its take-off roll can cause a jet blast on another runway or an aircraft at speed can cause a wake turbulence on the other runway. These combinations are depicted in Figure 2.1a. The separation requirement depends on the operating order, the type of aircraft and the operation type. However, the most important factor is the location of the intersecting lines.

- **Missed Approach** - Figure 2.1b and Figure 2.1c.

An arriving aircraft must have a safe path for a missed approach procedure if necessary. Two cases can arise. The first is where a departure is cleared after the arrival is (partly) completed. The second case is for two arrivals with intersecting missed approach paths. For this, ATC applies a staggering distance between the arrivals to ensure safe flight.

Intersecting Runways

For intersecting runways the same two types of dependencies arise as for converging & diverging runways. However, the intersection point is now located on the runway instead of the projected flight path. The separation requirements are heavily dependent on the situation, the type of operations and the type of aircraft. However, in general it can be said that it is most efficient to perform operations at the runway ends which are located closest to the intersection point as this requires the least amount of separation [49].

Mixed Mode Operations

When a runway is used for both arrivals and departures it is said to operate in mixed mode. The ratio between arrivals and departures gives an indication how the runway is used. The alternating mixed mode is used when this ratio is close to one (A-D-A-D-...). However, it can also occur that one of the two is higher in demand (A-A-A-D-A-A-...). For mixed mode operations separation requirements are not only important between consecutive operations but also for the preceding and following operations. The final requirement has to do with the inter-arrival and inter-departure times which should be respected as well, even if the operation order is split with another operation.

Ground Operations

The layout of the runways system has an impact on the ground operations as well. Aircraft that need to cross an active runway can pose further restrictions on the use of that runway. Multiple solutions are possible for this problem. The construction of end-arounds [10] or operating procedures such as the Land and Hold Short Operations (LAHSO) [40] decrease the negative influence of ground operations on the runway capacity. In general it can be said that the effect of ground operations depends heavily on the situation at the airport and that general rules are difficult to construct.

2.2.3. Air Traffic Management Constraints

Regulations around the airport have a constraining effect on the overall airport capacity. In this subsection first an overview is provided of the airspace structure around Amsterdam Airport Schiphol (AAS) to obtain a

general overview of the parties involved. The restrictions imposed by Air Traffic Control (ATC) are explained next.

Airspace Structure

The largest division of the airspace is in Flight Information Regions (FIR). Small countries usually consist of a single FIR while bigger countries can have multiple FIRs. Within a FIR the Air Navigation Service Provider (ANSP) is responsible for the management of air traffic on behalf of a company, region or country [29]. Inside the FIR multiple controlled areas exist to navigate traffic. The Upper Airspace (UTA) starts at Flight Level FL245. The Control Areas (CTAs) are areas in which ATC services are provided. CTAs are structured by means of airways and navigational aids. Flights landing at a specific airport then enter the Terminal Control Area (TMA) which is the area above an airport. The entry points into the TMA are called the Initial Approach Fixes (IAF). If the TMA is too busy, aircraft can be hold in a stack before given clearance to enter the TMA. Routes within the TMA are defined as Standard Instrument Departures (SIDs) or Standard Terminal Arrival Routes (STARs). Within the TMA aircraft can also be navigated by means of speed and altitude restrictions [29]. The final stage of an arrival is when the aircraft enters the Control Zone (CTR) at which the Tower takes control. In Figure 2.2 a schematic overview is given of the situation around AAS [29]. At AAS there are two ANSPs. UTA is managed by EUROCONTROL MUAC while lower airspace is managed by *Luchtverkeersleiding (LVNL)*.

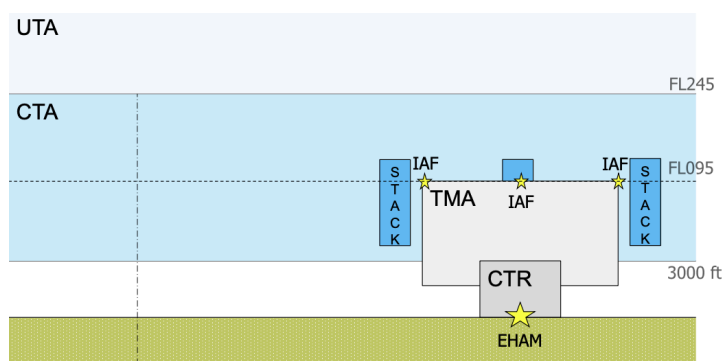


Figure 2.2: Dutch airspace around Amsterdam Airport Schiphol (EHAM) [29]

Wake Turbulence

Separation regulations are imposed by Air Traffic Control (ATC) to ensure the dissipation of wake turbulence of the preceding aircraft. Wake turbulence is the unwanted effect that comes from the pressure difference on both side of the wings. This pressure difference generates lift for the aircraft, but after the wings a rolling motion is created when the different airpockets collide. This spinning motion can last several minutes and can be potentially dangerous for the following aircraft. As wake turbulence is heavily correlated with aircraft size, four Wake Turbulence Categories (WTC) are created based on Maximum Take-Off Weights (MTOW) by ICAO [23]. The categories are displayed in Table 2.2. The Super Heavy (J) category was introduced later when the Airbus A380 was introduced. Because this aircraft was 4 times heavier than the threshold for Heavy aircraft and produced a bigger wake turbulence this new category was deemed necessary.

as this aircraft was 4 times heavier than the threshold for Heavy aircraft and produced a far bigger wake turbulence.

Table 2.2: Wake Turbulence Categories defined by ICAO [23]

WTC	Description	MTOW [kg]
J	Super Heavy	MTOW ~ 560,000
H	Heavy	$136,000 \leq \text{MTOW}$
M	Medium	$7,000 < \text{MTOW} < 136,000$
L	Light	$\text{MTOW} \leq 7,000$

As the categories defined by ICAO proved to be outdated for the current fleet, a new separation scheme was constructed which will be discussed in the next section. For each combination within the WTC separation

guidelines are constructed. For successive arrivals the distanced-based separation is presented in Table 2.3. The values between parentheses are based on minimum radar separation which is commonly taken as 3 *nmi*. For successive departures the metric time-based separation is used which is presented in Table 2.4.

Table 2.3: Distance-based separation minima in *nmi* [23]

Leading AC	Trailing AC			
	Super	Heavy	Medium	Light
Super	-	6	7	8
Heavy	-	4	5	6
Medium	(3)	(3)	(3)	5
Light	(3)	(3)	(3)	(3)

Table 2.4: Time-based separation minima in seconds [23]

Leading AC	Trailing AC			
	Super	Heavy	Medium	Light
Super	-	120	180	180
Heavy	60	90	120	120
Medium	60	60	60	120
Light	60	60	60	60

2.2.4. Aircraft Mix & Sequencing

Based on the previous part it can be deduced that the aircraft mix has an influence on the capacity. Both the WTC as the operation type poses restrictions and regulations on the separation. Having an aircraft mix which has a high percentage of heavy aircraft will lead to bigger separation minima, decreasing the runway capacity. The type of operation is also an important factor. Generally, for the same mix of aircraft, more departures than arrivals can be operated during one hour.

For airports with multiple runways, usually runways are used for solely one operation type. ATC prefers this as it simplifies ATM operations but it may not be the most optimal form for capacity. Some airports mix operations on the same runway but it is necessary to have an ATM system that is advanced enough to sustain this mode for a longer period of time.

Finally, sequencing can have a positive effect on the runway capacity as well. As the normal order of handling the demand is the First-Come, First-Served (FCFS) principle, it can be efficient to switch some orders, decreasing the overall separation.

2.2.5. Meteorological Conditions

The local meteorological condition is the final factor to consider in runway capacity. Cloud ceiling and visibility are the two parameters of interest and determine the weather category at which the airport will operate. Situational awareness and visibility are directly linked and ICAO [22] defines two categories: i) Visual Meteorological Conditions (VMC) and ii) Instrument Meteorological Conditions (IMC). Under IMC the pilot needs to be able to navigate using solely its instruments, while under VMC detection equipment is not necessary. For these categories different rules are in place and are listed below.

- **Visual Flight Rules - (VFR)**

VFR is allowed under VMC. The visibility must be 5 *km* or more when flying below FL100 or 8 *km* when flying above FL100. Furthermore, separation with the clouds should be 1500 *m* horizontally and 300 *m* vertically.

- **Special Visual Flight Rules - (SVFR)**

If the visibility or cloud rules are not met, an exception can be given by ATC to operate a flight at SVFR.

- **Marginal VFR - (MVFR)**

When the visibility is between 3-5 miles and the ceiling of the clouds between 1,000-3,000 *ft*, operations can be performed under MVFR. MVFR is an advisory term and no clearance from ATC is needed.

- **Instrument Flight Rules - (IFR)**

When VFR conditions are violated, flights need to operate under IFR. This is for a visibility between 1-3 miles and a cloud ceiling between 500-1,000 *ft*.

- **Low Instrument Flight Rules - (LIFR)**

Under really bad weather LIFR can apply. This means that the visibility is less than a mile and clouds are less than 500 *ft* above the ground.

For the meteorological conditions also the current wind conditions should be taken into account. Operations are preferred with head-wind conditions as this increases the True Airspeed (TAS) and decreases the take-off roll. Runways are oriented in the prevailing wind conditions at an airport. For airports with changing wind conditions it is important to note that operations can only take place on runways where the crosswind conditions are acceptable. This factor has a negative impact on the runway capacity and should be taken into account at all times.

2.3. RECAT-EU Separation

With the introduction of the A380 the obsolescence of the ICAO WTC became apparent. The A380 should be assigned to the 'Heavy (H)' category as no upper MTOW limit was defined. However, with a MTOW that was more than 4 times the threshold and the fact that the vortices generated were far greater than any other aircraft, an update of the current categories was necessary. After extensive research and cooperation with the FAA and European Stakeholders [43] a new categorisation was developed. The original 3 groups were extended to 6 groups and not only MTOW is taken into account, but wingspan as well. These revised groups also led to new distance-based and time-based separation requirements which are shown in Table 2.5 and Table 2.6. Further investigation was also performed into the runway occupancy times and averages were found which can be used in models. Those results are presented in Table 2.7

Table 2.5: Distance-based separation minima in nmi based on RECAT-EU [43]

RECAT-EU Scheme		"Super Heavy"	"Upper Heavy"	"Lower Heavy"	"Upper Medium"	"Lower Medium"	"Light"
<i>Leader / Follower</i>		A	B	C	D	E	F
"Super Heavy"	A	3	4	5	5	6	8
"Upper Heavy"	B	(3)	3	4	4	5	7
"Lower Heavy"	C	(3)	(3)	3	3	4	6
"Upper Medium"	D	(3)	(3)	(3)	(3)	(3)	5
"Lower Medium"	E	(3)	(3)	(3)	(3)	(3)	4
"Light"	F	(3)	(3)	(3)	(3)	(3)	3

Table 2.6: Time-based separation minima in seconds based on RECAT-EU [43]

RECAT-EU Scheme		"Super Heavy"	"Upper Heavy"	"Lower Heavy"	"Upper Medium"	"Lower Medium"	"Light"
<i>Leader / Follower</i>		A	B	C	D	E	F
"Super Heavy"	A	(60)	100	120	140	160	180
"Upper Heavy"	B	(60)	(60)	(60)	100	120	140
"Lower Heavy"	C	(60)	(60)	(60)	80	100	120
"Upper Medium"	D	(60)	(60)	(60)	(60)	(60)	120
"Lower Medium"	E	(60)	(60)	(60)	(60)	(60)	100
"Light"	F	(60)	(60)	(60)	(60)	(60)	80

Table 2.7: Runway occupancy times in seconds based on weight category [43]

RECAT-EU Category	DROT	AROT
"Super Heavy"	51.7	47
"Upper Heavy"	50	47
"Lower Heavy"	50	45
"Upper Medium"	40	45
"Lower Medium"	35.3	45
"Light"	30	44

2.4. Capacity Modeling & Calculation

To gain deeper knowledge of and to provide insights in the runway capacity, different modeling techniques are used. These models can provide reasonable estimates of the runway capacity under given conditions. The first capacity model was constructed by Blumstein (1959) [9] using a single runway used only for arrivals. This section covers the inter-arrival and inter-departure times for single runway use.

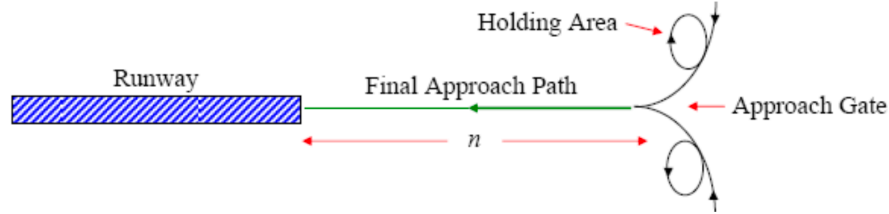


Figure 2.3: Situation for calculation of runway capacity in arrival mode[39]

2.4.1. Inter-Arrival Time

To calculate the minimum separation time between two consecutive arrivals on the same runway end, the inter-arrival time is used. Consider the situation depicted in Figure 2.3. The final approach path, indicated by n , is the final stage where different aircraft from different directions come together and line up for arrival. This path is typically between 5 and 8 nmi . Consider two aircraft i and j being the leading and trailing aircraft, respectively. Both have their own groundspeed indicated by V_i and V_j . The runway occupancy time of the leading aircraft is indicated by $AROT_i$. The longitudinal minimum separation is then defined by either ICAO WTC or RECAT-EU and is denoted as $s_{i,j}$. The goal is to determine the minimal acceptable time interval between arrivals, $T_{i,j}$. Two scenarios arise:

- **Closing or equivalent case** - $V_i \leq V_j$

The closing case occurs when the second aircraft has a higher or equal approach speed than the first aircraft. The separation at the approach gate needs to be larger than at the threshold as the minimum separation should be respected at all times. However, the first aircraft should have cleared the runway before the trailing aircraft is at the runway threshold. Therefore, the minimum required inter-arrival time is a maximum of two values, presented in Equation 2.5.

$$T_{i,j} = \max \left[\frac{s_{i,j}}{V_j}, AROT_i \right] \quad (2.5)$$

- **Opening case** - $V_i > V_j$

When the first aircraft has a faster approach speed the separation at the approach gate is the constraining factor. During the final approach path the separation will become larger. In this situation the $AROT_i$ should still be taken into account. The minimum required inter-arrival time is therefore a maximum function of those two values, presented in Equation 2.6.

$$T_{i,j} = \max \left[\frac{n + s_{i,j}}{V_j} - \frac{n}{V_i}, AROT_i \right] \quad (2.6)$$

Generally speaking, the required separation time is too strict in real-life situations as pilots and ATCo's tend to deviate from this exact value and mostly to the conservative side. Therefore, a buffer time is included to account for this. According to Roling [39] a buffer time of 10 seconds is sufficient.

2.4.2. Inter-Departure Time

To calculate the inter-departure time between consecutive departures only a single case need to be considered. The minimum time separation is the maximum of the time-based separation according to either ICAO WTC or RECAT-EU and the departure runway occupancy time, $DROT_i$. The calculation is presented in Equation 2.7. Again, a safety buffer is applied for the same reason as the arrival scenario.

$$T_{i,j} = \max [TBS_{ij}, DROT_i] \quad (2.7)$$

2.4.3. Maximum Throughput

To calculate the number of flights which can operate at a runway the maximum throughput capacity, μ , is used. As this number depends on the flight mix the expected value of the time interval is calculated first. This gives the average time interval between consecutive operations on the runway. Define $p_{i,j}$ as the probability that a pair occurs where aircraft i is followed by aircraft j . The average value of $T_{i,j}$ is then calculated according to Equation 2.8. The maximum throughput follows from Equation 2.9.

$$E[T_{i,j}] = \sum_{i=1}^k \sum_{j=1}^k p_{ij} \cdot T_{ij} \quad (2.8)$$

$$\mu = \frac{1}{E[T_{i,j}]} \quad (2.9)$$

2.5. Research on Runway Capacity Modeling

Over the years extensive research has been performed in the development of models for runway capacity. While the first models were analytic and rather simple, nowadays computer models can perform detailed analysis of every situation [37]. This gives decision makers better insights as to which action to take. In this section, the development of those different models is discussed. The first type of models are macroscopic and provide rough estimates of the capacity. The first models were developed decades ago, but still developments are made today. Macroscopic models are mostly analytic. Microscopic models on the other hand can provide runway capacity which is very accurate and detailed; tailored to a specific situation. Microscopic models make use of simulations to estimate the capacity. The trade-off between these types is the computing time. A mesoscopic model is the hybrid form which is also discussed. Furthermore, support tools which can help increase the runway capacity are discussed to get an extensive overview of what has been done in recent years.

2.5.1. Macroscopic Models

The first runway capacity model was developed by Blumstein in 1959 [9]. This simple model was constructed around the idea of calculating the capacity for a single runway with arrivals only. It formed the basis for a lot of models that followed. Blumstein constructed the model based on 5 assumptions [9][37]:

1. Aircraft land in order in which they arrive at the 'entry gate' (or approach gate)
2. Aircraft arrive at this gate independently and in a random sequence
3. Aircraft must maintain a minimum distance separation at the gate and a minimum time separation at the runway
4. The runway is used only for landing and is operating to capacity
5. Aircraft maintain a constant velocity from entry till runway.

Already then Blumstein concluded that the greatest improvements in runway capacity could be obtained through minimization of the separation requirements [9], something which is still researched today. Gilbo continued upon this model [19] and developed a model that was able to show multiple airport capacities under changing operating conditions and a method for allocating the airport resources between arrivals and departures for a given demand. He also developed the principal output which is still used today, the capacity envelope. Harris [20] made improvements by changing some of the parameters from constants to random variables. Taking into account the probability distribution for different parameters such as approach speed and runway occupancy times, the outcome became a better representation of the actual situation. Hockaday and Kanafani [21] developed the model further so that it could incorporate the strategy of "stretched" arrivals, which could improve the runway capacity.

The FAA constructed its own capacity model, called the FAA Airport Capacity Model (FAA-ACM). Starting in the early 1970s an preliminary version was created in collaboration with Peat, Marwick, Mitchell and Company (PMM&Co.) and McDonnell Douglas Automation (MCAUTO). Further development was done by the Systems Research and Development Service (SRDS) which is a branch of the FAA and which later was the basis for the FAA-ACM [15]. In 1981 they published their upgraded model in an advisory circular [47]. Together with the company MITRE they had developed a model which could now incorporate multiple different operations in a single run and added a number of different runway configurations. For complex airports consisting of numerous runways the user had to make use of combinations of consisting configurations which

could sometimes lead to a loss of dependencies. The FAA-ACM is able to calculate the capacity to a great extent and is still used today.

The LMI Capacity Model [15] is one of the models that incorporates the uncertainty factors of operations. The capacity model is able to compute the capacity of a single runway for different types of operation; arrivals only, departures only or mixed mode. Being both analytical as well as stochastic the LMI capacity model was one which could better predict the runway capacity. The model incorporates parameters such as speed and runway occupancy times but also communication between ATCos and pilots as random variables. The model computes 4 points on the capacity envelope and completes it by interpolating linearly between these points. The points are calculated as follows:

1. **All arrivals** - the capacity for the runway when only arrivals are handled.
2. **Free departures** - the point at which departures can be inserted given the same arrivals as point 1. This is done by filling in possible gaps between arrivals.
3. **Alternating** - this point is constructed when the mix of demand consist of as many arrivals as departures.
4. **All departures** - the capacity for the runway when only departures are handled.

The Approximate Network Delays (AND) [15] model is not so much a runway capacity model, but due to the fact that capacity plays an important factor it is mentioned here. The AND model is a network queuing model developed by the Massachusetts Institute of Technology (MIT) Operations Research Center together with the MITRE Corporation. AND is designed to analyse the impact of changes in schedules, volume and traffic on the delays of flights on a network level. AND operates with two main components at which it iterates between. A delay propagation algorithm is used to compute delays at each airport. A queuing engine is used to treat each airport as a M/E/1 queuing system within the network [36]. The DELAYS model is used to solve the differential equations that describe the distribution of delays over all airports. The DELAYS model assumes that demand is best approximated by a non-homogeneous Poisson process and that the service time per aircraft is approximated with a random variable. The AND model outputs a probability vector indicating the probability that an aircraft will be in the queue at a specific time at a specific airport. Based on this it can compute queue lengths, waiting times, total delays and delays above certain thresholds.

The MANTEA Capacity and Delay Model (MACAD) is a model that integrates several consisting models to analyse the runway capacity. As stated by Stamatopoulos [46], MACAD is able to consider parameters that influence capacity the most. Such parameters are airport geometry, operational characteristics, local air traffic management systems, airside and airfield access. One of the models that is integrated in MACAD is the LMI model described earlier. Also the DELAYS model is used to estimate the delays of the system. What makes MACAD unique is that it can compute the capacity of an airport in a short time. This makes it a very suitable tool for decision makers as changes in the system can be easily analysed.

2.5.2. Mesoscopic Models

Mesoscopic models are considered to be the hybrid form between macroscopic and microscopic models. It uses a simulation to arrive at its results, but by generalization of some parameters the simulation time is significantly reduced at the cost of less detail. One of the most significant models is the runwaySimulator [34]. Developed by MITRE, it is one of the first models that uses a Monte Carlo simulation to estimate the runway capacity. It is a combination of a trajectory model, airport and fleet characteristics and separation rules and is able to analyse complex interactions within the system. RunwaySimulator outputs a capacity curve for an airport considering a demand that is sufficient. The model can be used to evaluate effects on the capacity when parameters are changed (such as the fleet mix or certain regulations), but it can also be easily incorporated as inputs for other models. Koch et al. [34] did a validation of the model on six of the most delayed airports in the US. The output capacity curves were compared with the actual data and it was found that the results match up well and that the model is able to provide better insights in the trade-off between departures and arrivals. In another research performed by Kim and Hansen [1] the runwaySimulator and FAA-ACM were compared with two airports in the US. It was found that, although both models tend to overestimate capacity, the runwaySimulator provides more accurate runway capacities under a number of operating conditions.

2.5.3. Microscopic Models

Microscopic models use simulations to estimate the runway capacity. Simulations are more detailed compared to analytical models. This can be directly seen in the fact that simulations usually require a lot more inputs and can have very long simulation times. Some of the most used simulation models are discussed; the Airport Machine, SIMMOD, TAAM, HERMES and the Airport Business Suite.

The Airport Machine is able to simulate the entire area of an airfield. This includes taxiways and aprons as well. The Airport Machine has outputs of flows and throughput capacity as well as delays at different facilities at the airport. The structure is a node-link system and simulates all activities from a few minutes before landing until a few minutes after departure. The node-link structure considers aircraft travelling over the links, but two aircraft are not allowed to be on the same link at the same time. When this happens the model decides which aircraft goes first, based on input operating strategies. The other aircraft is then assigned a delay. The Airport Machine can have up to eight different aircraft types defined by the user, which has an effect of the output values. The Airport Machine is considered to be a thoroughly developed model, but users need to have a lot of training before being able to operate it. [15]

Closely related to the Airport Machine is the SIMMOD model. SIMMOD is also a node-link model and solves converging aircraft at the same link in the same way as the Airport Machine. SIMMOD has some more outputs which also include aircraft travel times and fuel consumption. Setting up a simulation in SIMMOD requires a lot of time as the whole airspace and airfield network need to be specified by the user. One can use a digitizer which can evaluate the entire airport layout from a map but it is considered that it still takes up to 2 days to get an accurate representation [15]. SIMMOD already has more aircraft types than the Airport Machine, making it possible for a more accurate representation. One of the perceived drawbacks of SIMMOD is that it requires a user with good understanding of ATM and airport operations. SIMMOD is a 1-D model which is not able to check for conflicts in vertical separation, so the user need to define the network accordingly. [37] [15]

The Total Airspace & Airport Modeller (TAAM) is very suitable for analysis of ATM concepts. TAAM is able to model entire air traffic systems in detail and covers the entire gate-to-gate ATM process [15]. The user needs to input an air traffic schedule, environmental descriptions, flight plans and regulations. TAAM is a 3-D model which makes it more complete when comparing it to SIMMOD. TAAM can output a number of parameters such as delays, airport movements, noise contours, fuel burn and also controller workloads. It is also possible to link TAAM with the FAA Integrated Noise Model (INM), which is explained in the next chapter. In the research performed by Bazargan et al. [33] a simulation is performed with different runway configurations to compare ultimate airport capacities using TAAM. In their research they summarize the capabilities of the model and findings of previous researches.

The Heuristic Runway Movement Event Simulation (HERMES) is a parallel runway capacity tool which can evaluate the capacity under current and future demand and is able to evaluate capacity changes due to technological or structural improvements of the runway. HERMES is found to be a very accurate tool with inaccuracies of 3-4 movements in a 24hr period [15]. A major shortcoming is that HERMES is specifically designed for two use-cases, London Heathrow and Gatwick, making it difficult to apply to other airports. Besides that, HERMES is not compatible for airports with crossing runways.

The Airport Business Suite (ABS) is a set of models developed by Delft University of Technology [51] and can be used in the Airport Strategic Exploration (ASE). ABS consist of 5 modules: i) a model for the calculation of the demand for an airport, ii) a model for the supply or available capacity, iii) a tool which matches demand and supply, iv) an airport turnover module and v) a financial tool for the calculation of investments and operational costs. The last two models later proved to be inconsistent and were removed, leaving only the first three models in the ABS. In 2008 Wijnen et al. published an article [41] stating the need for a decision support system (DSS) that integrates the collaboration between different stakeholders. They developed a conceptual design called HARMOS which is able to integrate the planning process in a multi-stakeholder context [41]. Continued development led to the addition of a runway allocation optimization model [45]. This model incorporated a noise module by means of the Integrated Noise Model (INM) and a third-party risk module developed by the UK National Air Traffic Service (NATS). Making use of a Multi-Integer Linear Program (MILP) the model is able to assign all flights to different runways at an airport.

Some shortcomings in the runway allocation model were resolved later on. Van der Klugt [49] used a discrete-event simulation model which was able to incorporate all factors influencing the runway capacity. Especially the dependency between runways in a complex runway layout were now considered. Delsen [12] was the first to develop an algorithm that assigns flights to runways based on a trade-off between noise emission and fuel burn. However, this algorithm was limited in the sense that it only considered two separation categories (Medium and Heavy). This was further optimized by Van der Meijden [50] by means of pair-wise flight dependencies. At this point the algorithm created by Delsen and Van der Meijden could be improved by incorporating the dependency rules as created by Van der Klugt.

2.5.4. Decision Support Tools

Next to models describing the runway capacity, resources are also put in the development of decision support tools which can help increase the efficiency of the whole system. These tools are mostly microscopic models describing one airport element. Mirkovic [6] summarizes a great number of tools. The first tools were developed for runway system capacity management. Arrival Managers (AMANs) and Departure Managers (DMANs) were developed to support sequencing and to prevent delays in queues (both in air and on ground). Later, Surface Managers (SMANs) and Turnaround Managers (TMANs) were developed to optimize the operations performed on the ground. The combination of AMAN and DMAN proved to be an useful tool for airports operating in mixed mode. The German Aerospace Center (DLR) developed the Complete Arrival Departure Manager (CADM) for this purpose. A lot more managers are present, but the general goal is to integrate all those in one single manager. The Total Airport Management (TAM) is the tool for this. Together with the concept of Collaborative Decision Making (CDM) in which the exchange of information between all stakeholders is handled, the decision support tools become bigger and more extensive. [6]

3

Noise Modeling

Starting from the 1970s the International Civil Aviation Organization (ICAO) published Annexes regarding noise emission and environment [26]. In this chapter aircraft noise is reviewed. First, in Section 3.1 the different sources of aircraft noise are considered. Second, in Section 3.2 noise metrics are presented to measure noise emissions. Multiple mitigation techniques and regulations are in place today which are reviewed in Section 3.3. Noise visualization can be a powerful tool to gain insights in noise annoyance in the vicinity of airports, this is discussed in Section 3.4. Finally, in Section 3.5 three different noise models are reviewed.

3.1. Aircraft Noise

Aircraft noise can be divided into 2 categories: engine noise and airframe noise. In the past, a lot of research and development was directed to decrease engine noise as this was the predominant source. Nowadays, engine noise has become more quiet, moving the objective for noise reduction also towards airframe noise. In this section both are analysed.

3.1.1. Engine Noise

Bertsch, Simons and Snellen [31] define 5 different components in the engine that contribute to engine noise. These are depicted in Figure 3.1. i) Fan noise is always present and depends mainly on the inlet geometry, the number of blades and vanes, the fan pressure ratio and the relative Tip Mach number. ii) Jet noise is mainly important under take-off conditions and can be observed at the back of the engine. Jet noise is dependent on velocity differences between air streams and research has proved that higher bypass ratios lead to both a lower jet noise and a lower fuel consumption [4] [13]. iii) Combustion noise is important during the approach phase and departure phase after thrust cutback. Combustion noise is driven by the pressure and temperature ratio and the fuel mix (lean or rich). Combustion noise is becoming the predominant source as other sources are effectively reduced. iv) Turbine noise is determined by the number of blades and vanes together with the Mach number and number of stages in the engine. v) Compressor noise is the last source which is predominant during the second stage.

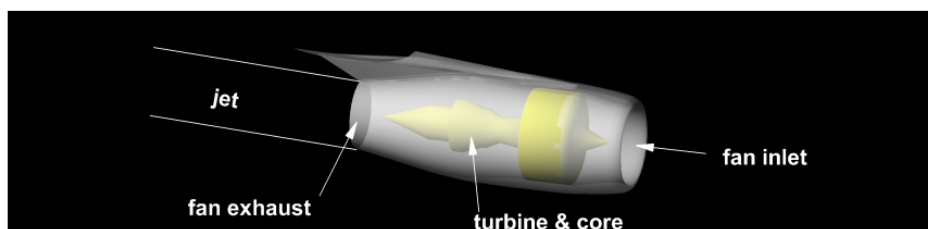


Figure 3.1: Different sources of engine noise [31]

3.1.2. Airframe Noise

The different sources of airframe noise are presented in Figure 3.2 and are defined by Bertsch, Simons and Snellen [31]. Airframe noise is mainly present during the approach phase as thrust settings are set to low or idle, making airframe the predominant source. i) The landing gear is considered to be one of the most dominant sources. During approach the landing gear is placed in turbulent airflow, causing broadband noise and tonal noise due to cavities in the structure. ii) Flaps and slats provide broadband noise due to turbulence in the gaps and side edges of the devices. iii) Lift and control devices such as the wing provide some noise, but these are not dominant noise sources. iv) Spoilers, speed brakes and Krueger devices are also small contributing factors.

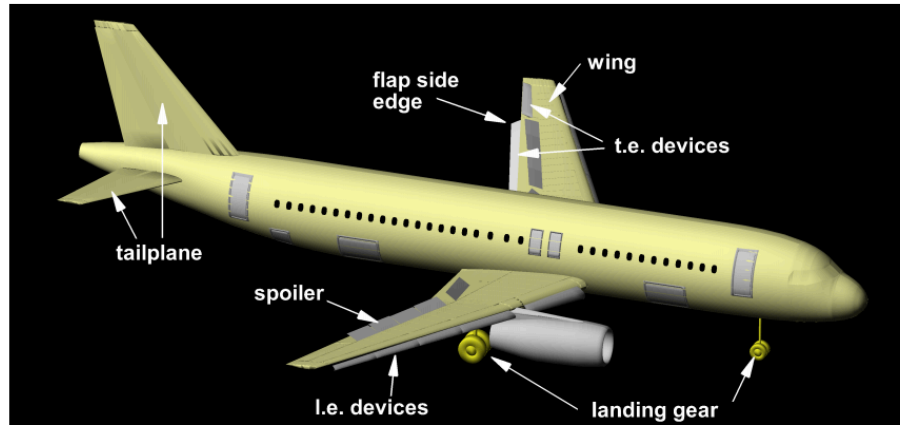


Figure 3.2: Different sources of airframe noise [31]

3.2. Noise Metrics

To define noise and how humans perceive it, several noise metrics are defined. In the first part of this section the perceived noise levels are discussed. In the second part, the effect of duration is analysed which is especially important for aircraft fly-over noise. The formulae presented are based on Ruijgrok [44] and Simons [13]. Finally, a metric is presented relating aircraft noise to annoyed people.

3.2.1. Noise Levels

The way sound is perceived by humans can be defined by the Sound Pressure Level (SPL) and is the ratio of the absolute sound pressure against a reference level of sound in the air [13]. The absolute pressure level is indicated by p_e with units Pa and is compared to the reference sound pressure, p_{e0} , with a value of $2.0 \times 10^{-5} \text{ N/m}^2$. The unit of the SPL is decibels (dB) and the equation is shown in Equation 3.1.

$$SPL = 10 \log \left(\frac{p_e^2(t)}{p_{e0}^2(t)} \right) \quad (3.1)$$

Loudness of a sound as perceived by humans is not only dependent on the SPL but also on the frequency [13]. Loudness levels of tones have been established and given the unit *phon*. The definition of a phon is described by Simons [13] as follows: "a tone (or narrowband noise) has a loudness level of X phons if it is equally loud as a tone with a SPL of X dB at 1 kHz". Phon levels range from 0 (threshold of hearing) till 120 (threshold of pain). The different contours are shown in Figure 3.3. An increase in loudness with 10 phons is perceived as twice as loud [13], for which another scale is developed: the "sone" scale. This is also shown in Figure 3.3. The relation between s and p is given with Equation 3.2 and Equation 3.3.

$$s = 2^{\frac{p-40}{10}} \quad (3.2)$$

$$p = 40 + 10^2 \log s = 40 + 33.3^{10} \log s \quad (3.3)$$

When considering aircraft noise, another metric is defined, the so-called perceived noise level. Noisiness curves were established by means of sound juries and their contours are shown in Figure 3.4. The unit in

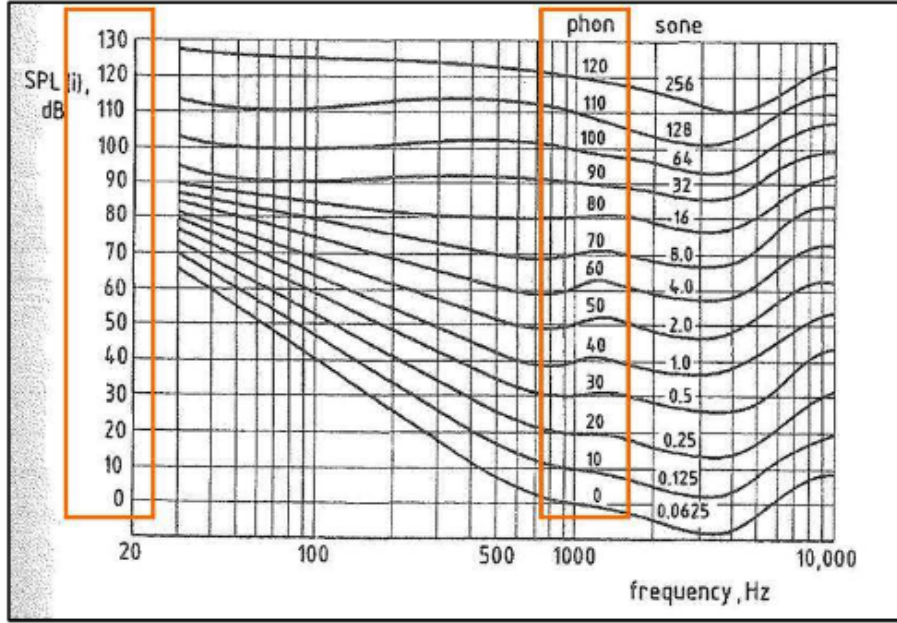


Figure 3.3: Equal loudness contours and corresponding phon and sone values [13]

which noisiness is measured is called the "noy". Overall noy values and perceived noise level (in PNdB) are given in Equation 3.4 and Equation 3.5, respectively.

$$N = n_{max} + F \left(\left(\sum_{i=1}^n n_i \right) - n_{max} \right) \quad (3.4)$$

$$L_{PN} = 40 + 33.3 \log N \quad (3.5)$$

To measure the loudness of a signal different frequency weighting filters can be applied which correspond to a certain loudness contour. Different weighting filters are present, labeled as A-, B-, C- or D-weighting filters. The most-used weighting filter is called A-weighting, which corresponds to a loudness contour at 40 phon. The overall A-weighted sound pressure level L_A is defined in Equation 3.6. The corrective factor ΔL_A is shown in Figure 3.5 and can be approximated with Equation 3.7 which is dependent on the frequency f [Hz] [44] [13].

$$L_A = 10 \log \sum_i 10^{\frac{SPL(i) + \Delta L_A(i)}{10}} \quad (3.6)$$

$$\Delta L_A = -145.528 + 98.262 \log(f) - 19.509 (\log(f))^2 + 0.975 (\log(f))^3 \quad (3.7)$$

3.2.2. Effect of Exposure

Aircraft fly-overs are considered to be non-stationary signals. This means that the duration of the signal should be taken into account somehow. Where the previous metrics are all defined for stationary signals, in this section new metrics are defined. The first is called the "equivalent A-weighted sound level" (EAL) and is a noise metric that integrates L_A over time, which is shown in Equation 3.8. The A-weighted sound is computed the same as Equation 3.6 [13].

$$L_{Aeq,T} = 10 \log \left[\frac{1}{T} \int_0^T 10^{\frac{L_A(t)}{10}} dt \right] \quad (3.8)$$

The integration time T is chosen such that it only covers the interval at which L_A is not less than 10 dBA below the value of $L_{A,max}$, called the 10 dBA down time. This value is chosen because only the highest levels of a non-stationary noise contribute to the integral.

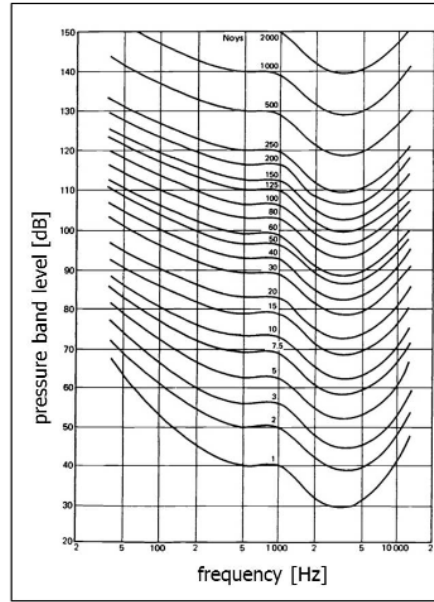


Figure 3.4: Equal noisiness contours in terms of frequency and pressure band [13]

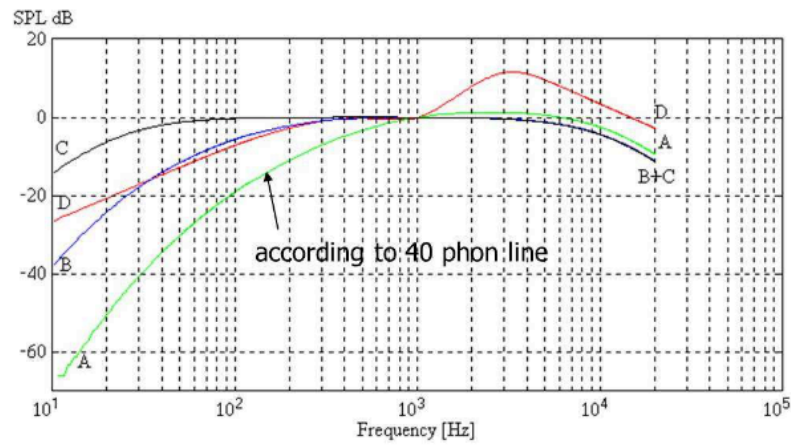


Figure 3.5: A-, B-, C- and D-weighting functions [13]

Removing the integration time and replacing it with a constant of $T_1 = 1$ s the sound exposure level (SEL) metric is defined. This is given in Equation 3.9 and also has units of dBA.

$$L_{AE} = 10 \log \left[\frac{1}{T_1} \int_0^T 10^{\frac{L_A(t)}{10}} dt \right] \quad (3.9)$$

In order to quantify noise impacts on communities in the vicinity of airports the "Day-Night average Level" (DNL) metric is defined. This metric can be used to show the noise dose for a 24-hour period. DNL applies weighting factors which are based on the time of day the noise event takes place, incorporating penalties for noise events happening at night. The equation is presented in Equation 3.10. The day time window is defined from 07.00 - 22.00h and the weighting factor is $w = 1$ (0 dB). The night window is from 22.00 - 07.00h with a weighting factor of $w = 10$ (10 dB).

$$L_{DN} = 10 \log \left[\frac{1}{86400} \int_0^{86400} w(t) 10^{\frac{L_A(t)}{10}} dt \right] \quad (3.10)$$

The Day-Evening-Night average level, L_{DEN} is defined in the same way, but divides a 24 hour period up into three parts. The extra evening window is from 19.00h - 22.00h and has a weighting factor of $w = 3$

(5 dB). When non-stationary events are considered (landings or take-offs) and the SEL values are known, Equation 3.9 can be redefined to Equation 3.11 [13].

$$L_{DN} = 10 \log \left[\frac{1}{86400} \sum_{i=1}^N 10^{(SEL_i + w_i)/10} \right] = -49.4 + 10 \log \left[\sum_{i=1}^N 10^{(SEL_i + w_i)/10} \right] \quad (3.11)$$

3.2.3. Noise Annoyance

Halperin [11] investigated the effects of sleep disturbance due to noise exposure. The World Health Organization (WHO) [53] [11] defines 7 different categories of negative health or social effects due to noise pollution. Ranging from hearing impairment to mental health issues and sleep disturbance. In his research Halperin concludes that sleep disturbance due to noise pollution from transportation can lead to higher stress levels, daytime sleepiness, annoyance, mood changes and overall well-being and cognitive performance. Sleep disturbance can already happen at noise levels as low as 48 dB [11]. Also day-time noise can lead to disturbance in the well-being of people and can have negative health effects. Noise disturbance, especially caused by aircraft, is therefore a major political and societal issue. Expansion of airports or airport operations in densely populated areas heavily regulated due to noise effects. Airports closely monitor noise annoyance of people in the vicinity. Amsterdam Airport Schiphol (AAS) for example has a committee, Bewoners Aansprekpunt Schiphol (BAS), which registers all noise complaints from residents and publishes this in an annual report. This report serves as guidance for the operations at AAS. [8]

The WHO investigated the relation between L_{DN} or L_{DEN} values and the percentage of highly annoyed (%HA) persons. This metric is used to indicate the effects of noise disturbance and is used throughout Europe, North-America and Australia. The WHO combined raw data from 54 countries in the aforementioned regions and found the relationship between L_{DEN} and %HA and is given in Equation 3.12. This value is specific for aircraft noise disturbance, as other relationships were found for other transportation means. [53]

$$\%HA = -9.199 \cdot 10^{-5} (L_{DEN} - 42)^3 + 3.932 \cdot 10^{-2} (L_{DEN} - 42)^2 + 0.2939 (L_{DEN} - 42) \quad (3.12)$$

3.3. Noise Mitigation & Regulation

In 2011 the International Civil Aviation Organization (ICAO) proposed their policy for noise procedures and how to cope with the growing noise pollution around airports. In their Balanced Approach to Aircraft Noise Management [26] they provide guidelines for the identification of noise and proposed four principal elements for the reduction of noise which are depicted in Figure 3.6. These elements are discussed in this section.

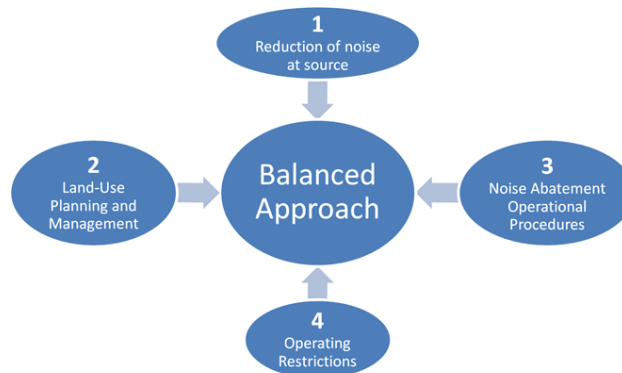


Figure 3.6: Four principal elements of the ICAO's Balanced Approach to Aircraft Noise Management [26]

3.3.1. Reduction of Noise at the Source

The first pillar is constructed to reduce the noise directly at the source. In the 1970s Standards and Recommended Practices (SARPs) were assembled in the "*Chicago Convention*" and contained noise limits for aircraft. Over the years those limits have become stricter and noise certification of aircraft is now an important

topic in the design of aircraft. In Annex 16 [28] noise provisions are stated and the primary purpose of this is to ensure the fact that the newest technology is incorporated in the design of aircraft. In the SARPs reference measurement points are defined at which noise certification is performed. These three points are at the approach, a sideline from the runway and a fly-over point. The certification is based on the MTOW of aircraft as heavier aircraft produce more noise than lighter ones and is documented in the so-called "Chapter 2 Noise Standard" [28]. Improvements in technology such as higher bypass ratio engines led to more stringent noise standards, documented in Chapter 3 and Chapter 4. In 2013 a new chapter was introduced, Chapter 14, which had even more stringent standards reducing the Effective Perceived Noise (EPNdB) with 7 with respect to the Chapter 4 level. The standards are shown in Figure 3.7. Every aircraft that is submitted for certification at or after December 31, 2017 must comply with these values. An example of a noise certification measurement is presented in Figure 3.8

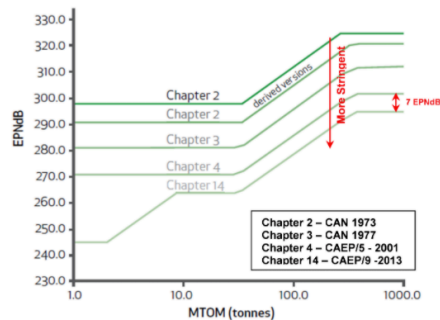


Figure 3.7: Progression of ICAO noise standards [26]

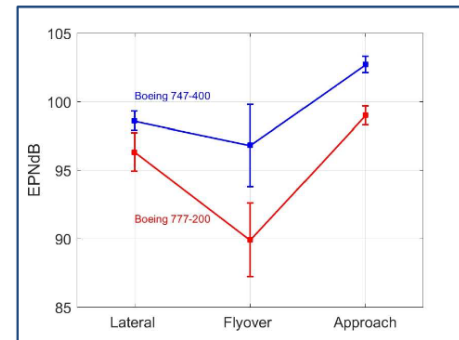


Figure 3.8: Noise certification for Boeing 747-400 and Boeing 777-200 [13]

3.3.2. Land-Use Planning and Management

The main objective of land-use planning and management is to ensure that the population surrounding airports has the least possible hindrance of noise. The main policies for land-use are provided by ICAO in "Assembly Resolution A39-1 Appendix F" and describe several preventive measures. One of those advices is for airports to enable user-friendly information on airport and aircraft operations for people living in the vicinity of the airport. Another measure advised by ICAO is to make use of so-called noise charges [27] as a way to manage noisy aircraft. Regardless of the fact that new-generation aircraft are becoming less noisy, it is still necessary for airports to apply noise alleviation or prevention measures. Noise charges could then be charged to the user, but it is recommended that the revenue is solely used for noise related costs.

3.3.3. Noise Abatement Operational Procedures

Aircraft operations have a large impact on the noise emission and how the noise is distributed in areas surrounding the airport. Airports, together with ICAO, developed low noise operational procedures which reduces the noise emission in the vicinity of the airport. Two possibilities that are widely used are the Noise Preferential Runways and Routes (NPRs) and Noise Abatement Procedures for both take-off and landing. In this remaining part the concept of those possibilities are analysed for both types of operation.

Departure Procedures

For departing aircraft two noise abatement departure procedures (NADPs) are developed and are identified as NADP-1 and NADP-2. NADP-1 is designed to mitigate noise emission in close vicinity of the airport, while NADP-2 is designed for noise mitigation further along the departure path [25]. NADP-1 can be considered as a three stage procedure. In the first stage, aircraft climb with a given speed ($V_2 + 15/20 kts$) to 800 ft above the airport. At 800 ft the departure will continue under normal procedures, but in the event of an engine-failure the transition to single-engine departure is initiated here. Otherwise the climb will be continued to 1500 ft at which the thrust will be reduced and the aircraft will climb to 3000 ft with this thrust setting. At the same time the speed is kept constant. At 3000 ft the pitch angle is decreased and the flaps are retracted. The climb speed will be initiated and NADP-1 is completed. [25] NADP-2 consist only of a single stage. At 800 ft the aircraft will reduce its thrust, retract the flaps and accelerate to climb speed. [25]

Noise Preferential Routes are also used to mitigate negative noise effects. This is done with the so-called Standard Instrument Departures (SIDs). SIDs are pre-specified routes which aircraft have to follow at order of ATC. Airports usually have multiple SIDs for different outbound directions. SIDs are defined up to the en-route flight segment.

Arrival Procedures

During the approach phase noise emission is also present. One of the procedures that can be used is the so-called Continuous Descent Approach (CDA). Conventional approaches involves step-wise descent until the runway is reached. CDA is a constant descent along a constant angle and causes both fuel reduction and noise reduction. CDAs are used mostly during night times as larger separation is necessary which is not optimal during day-time operations at busy airports.

NPRs are also constructed for arriving aircraft. These are called Standard Terminal Arrival Routes (STARs). STARs ensure that aircraft arriving from different directions are structured into specified airways leading to the runway. STARs could be constructed such that they circumvent densely populated areas and therefore mitigate noise pollution.

3.3.4. Operating Restrictions

The final pillar presented by ICAO has to do with operating restrictions. The restriction with the most impact was constructed around banning aircraft with certain noise certification by member States. In the 1980s this began by certain airports banning Non-Noise Certificated (NNC) aircraft. In the years following, Chapter 2 and eventually Chapter 3 aircraft were banned on some airports. Banning aircraft can have substantial economic impact on airlines and airports. The ICAO Assembly so far is able to reach an agreement every time between the States and airlines when such restrictions were proposed. The phase-out of noisy aircraft is not the only operating restriction that airports apply. In Chapter 7 of "*Doc 9829 Guidance on The Balanced Approach To Aircraft Noise Management*" other restrictions are presented such as curfews, night-time restrictions, quotas, cap-rules and restrictions to the nature of the flight [26].

3.4. Noise Visualization

Noise monitoring is becoming increasingly more important in the debate about noise pollution around airports. Amsterdam Airport Schiphol measures noise at 41 locations surrounding the airport [8] and evaluates with its stakeholders if the criteria were met. In the debate about noise pollution a visualization of noise contours could provide insights to all stakeholders involved and provides clear and understandable information. In this section two different types of visualization are presented: the noise contour and the noise grid.

3.4.1. Noise Contour

Noise contours are lines where some noise metric has a constant value. This can either be $L_{A,max}$ or SEL . Multiple contours in one plot are also possible, showing different values. In Figure 3.9 a typical contour is shown for an aircraft taking off. Different phases can be seen such as the take-off point and the thrust cutback point. In Figure 3.10 the noise contours of multiple events around AAS is shown. The runway layout is also shown and some of the characteristics of the single event figure can be observed.

3.4.2. Noise Grid

In the study performed by Delsen [12] another visualization technique is shown. An example of the noise grid is shown in Figure 3.11. While a noise grid is not that detailed with respect to a noise contour, it can provide fast information about locations where noise limits (as set by the user) are violated. In the noise grid shown, three different colors can be observed. Blue grid points indicate the presence of a certain population, green points indicate the area which is considered in an optimization and the red points indicate a violation of the set noise limit. The noise grid is especially useful for linear optimization problems as each gridpoint can easily be modeled by a single decision variable.

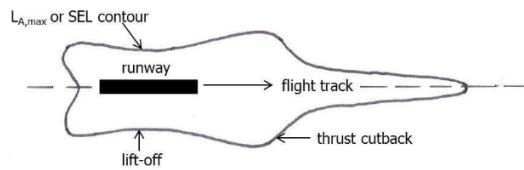


Figure 3.9: Noise contour of single aircraft take-off

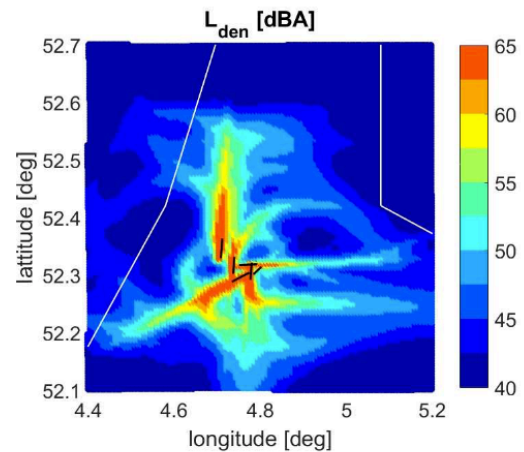
Figure 3.10: Noise contour Amsterdam Airport Schiphol for different L_{DEN} values

Figure 3.11: Noise grid of AAS [12]

3.5. Research on Noise Modeling

To better evaluate the impact of noise on populations research has been performed in the development of noise models. These models can be used for airport noise studies based on present day operations or for future developments of the runway system. In this section three major noise models are presented. The Integrated Noise Model (INM) which was designed by the Federal Aviation Administration (FAA), the Aviation Environmental Design Tool (AEDT) and the Dutch Aircraft Noise Model (NRM).

3.5.1. The Integrated Noise Model (INM)

In 2008 the FAA published the 7th version of the Integrated Noise Model (INM) [18]. The INM was developed out of the need for a model that could compute noise impacts in the vicinity of airports. For the noise computation the INM needs input about the airport conditions, the type of aircraft operating at the airport, the operational and geometry parameters and finally the type of metric to be calculated. The INM is able to output contours about exposure-based, maximum-level-based or time-based noise emissions. The INM is a very extensive model and requires a lot of input. The big advantage of this is that the user can analyse to a great detail a wide variety of airports and operations. The downside is that the set-up of a simulation can take up a lot of time. [18]

The INM needs the following airport inputs for an analysis. A reference point in longitude/latitude must be given and the runway locations relative to this point. Also elevation of the airport is needed. Meteorological conditions such as annual day temperature (Fahrenheit), relative humidity and annual barometric pressure are also needed as inputs from the user. Optionally terrain inputs can be used from other models

to account for terrain blocking in the noise calculation. Noise profiles can be calculated by the inputs about the SIDs and STARs. Along the flight path noise computations are performed, leading to the noise contours as seen in the previous section. [18]

The INM also needs aircraft data as inputs. Aircraft operation, type and number of operations for each of the three time periods (day, evening, night) are needed from the user. The three-dimensional flight path for an operation is also needed. The INM has a large database which can compute the Noise vs Power vs Distance (NPD) values for a large variety of aircraft. [18]

3.5.2. The Aviation Environmental Design Tool (AEDT)

The successor of the INM is the Aviation Environmental Design Tool (AEDT) and is the current calculation tool of the FAA since 2015. The AEDT can be considered as a model which combines several consisting models into one and is able to provide full "gate-to-gate" analysis ranging from a single flight till a full scale global level. The INM and also the Emissions and Dispersion Modeling System (EDMS) are incorporated in the AEDT. The AEDT has three databases which makes the model user friendly. The amount of data that is specified by the user is reduced as the user now has access to all databases with information. The three databases are: i) an airport database with detailed information about different aspects of the airports. This ranges from runway information, taxi-systems as well as route information. ii) a fleet database where extensive information about almost all aircraft types and engines can be found. This data is retrieved from the Base of Aircraft Data (BADA), which will be explained in the next chapter. Finally, iii) there is a movements database for various operations and trajectories such as the noise preferential routes and procedures explained before. [48]

3.5.3. The Dutch Aircraft Noise Model (NRM)

The last model considered is specific for Amsterdam Airport Schiphol and is called the Dutch Aircraft Noise model or *Nederlands Rekenmodel (NRM)*. It uses different tables containing data to compute noise calculations. First a classification of aircraft types into classes is performed. These classes are based on MTOW and divided into nine categories. Each category is then linked to one of four noise categories based on ICAO's certification procedure. This leads to a total of 36 different classes and each class has its own representative aircraft type. Then flight profiles and NPD tables are formed and a combination can be formed with the type of aircraft, depending on the operation to be performed. Flight procedures are divided into three categories: start, landing and circuit with each its own set of characteristic procedures. Finally, NPD data is used for different aircraft which can output the overall A-weighted sound pressure levels to determine the noise created by an aircraft. For various thrust settings the L_A values can then be computed. [13]

4

Fuel Burn Modeling

The final subject of the literature review is about aircraft fuel burn. This chapter is rather short with respect to the previous chapters because fuel models will not be considered in this research, but rather a fuel burn calculation method is presented. In Section 4.1 the airline cost structure is presented to underline the importance of fuel cost. The fuel trend is an important parameter to take into account and this is reviewed in Section 4.2. The fuel burn calculation method is based on earlier research performed by Delsen and Van Der Meijden [12] [50] and an overview of this method is given in Section 4.3. Finally, the parameters necessary for the calculation of fuel burn are obtained from an aircraft database which is presented in Section 4.4.

4.1. Airline Cost Structure

To get an understanding of the importance of fuel cost, the cost structure of an airline is analysed first. In Figure 4.1 this cost breakdown is shown. According to Doganis [14] and Belobaba [7] the Total Cost (TC) can be subdivided into non-operating cost (NOC) and total operating cost (TOC). Non-operating cost can be any such cost that has no connection to the operation of the fleet. Interest is an example of NOC. The TOC can be subdivided into indirect operating cost (IOC) and direct operating cost (DOC). For IOC one could think of station and ground expenses (which are not identifiable to a specific flight), passenger services and promotions. The DOC is divided into fixed direct operating cost (FDOC) and variable direct operating cost (VDOC). VDOC are cost which are flight dependent and fuel is assigned to this category. According to Doganis and Belobaba [14] [7] fuel cost can make up 25% of the VDOC. A reduction therefore in fuel usage has a direct positive effect on the airline cost structure.

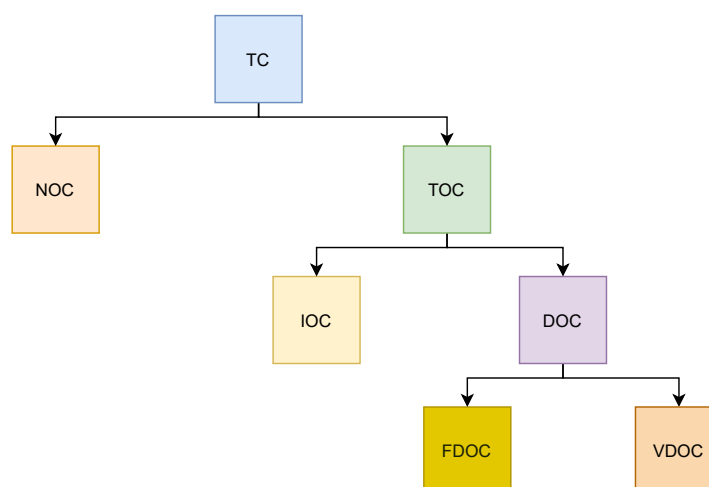


Figure 4.1: Airline cost breakdown [50]

4.2. Fuel Trend

Fuel cost is driven by two factors. The first being the fuel efficiency and is determined by the type of engine. Newer engines are more efficient, lowering the fuel used during operations and hence the fuel cost. The second factor is the fuel price. Over the years fuel prices of Jet-A fuel varied as can be seen in Figure 4.2. Large fluctuations in the fuel price makes strategic planning difficult. For instance, the fuel price in the 2010s is a level 6 times higher than in the 1990s. Fuel prices are related to the oil price and geopolitical events have huge impact on the price [42]. In a study performed by Mordor Intelligence the compound annual growth rate (CAGR) for the jet fuel market is expected to be around 11% for the period 2020-2025 (with base year 2019). Increasing passenger traffic, more Low-Cost Carriers (LCC) and an increasing demand for air cargo is expected to be the main drivers for this growth. The market is consolidated and typically 5 major companies are supplying jet fuel. Although factors such as the recent covid-19 crisis heavily influence the demand, the overall growth is still expected. The growth of the jet fuel market is inherently linked to the jet fuel price and a growing market could lead to an increase in the price as well. [35]



Figure 4.2: Fuel prices 1990-2019 [42]

To avoid risks of certain surges in jet fuel prices, some airlines lock in their fuel prices by means of fuel hedging. For a certain period of time (week, month or year) the price of jet fuel is fixed. If jet fuel prices then rise the fixed price is still paid. However, the downside of this could happen when fuel prices drop and the fixed price still has to be paid. Fuel pricing is done especially when airlines predict a rising price. Due to the Corona virus oil prices experienced a large drop which is very unfavorable for some airlines as expressed in the article by Horton [52].

4.3. Fuel Burn Modeling

Fuel calculation is done according to the method introduced by Delsen [12] in 2016. For the runway allocation model to incorporate the fuel dependency, an accurate representation of the fuel cost must be implemented. To calculate fuel burn different segments of the flight path are constructed and for each segment the fuel burn can be calculated based on the distance flown (D), the fuel flow mass rate (\dot{m}_f) and the True Airspeed (V_{TAS}). The calculation for the Total Fuel Used (TFU) is given in Equation 4.1. The summation is over all segments in the considered path. For an arriving flight these segments consist of a part from the Initial Approach Fix (IAF) to the Final Approach Fix (FAF), from the FAF to the runway and the taxi operation from the runway to the gate. For departing aircraft the taxi distance is taken first and the second segment is from take-off to the first waypoint indicator on the standard instrument departure (SID). For accurate modeling it is necessary to have distances for all these segments. The allocation model considers a constant airspeed during a segment. This assumption is true for most controlled regions around airports as the speed is determined by ATC. Fuel flow is dependent on the type of engine used, the number of engines, the thrust production and the age of the engines. As stated by Delsen it can be assumed that during a segment the fuel flow of an aircraft remains constant. The fuel flow can be calculated with the Thrust Specific Fuel Consumption (TSFC) and the thrust setting (T).

$$TFU = \sum_{s \in S} \frac{D \cdot \dot{m}_f}{V_{TAS}} \quad (4.1)$$

4.4. Base of Aircraft Data (BADA)

Because fuel consumption during different stages is aircraft dependent, a detailed analysis is needed to accurately represent fuel burn in the runway allocation model. To do this, use can be made of the Base of Aircraft Data (BADA). BADA is a database providing a set of data files in ASCII language and has information about performance and operation. Coefficients for thrust setting, fuel flow and drag calculation as well as nominal speeds in climb, cruise or descent can be found for 318 different aircraft types. BADA is constructed around the idea of the Total Energy Model [2] and the BADA Family 3 covers more than 95% of the aircraft which are operated in the European area.

For a jet aircraft the mass fuel flow, \dot{m}_f , is calculated with Equation 4.2. Where C_T is an aircraft specific parameter and T_{hr} is dependent on the operating segment considered.

$$\dot{m}_f = C_T \cdot T_{hr} \quad (4.2)$$

For each segment the thrust specific fuel consumption, C_T , can be calculated using Equation 4.3 [17]. The unit is $\frac{kg}{min \cdot kN}$ and C_{f1} and C_{f2} are coefficients which are aircraft specific and obtained from BADA. The True Airspeed changes per segment and is regulated by ATC.

$$C_T = C_{f1} \times \left(1 + \frac{V_{TAS}}{C_{f2}} \right) \quad (4.3)$$

To calculate the thrust for each segment, BADA uses a maximum thrust setting which is multiplied by coefficients for the segment considered. The maximum thrust calculation is shown in Equation 4.4 where $C_{Tc,1}$, $C_{Tc,2}$ and $C_{Tc,3}$ are aircraft specific coefficients and H_P is the geopotential altitude.

$$T_{hr,max} = C_{Tc,1} \cdot \left(1 - \frac{H_P}{C_{Tc,2}} + C_{Tc,3} \cdot H_P^2 \right) \quad (4.4)$$

Furthermore, during the modeling phase of fuel burn some considerations are made. It is assumed that fuel flow during a segment is constant by taking the average altitude. For taxi operations it is assumed that the thrust used is 7% of the maximum engine thrust [30]. The runway allocation model is able to assign delay to certain flights if this is favorable for the whole system. Delay comes at the cost of extra fuel burn and so this is modeled as well. In this research, and previous research as well, it is assumed that delay can be assigned to flights at the IAF (arrival) or during taxi operations (departure). For these locations the fuel burn can be calculated with units kg/s . It is also assumed that extra delay does not come at the cost of extra noise disturbance. When delay is assigned to arrival flights the height at which this occurs is such that the extra noise is negligible on the ground. For noise at the ground the gridpoints at the airport will always be violated, and therefore extra modeling for delay is not necessary.

III

Supporting work

Note: This part serves as a substantiation of the claims made in the scientific paper

5

Previous Work

The newly developed Flexible Runway Scheduling Model (FRSM) is an improvement and combination of earlier research performed by Delsen [12], Van Der Meijden [50] and Van Der Klugt [49]. This chapter presents an overview of the work performed by those authors to place the current work in perspective. For a detailed analysis the reader is referred to their publications. The structure of this chapter is as follows. The Flexible Runway Allocation Model (FRAM) is presented in Section 5.1 and the runway dependency calculations are presented in Section 5.2.

5.1. Flexible Runway Allocation Model

The first two versions of the model are allocation models and are constructed differently with respect to the newly developed FRSM. As the models from Delsen [12] and Van Der Meijden [50] are closely related, only the last version is presented here. First the objective function is presented and its decision variables. Second, the constraints are given and evaluated. Finally, some improvement areas are shown and compared to the new FRSM.

5.1.1. Objective Function

The objective function of the FRAM is a multi-objective minimization problem with two objectives, fuel burn and noise emission. The overall measure of performance is indicated by Z . Fuel burn characteristics are determined and these are proposed as costs for the airline. Noise annoyance is determined for the residents living in the vicinity of an airport who experience noise caused by departing or arriving flights. The objective function is presented in Equation 5.1.

$$\text{minimize } Z = \alpha \cdot n_f \sum_{f \in F} \sum_{r \in R} \sum_{d \in D} C_{f,r,d}^F \cdot x_{f,r,d} + \beta \cdot n_n \sum_{xy \in P} C_{xy}^G \cdot g_{xy} \quad (5.1)$$

The first part of the objective function is the fuel burn objective. The decision variable is defined in Equation 5.2 and it can be observed that it is a binary variable. The fuel burn decision variable has three types of information. The flight number, f , the allocated runway, r , and the operation time including possible delay steps, d . The operation window in this optimization is divided into segments of 20 seconds starting at 00.00h.

$$x_{f,r,d} = \begin{cases} 1 & \text{if yes} \\ 0 & \text{if no} \end{cases} \quad (5.2)$$

The cost variable related to fuel burn is presented in Equation 5.3. The cost coefficient is specific for each flight, runway and operating time (which includes delay). This is calculated using a pre-processor which analyses the flight schedule beforehand.

$$C_{f,r,d}^F = TFU_{f,r,d} \quad (5.3)$$

The second part of the objective function is the noise annoyance objective. This decision variable is shown in Equation 5.4. This decision variable has binary states as well and indicates whether or not a user-defined

noise limit is violated. In the research performed, these decision variables present the grid measurement points which had a spacial resolution of $1 km^2$.

$$g_{xy} = \begin{cases} 1 & \text{if yes} \\ 0 & \text{if no} \end{cases} \quad (5.4)$$

The cost variable related to noise annoyance is the population living at a gridpoint and is presented in Equation 5.5. For this cost variable a distinction can be made between households or population, depending on the preference of the user. The population data need to be obtained from local sources.

$$C_{xy}^G = POP_{xy} \quad (5.5)$$

It can be furthermore noted that a normalization is applied for fuel and noise to ensure that the ranges of both objectives are in the same margin. Furthermore, weights are applied by means of α and β to define the importance of both objectives with respect to each other.

5.1.2. Constraints

The constraints are presented in Equation 5.6 to Equation 5.9. All flights should be assigned to one runway at one operational time step with an optional accompanying delay. This is shown in Equation 5.6. To implement the possibility of closed runway operations, for instance due to maintenance or because of the absence taxi ways, Equation 5.7 is constructed. Separation between flights is ensured with Equation 5.8. A dependency matrix, $n_{f,r,d}^{DM}$, is constructed for the separation between consecutive flights within a certain operating window on runways that are conflicted with this operation. Finally, in Equation 5.9 the noise limit switching constraint is introduced. By means of the big-M method the indicator constraint is activated at a high penalty to ensure the constraint is satisfied.

$$\sum_{r \in R} \sum_{d \in D} x_{f,r,d} = 1 \quad \forall f \in F \quad (5.6)$$

$$\sum_{f \in F} \sum_{d \in D} x_{f,r,d} = 0 \quad \forall r \in R_{\text{closed}} \quad (5.7)$$

$$\sum_{f \in F} \sum_{d \in D} n_{f,r,d}^{DM} \cdot x_{f,r,d} \leq 1 \quad \forall r \in R_{\text{conflict}} \quad \forall t \in T \quad (5.8)$$

$$\sum_{f \in F} \sum_{r \in R} \sum_{d \in D} C_{xy(f,r,d)}^G \cdot x(f,r,d) - M \cdot g_{xy} \leq L_{\text{limit}} \quad \forall xy \in G \quad (5.9)$$

5.1.3. Improvement Areas

From the research performed by Delsen [12] and Van Der Meijden [50] and from the research performed in this report several improvement areas are determined to incorporate in the FRSM. The first improvement to be made has to do with the allocation of delay. In the FRAM the operating time and assigned delay is divided into segments of 20 seconds and is captured in one and the same decision variable. This discrete representation has the disadvantage that accuracy is lost. Runway capacity can be severely impacted with this discretization as minimum delays are always rounded up to the nearest 20 seconds. By changing the model to have continuous operating windows and delays the accuracy of the model will improve. Another advantage is the fact that the model will never become infeasible as endless delays are possible to solve the problem.

Another improvement can be made in the separation constraint. The FRAM considers a dependency matrix with discrete time steps between runways in conflict with each other. These matrices have to be constructed for every possible flight combination within the runway system and do not provide an easy possibility to apply the model to other airports. By changing the separation constraint to implement the operating time a more accurate separation can be provided.

5.2. Runway Dependencies for Complex Runways

In the work done by Van Der Klugt [49] research is performed for the modeling of dependencies between runways in complex runway systems. Multiple different dependencies are defined and equations are constructed to calculate the minimum required separation time between operations. In this section only the dependencies between different runways are considered. Separation requirements on the same runway are analysed

in the literature review. For opposite direction operations equations used by Van Der Meijden [50] are presented. This section is divided into four parts. The first part is about operations on converging & diverging runways. The second part is for separation requirements on intersecting runways. The third part provides an overview for operations on parallel runways. The final part is for the opposite direction operations. Ground operations are not considered in this research and therefore not stated here.

5.2.1. Converging & Diverging Runways

Converging or diverging runways are those which are oriented such that their centerlines intersect at some point. There are three types of dependencies which arise for this combination. The jet blast and wake turbulence on the ground and the missed approach path in the air. In this part the dependencies which arise for the different operating combinations (AA, DD, AD and DA) are presented.

The first situation is shown in Figure 5.1. Two departures are scheduled on diverging runways and the jet blast and wake turbulence caused by one aircraft creates a dependency on the other runway. For the situation in Figure 5.1a the minimum time between the start of the departure on runway 2 and the start on runway 1 is defined in Equation 5.10. The time to the intersection point, $R_{D2,int}$, is given as a percentage of the departure runway occupancy time. The line-up time, $t_{D1,lu}$, is dependent on the weight class of the aircraft. A communication buffer, \bar{c}_{D1} , is applied of 10 seconds in all cases.

The second scenario, depicted in Figure 5.1b, is similar only that the aircraft on runway 2 can already be lined up. Furthermore, the clearance point, $R_{D1,cl}$, is a significant smaller time as jet blast of a departing aircraft at the beginning of the take-off roll is small.

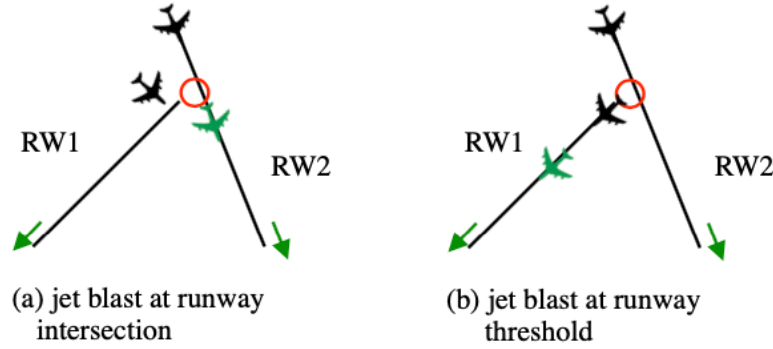


Figure 5.1: Jet blast and wake turbulence between two departures on diverging runways [49]

$$\Delta t_{\min} = R_{D2,int} + t_{D1,lu} + \bar{c}_{D1} \quad (5.10)$$

$$\Delta t_{\min} = R_{D1,cl} + \bar{c}_{D2} \quad (5.11)$$

When an departure and arrival are scheduled at two runways one has to take into account the jet blast, wake turbulence and missed approach path of the arrival. The first situation is shown in Figure 5.2. When the departure is scheduled first, as shown in Figure 5.2a the arriving flight must be at a specified distance from the runway threshold. The minimum time separation is then calculated with Equation 5.12, where V_{A2} is the approach speed of the arriving aircraft.

If the scenario is reversed, and the arrival is scheduled first, the departing flight can start the line-up after the arriving flight has cleared the intersection point as depicted in Figure 5.2b. The corresponding equation is shown in Equation 5.13, where $R_{A2,int}$ is again indicated as a percentage of the arrival runway occupancy time.

$$\Delta t_{\min} = \frac{D_{min}}{V_{A2}} - \bar{c}_{D1} \quad (5.12)$$

$$\Delta t_{\min} = R_{A2,int} + t_{D1,lu} + \bar{c}_{D1} \quad (5.13)$$

Another dependency arises for converging runways and the missed approach path of an arrival. This is shown in Figure 5.3. If the departure is scheduled first, the minimum separation with the arrival is given

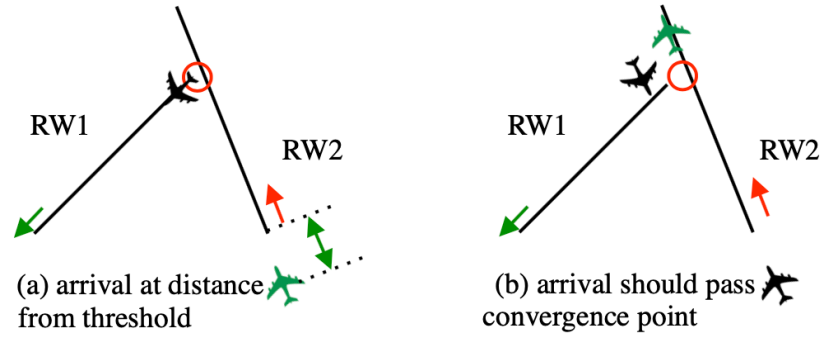


Figure 5.2: Jet blast and wake turbulence between a departure and arrival on converging/diverging runways [49]

with Equation 5.14. The minimum distance is not the same as in Equation 5.12. If the arrival is scheduled first, the departing aircraft can start its take-off roll after a certain time which is given by Equation 5.15. The completion time, $R_{A2,com}$, is the ROT time after touch-down and can be a full completion or only part of the completion. If it can be made sure that the missed approach path separation is not needed, earlier clearance can be given.

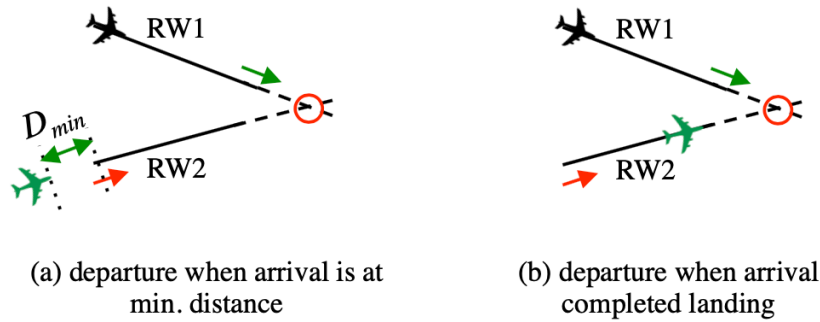


Figure 5.3: Missed approach path intersects with departure path [49]

$$\Delta t_{\min} = \frac{D_{\min}}{V_{A2}} - \bar{c}_{D1} \quad (5.14)$$

$$\Delta t_{\min} = R_{A2,com} + \bar{c}_{D1} \quad (5.15)$$

The final dependency for converging/diverging runways is between two consecutive arrivals. This situation is shown in Figure 5.4. For that operation the intersection of the missed approach path must be considered and a staggering distance is applied between the arrivals. The minimum time separation is given in Equation 5.16.

$$\Delta t_{\min} = \frac{D_{st}}{V_{A2}} \quad (5.16)$$

5.2.2. Intersecting Runways

For intersecting runways similarities arise with converging/diverging runways. The difference is that the intersection point is now at the runway and not on a projected path. The same operation combinations need to be examined.

If two consecutive operations are performed the location of the intersection point is of importance. If the intersection is located closest to the starting point, Equation 5.17 is used to determine the time separation for two consecutive departures. In this equation, $R_{D1,int}$ is calculated as a percentage of the departure ROT

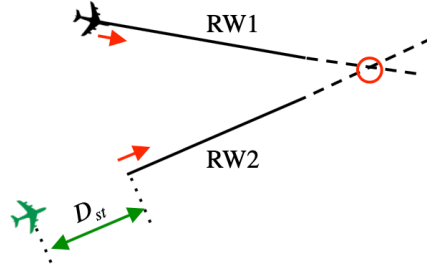


Figure 5.4: Intersecting Missed Approach Paths of two arrivals [49]

with respect to the location of the intersection point. If the location of the intersection is located at the far end of the runways an increased inter-departure separation, $G_{i,j}$, is introduced. The separation is then given in Equation 5.18.

$$\Delta t_{\min} = R_{D1, \text{int}} + \bar{c}_{D2} \quad (5.17)$$

$$\Delta t_{\min} = G_{i,j} + \bar{c}_{D2} \quad (5.18)$$

When a departure is followed by an arrival, the arrival should be at a minimum distance from the runway, D_{\min} , and to minimise the risk of a missed approach procedure the arrival should be at or before the missed approach distance, D_{MAP} , before the departure has cleared the intersection. This maximum function is displayed in Equation 5.19. If the procedure is in the opposite direction, the departure can take-off after clearance of the intersection point by the arriving aircraft. This is given in Equation 5.20.

$$\Delta t_{\min} = \max\left(\frac{D_{\min}}{V_{A2}} - \bar{c}_{D1}, \frac{D_{MAP}}{V_{A2}} + R_{D1, \text{int}}\right) \quad (5.19)$$

$$\Delta t_{\min} = R_{A2, \text{int}} + \bar{c}_{D1} \quad (5.20)$$

The separation for the final combination, two arrivals, is resolved by the same separation equation as for the converging and diverging scenario, Equation 5.16. It can be noted that the location of the intersection point has an influence of the applied staggering distance. This distance will be greater if the intersection is located at the far end of the runway.

5.2.3. Parallel Runways

For operations on parallel runways the separation between centerlines is of importance as is stated in the literature review. The exact rules for the different operations are stated in Table 2.1. If the centerlines are less than 2500 *ft* the runways are considered as a single runway for two consecutive arrivals, departures or a departure followed by an arrival. For these separation times the normal inter-departure and inter-arrival times can be used. When an arrival is followed by a departure the operation can start after touchdown.

When the distance between the centerlines is less than 4300 *ft* a 1.5 *nmi* direct separation must be applied for two consecutive arrivals. To calculate the in-trail separation Equation 5.21 can be used and replaced for $s_{i,j}$ to calculate the separation time.

$$S_p = \sqrt{D_{dia}^2 - s^2} \quad (5.21)$$

5.2.4. Opposite Direction Operations

The final dependency which should be considered is the opposite direction operation dependency. When operations are performed on the same runway but on opposite runway ends, different separation requirements are necessary. The four possibilities are depicted in Figure 5.5. For two opposite arrivals a separation should be implemented where a missed approach procedure by the first aircraft does not affect the second aircraft. If a missed approach procedure is initiated, the second aircraft must be vectored away from the runway which is only possible above a certain Minimum Vectoring Altitude (MVA). This MVA is not dependent on

the weight class but on local regulations. The separation is then determined with the Rate of Descent (ROD) of the aircraft and shown in Equation 5.22.

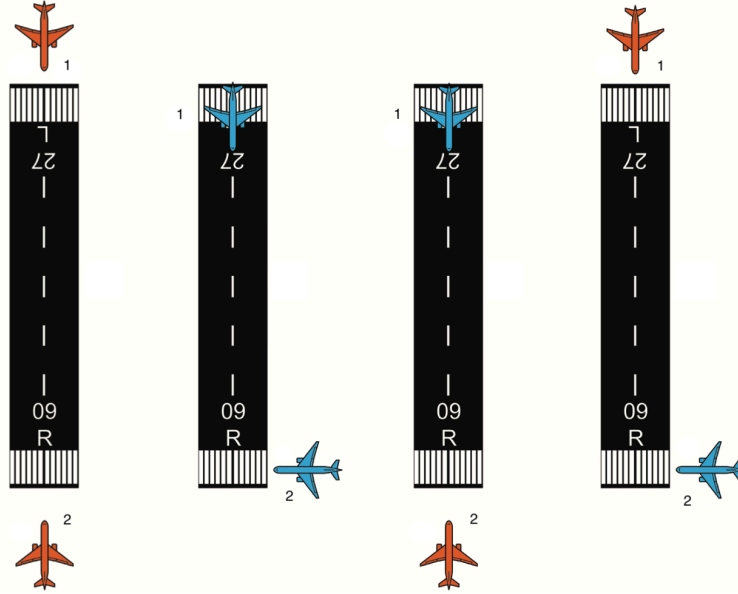


Figure 5.5: Opposite Direction Operations on the same runway [50]. The order of operation is indicated with numbers.

$$T_{ij} = \frac{MVA}{ROD} + c \quad (5.22)$$

For two opposite departures the separation between them is determined by the runway occupancy time of the first departure. This is given in Equation 5.23. No communication buffer is necessary as the second aircraft is given clearance based on visual inspection of the runway and can therefore be determined by the pilot itself.

$$T_{ij} = DROT_i \quad (5.23)$$

For a departure followed by an arrival, as depicted in the third figure from the left, the largest separation is necessary. The departing aircraft should be vectored away from the runway centerline, which is only possible at or above the MVA. The arriving aircraft should also be at the MVA and the departure should be completed as well. Therefore, the total separation for this combination is stated in Equation 5.24.

$$T_{ij} = \frac{MVA}{ROD} + DROT_i + \frac{MVA}{ROC} \quad (5.24)$$

The final combination is an arrival followed by a departure. The arrival runway occupancy time suffices for the minimum separation between this operation. This equation is stated in Equation 5.25.

$$T_{ij} = AROT_i \quad (5.25)$$

6

Flexible Runway Scheduling Model

This chapter serves as a guide for the flexible runway scheduling model to gain an understanding of its processors and flows. In Section 6.1 the top-level architecture of the model is explained and elaborated upon further with respect to the scientific paper. In Section 6.2 the algorithms developed for the pre-processors are presented and explained. Finally, in Section 6.3 some additional remarks about the optimization tool are given.

6.1. Model Architecture

An overview of the model architecture is presented in Figure 6.1. The main structure of the model is presented in blue where the different systems are present. A single run starts with input by the user. This input is related to the simulation to be performed and to the situation which is analysed. For simulation parameters some inputs are: the objective weights and their range, the time period of optimization, the noise limit and the specified window (SW). For situation parameters some inputs are: the number of runways and which are closed for operation and the normalization parameters.

Further input requires a flight schedule with information about the ETA/ETD, O/D data, SID/IAF data, aircraft type data and gate/pier/terminal data. If only O/D data is present, the user needs to define SID/IAF procedures for every flight. Based on the aircraft type data different weight classes can be determined as well as the noise profiles for these types.

Fuel profiles are obtained through BADA and require information of the different aircraft considered. Furthermore, operating altitudes are necessary for the calculation of thrust parameters which are necessary for fuel calculations. Finally, distances between several locations are necessary. These are ground and air distances.

Noise profiles are obtained through AEDT. After determination of the aircraft types and the noise preferential routes the AEDT can be set-up to create profiles for every combination for every flight. The measurement grid is defined at this step by the user and population data should coincide with the measurement points.

Finally, the separation regulations need to be determined by the user. The first step is to determine the separation scheme and corresponding weight classes. The second step is then determining dependencies between the runways.

The input data is first pre-processed. This is explained in the next section. After this, the linear problem is formed with the objective function and constraints as described in the scientific paper. The CPLEX Optimizer writes an LP file which can be used to re-examine the analysed problem. After the problem is solved, the program writes two files; a MIP file and SOL file. This is explained in the final section of this chapter.

The post-processor returns the solved output into results which can be examined. The linear problem translates all inputs to a list of numbered decision variables and the information is not accessible right away. The output consist of a flight allocation scheme where the number of flights per runway is visible. Together with a timetable, the number of operations can be analysed for the period of time considered. A noise grid is presented to examine the places where the noise limit is violated. Finally, other data is processed such as the delay per flight, the total fuel and the people exposed.

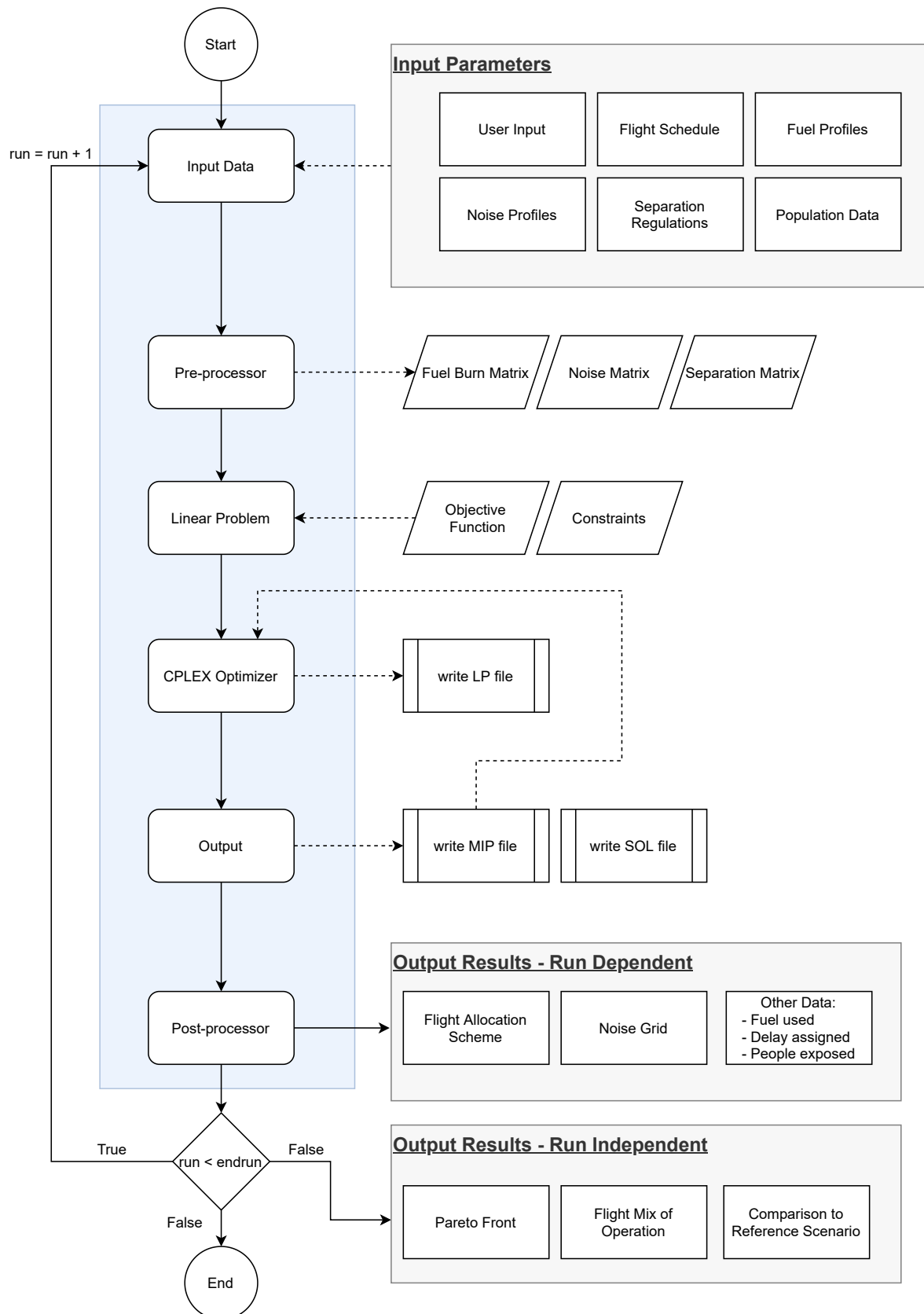


Figure 6.1: Architecture of the Flexible Runway Scheduling Model

When the model is initiated to perform several simulations a 'continue' statement is used. Several simulations can be performed when the analysis of different weights is examined. As long as the range is not complete the model will continue to run. If the range is completed, the model will output the final results. If several simulations are performed a Pareto front can be constructed to visualize the effect. Furthermore, a visualization of the flight mix is given. Finally, if the simulation is ran against a reference scenario this can be compared with this output.

6.2. Pre-processors

The data given by the user is pre-processed such that the FRSM can easily access the information. In this section three pre-processors are explained and an overview of their algorithms are presented including their inputs and outputs.

6.2.1. Fuel Pre-processor

The fuel burn pre-processor produces information for the fuel use for every flight to every runway possible. The inputs necessary are stated in Algorithm 1. The algorithm differentiates between arrivals and departures as their trajectories and segments differ. Fuel flow parameters are obtained from calculations through BADA which are specific for each flight and thus the algorithm considers the type of aircraft as well. If flights are not possible to a runway, for instance due to closed runway operations, the algorithm can be altered to take this into account. However, this procedure is not specifically necessary for the FRSM.

Algorithm 1 Flight-Runway specific Fuel Burn Pre-processor

Input: The set of flights, BADA coefficients, a matrix with lengths for different arrival and departure trajectories, a matrix with taxi distances and the number of runways.

Output: A fuel burn matrix with dimensions $f * r$

```

1: Initialize Fuel Burn matrix  $\mathbf{TFB} = [\mathbf{0}]$  and fuel flow parameters from BADA [17]
2: for all flights  $\in F$ , all runways  $\in R$  do
3:   if flight is Arrival then
4:      $TFU_{appr} = \frac{D_{LAF|FAF} \cdot \dot{m}_f(LAF|FAF)}{V_{LAF|FAF}} + \frac{D_{FAF|RWY} \cdot \dot{m}_f(FAF|RWY)}{V_{FAF|RWY}}$ 
5:      $TFU_{taxi} = \frac{D_{RWY|PIER} \cdot \dot{m}_f(TAXI)}{V_{TAXI}}$ 
6:      $TFB(f, r) = TFU_{appr} + TFU_{taxi}$ 
7:   else if flight is Departure then
8:      $TFU_{taxi} = \frac{D_{PIER|RWY} \cdot \dot{m}_f(TAXI)}{V_{TAXI}}$ 
9:      $TFU_{dep} = \frac{D_{RWY|SID} \cdot \dot{m}_f(RWY|SID)}{V_{RWY|SID}}$ 
10:     $TFB(f, r) = TFU_{taxi} + TFU_{dep}$ 
11:   end if
12: end for
13: return  $\mathbf{TFB}$ 

```

6.2.2. Noise Pre-processor

The noise pre-processor gives the noise matrix N as principle output. For all aircraft and all runway combinations AEDT profiles are loaded into the algorithm. These profiles contain a list of SEL values for every gridpoint considered. The algorithm examines the trajectory of the flights and the aircraft type and then selects the corresponding profile. As the information obtained through AEDT are SEL values and those need to be linearised, the AEL values are computed first for every gridpoint before storage in the noise matrix.

6.2.3. Separation Pre-processor

The separation pre-processor is airport specific and produces separation times for all different operation combinations, weight classes and runways. The algorithm produces four separation matrices, one for each operational combination. The general equations can be provided for operations on the same runway end and for operations on opposite runway ends. However, for dependencies between runways an analysis from the user is necessary and equations according to those dependencies should be activated for every runway combination.

Algorithm 2 Flight-Runway specific Noise Emission Pre-processor

Input: The set of flights including aircraft type, the set of trajectories, the number of runways and AEDT profiles.

Output: A noise emission matrix with dimensions $xy * f * r$

```

1: Initialize Noise Emission Matrix  $\mathbf{N} = [\mathbf{0}]$  and AEDT profiles [48]
2: for all flights  $\in F$ , all runways  $\in R$  do
3:   if flight is Arrival then
4:     IAF = Trajectory{f}
5:     AC = Aircraft-type{f}
6:     SEL = AEDT-Arrival-Profile{AC, (r & IAF)}
7:     for all gridpoints  $\in P$  do
8:        $N(xy, f, r) = 10^{\frac{SEL(xy)}{10}}$ 
9:     end for
10:  else if flight is Departure then
11:    SID = Trajectory {f}
12:    AC = Aircraft-type{f}
13:    SEL = AEDT-Departure-Profile{AC, (r & IAF)}
14:    for all gridpoints  $\in P$  do
15:       $N(xy, f, r) = 10^{\frac{SEL(xy)}{10}}$ 
16:    end for
17:  end if
18: end for
19: return  $\mathbf{N}$ 

```

6.3. IBM ILOG CPLEX

The FRSM uses the commercial solver IBM ILOG CPLEX to solve the linear problem. With the pre-processed information, objective function and constraints the linear problem is formed first. CPLEX uses a combination of Branch & Bound and Dynamic Search and the program is set to default, where it chooses the best combination depending on the problem.

CPLEX is then initiated to first write a LP file. This file contains all decision variables, costs, objective function and constraints and can be used for further evaluation if necessary. Also, if another solver is preferred the LP file created can be used as well in that particular solver.

If CPLEX finds a feasible solution it creates a MIP file. This file contains the information of all the values for all decision variables and is used in a consecutive simulation run. When optimizing for multiple weights, the MIP file ensures that a solution is always found and that the solution cannot be worse than the previously found solution. If complex problems are solved by CPLEX the MIP file has a positive impact on the optimization time. The second file that is created is a SOL file. This file contains the solution of the problem and can be directly analysed without any processors. The SOL file is also accessible with other solvers.

Algorithm 3 Airport specific Separation Pre-processor**Input:** A set of operations, weight-classes and corresponding separation scheme and local safety regulations.**Output:** 4 separation matrices for every combination of operations with dimensions $r * r$

```

1: Initialize separation matrices S-AA, S-DD, S-DA and S-AD = [0] and RECAT separation [43]
2: for all combinations  $\in$  operations, all runways(i)  $\in$  R, all runways(j)  $\in$  R, and all weight classes do
3:   if Combination == "AA" then
4:     if  $r_i == r_j$  then
5:       S-AA( $r_i, r_j$ ) = Equation 2.5 or Equation 2.6
6:     else if  $r_i$  is opposite  $r_j$  then
7:       S-AA( $r_i, r_j$ ) = Equation 5.22
8:     else if  $r_i$  creates dependency on  $r_j$  then
9:       S-AA( $r_i, r_j$ ) = Equations according to [49]
10:    else if  $r_i$  creates no dependency on  $r_j$  then
11:      S-AA( $r_i, r_j$ ) = 0
12:    end if
13:  else if Combination == "DD" then
14:    if  $r_i == r_j$  then
15:      S-DD( $r_i, r_j$ ) = Equation 2.7
16:    else if  $r_i$  is opposite  $r_j$  then
17:      S-DD( $r_i, r_j$ ) = Equation 5.23
18:    else if  $r_i$  creates dependency on  $r_j$  then
19:      S-DD( $r_i, r_j$ ) = Equations according to [49]
20:    else if  $r_i$  creates no dependency on  $r_j$  then
21:      S-DD( $r_i, r_j$ ) = 0
22:    end if
23:  else if Combination == "DA" then
24:    if  $r_i == r_j$  then
25:      S-DA( $r_i, r_j$ ) = DROT
26:    else if  $r_i$  is opposite  $r_j$  then
27:      S-DA( $r_i, r_j$ ) = Equation 5.24
28:    else if  $r_i$  creates dependency on  $r_j$  then
29:      S-DA( $r_i, r_j$ ) = Equations according to [49]
30:    else if  $r_i$  creates no dependency on  $r_j$  then
31:      S-DA( $r_i, r_j$ ) = 0
32:    end if
33:  else if Combination == "AD" then
34:    if  $r_i == r_j$  then
35:      S-AD( $r_i, r_j$ ) = AROT
36:    else if  $r_i$  is opposite  $r_j$  then
37:      S-AD( $r_i, r_j$ ) = Equation 5.25
38:    else if  $r_i$  creates dependency on  $r_j$  then
39:      S-AD( $r_i, r_j$ ) = Equations according to [49]
40:    else if  $r_i$  creates no dependency on  $r_j$  then
41:      S-AD( $r_i, r_j$ ) = 0
42:    end if
43:  end if
44: end for
45: return S-AA, S-DD, S-DA and S-AD

```


7

Amsterdam Airport Schiphol Results

The results and conclusions presented in the scientific paper have accompanying results to substantiate the claims made. In this chapter these results are presented for the three scenarios. Some extra explanation is given if necessary, however, most information can be obtained from the paper. In Section 7.1 the composition of aircraft in each scenario is presented together with the O/D data. The runway dependencies constructed by Van Der Klugt [49] are applied to Amsterdam Airport Schiphol (AAS) and an overview is presented in Section 7.2. To provide insights in the runway allocation a timetable for each scenario is analysed in Section 7.3. Finally, in Section 7.4 the assigned delays are presented.

7.1. Aircraft Mix & O/D Data

To provide insight in the flight composition, the different aircraft types are presented for each scenario. Some remarks can be made for each scenario. Note that the axes for each figure are not the same. In general it can be said that the predominant aircraft types at Amsterdam Airport Schiphol are the Boeing 737 series and the Embraer E190-E2. In the first scenario, Figure 7.1, the number of different flights is lowest; which is partly explained by the fact that this scenario also contains the lowest number of flights in general. The occurrence of the DH8D made it necessary to incorporate fuel schemes for turboprops as well. For the second scenario the flight mix is dominated by three types. The B737 series, the smaller Embraers and the A320 family. For scenario three a relative high occurrence of the heavy B777 and B787 series can be noted.

The Flexible Runway Scheduling Model considers both fuel burn and noise emission in the trade-off. To analyse the results and to compare these results with a reference scenario it is important to observe the origin or destination of the flights. This data can provide insights in trade-offs made within the program. For the first scenario the number of flights with a destination located south of the airport is significant. Waypoint indicators "*LEKKO*" and "*IDRID*" make up almost 60% of the destinations for the outbound peak. This makes the preference for south-oriented runways visible. The scheduling of flights on *R18L* and *R24* is a result of this. For the second scenario an equal spread can be observed. However, as the number of departures in the second scenario is lower, the influence is also less. The origins of the arrivals are somewhat more located from the north, as the indicators "*ARTIP*" and "*SUGOL*" are the IAFs located north of the airport, but this influence is smaller. In the third scenario it can be observed that all locations are spread fairly equal. Although northern departures are still in minority, this difference is small. An equal division of locations for both departures and arrivals can lead to a more effective outcome of the FRSM. Because more flights can benefit from another runway with respect to the reference scenario more fuel savings can be obtained.

7.2. Runway Dependencies for EHAM

The dependency calculations as provided by Van Der Klugt [49] are applied to the runway system of Amsterdam Airport Schiphol (AAS). AAS has a runway system with 6 runways oriented in different directions to cope with the changing wind conditions throughout the year. The small runway *R04/R22* is used for general aviation only and is therefore not considered in this research. It can be observed from Figure 7.10 that multiple dependencies arise within the runway system. The calculations for this specific case are presented here. Each consecutive operation combination is considered and the assumptions are stated.

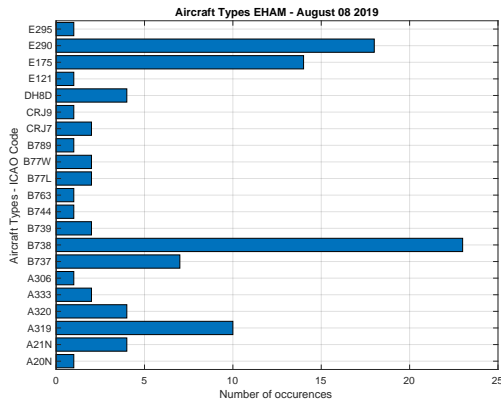


Figure 7.1: Aircraft Composition Scenario 1: Outbound Peak

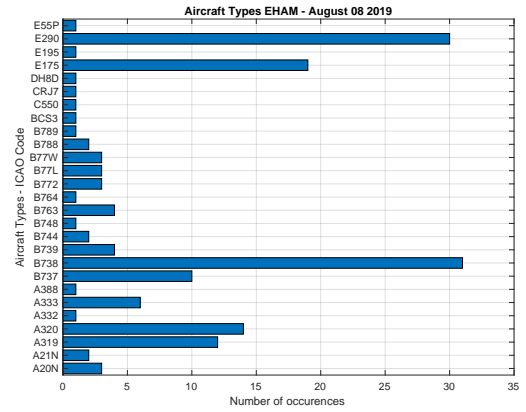


Figure 7.2: Aircraft Composition Scenario 2: Inbound Peak

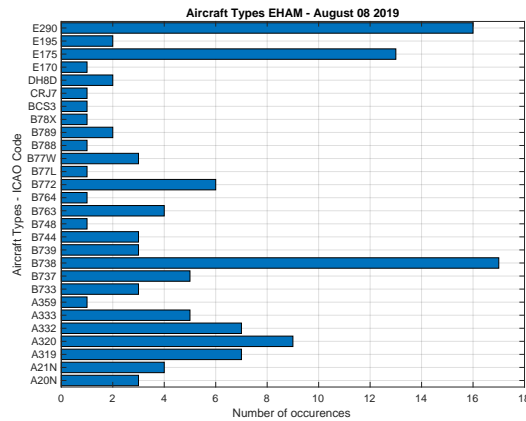


Figure 7.3: Aircraft Composition Scenario 3: 2 + 2

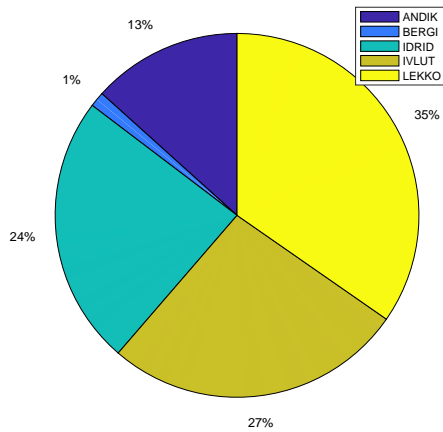


Figure 7.4: Departing directions for Scenario 1

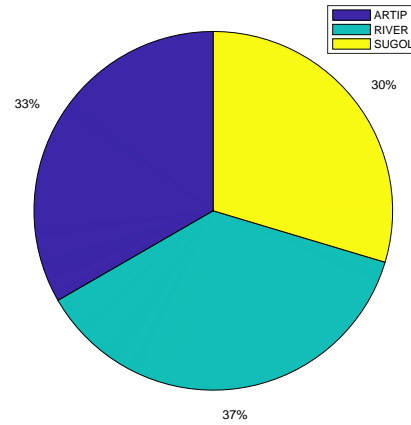


Figure 7.5: Origins of arrivals in Scenario 1

7.2.1. Arrival - Arrival

For two consecutive arrivals there are two dependencies to consider. The first dependency arises in the air when either the missed approach path or the final approach paths intersect with each other. The second dependency arises for an intersection point on the runway. Both these dependencies are resolved by applying a staggering distance to the second aircraft. An overview of the different distances is given in Table 7.1. The minimum staggering distance is determined to be 1.5 *nmi* and corresponds to a time separation of about 40 seconds, depending on the aircraft approach speed. In this research the distance is increased to 2.0 *nmi* if

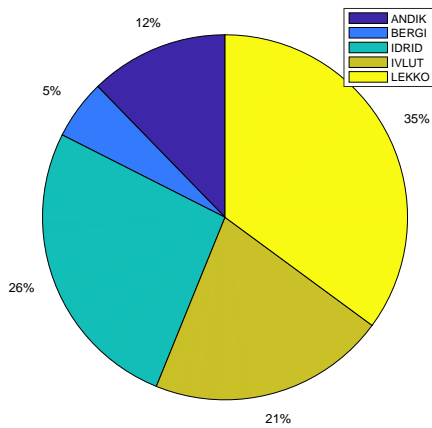


Figure 7.6: Departing directions Scenario 2

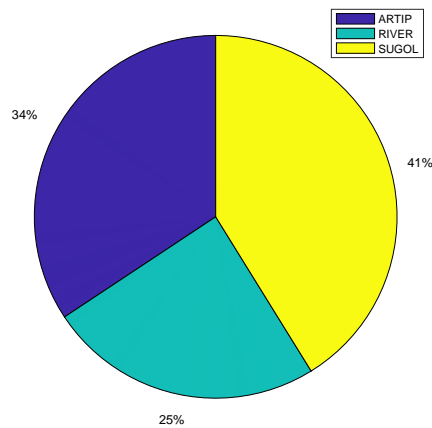


Figure 7.7: Origins of arrivals in Scenario 2

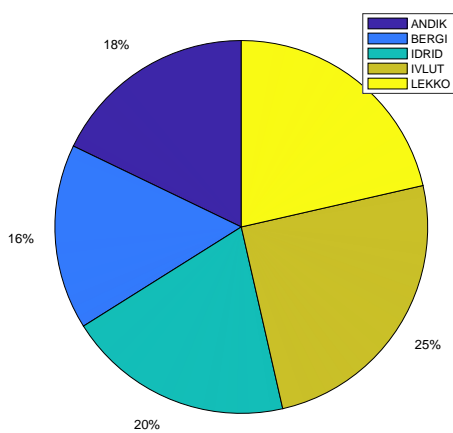


Figure 7.8: Departing directions Scenario 3

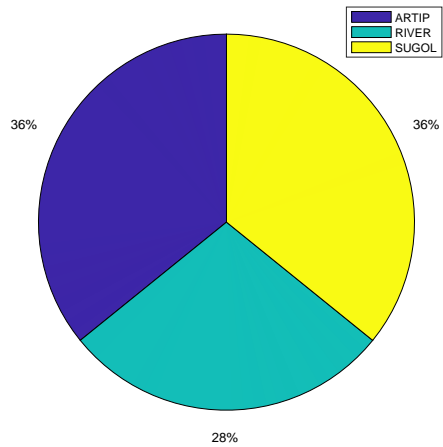


Figure 7.9: Origins of arrivals in Scenario 3

the intersecting paths are at the halfway point of one of the runways, which is the case for two arrivals on the combination R36C - R27. If the intersection of the projected paths is at the end of one of the runways the distance is further increased to 2.5 nmi. An example of this arises for the combination R24 - R36C.

Table 7.1: Staggering distances in nmi between two consecutive arrivals on EHAM

	First RWY	Second RWY									
		R36L	R18R	R36C	R18C	R36R	R18L	R09	R27	R06	R24
	R36L	-	-	-	-	-	-	-	-	-	-
	R18R	-	-	-	-	-	-	-	1.5	-	-
	R36C	-	-	-	-	-	-	-	2	2.5	1.5
	R18C	-	-	-	-	-	-	-	2	2.5	1.5
	R36R	-	-	-	-	-	-	-	2.5	2	2
	R18L	-	-	-	-	-	-	-	-	-	-
	R09	-	-	-	-	-	-	-	-	-	-
	R27	-	1.5	2	2	1.5	-	-	-	-	-
	R06	-	-	2	1.5	2.5	-	-	-	-	-
	R24	-	-	2.5	1.5	1.5	-	-	-	-	-

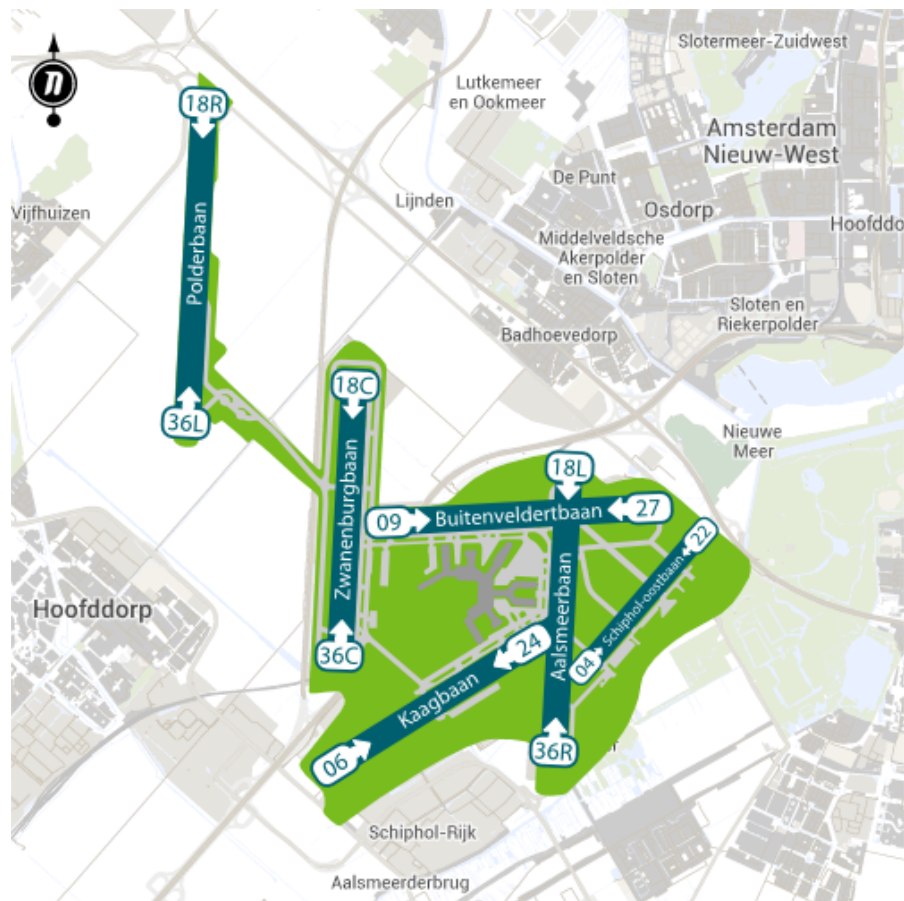


Figure 7.10: Runway System for Amsterdam Airport Schiphol (AAS/EHAM) [5]

7.2.2. Departure - Departure

When two consecutive departures take place jet blast and wake turbulence should be considered as well as intersecting flight lines. The main parameter of interest is the time it takes for a departure to reach the location where the dependency arises. This is either indicated with the time to intersection $R_{D,int}$ or the time to clearance $R_{D,cl}$. In each scenario it can differ whether or not the second aircraft is allowed to line-up during the operation or only after the first departure has cleared the location. For the calculation of the runway occupancy times a percentage of the complete runway occupancy time is taken which can be used in Equation 5.10 and Equation 5.11. An overview is provided in Table 7.2. For a departure which has an influence on another runway at the start of its take-off roll, clearance is given after 20% of the first departure is completed. An example arises for the case of two departures on the combination $R09 - R36C$, where a departure on $R36C$ can already be lined-up. If the operating order is reversed, e.g. $R36C - R09$, the separation time is increased and the second aircraft is only allowed to line-up after clearance. Finally, if the first section of the departing trajectory intersects with another runway, the separation time can be larger than the ROT. An example arises for the case of two consecutive departures on $R27 - R36C$ where the first aircraft has to clear the second runway as well.

7.2.3. Departure - Arrival

For a departure followed by an arrival the main parameter of interest is the distance the arrival should be removed from the runway threshold at the beginning of the departure. The minimum separation distance is $1.5 nmi$. These are mainly applied to situations where the jet blast of an operation has an influence on the arriving flight, a situation which arises for instance between $R09 - R36C$. If the point of conflict is at the end of a departing trajectory an extra separation is applied of $2.5 nmi$ which is the occasion for the combination $R24 - R36C$. Here, extra separation is necessary as the arriving flight must be further away than the threshold of the runway at the moment the departure is lifting off.

Table 7.2: Percentage of the DROT for two consecutive departures on EHAM

		Second RWY									
		R36L	R18R	R36C	R18C	R36R	R18L	R09	R27	R06	R24
First RWY	R36L	-	-	-	-	-	-	-	-	-	-
	R18R	-	-	-	-	-	-	-	-	-	-
	R36C	-	-	-	-	-	-	50	50	-	-
	R18C	-	-	-	-	-	-	50	50	-	120
	R36R	-	-	-	-	-	-	-	-	-	-
	R18L	-	-	-	-	-	-	20	20	-	50
	R09	-	-	20	20	-	70	-	-	-	-
	R27	-	-	110	110	-	30	-	-	-	-
	R06	-	-	-	-	-	-	-	-	-	-
	R24	-	-	-	100	-	20	-	-	-	-

Table 7.3: Staggering distances in nmi for aircraft arriving after a departure on EHAM

		Second RWY									
		R36L	R18R	R36C	R18C	R36R	R18L	R09	R27	R06	R24
First RWY	R36L	-	-	-	-	-	-	-	-	-	-
	R18R	-	-	-	-	-	-	-	-	-	-
	R36C	-	-	-	-	-	-	-	1.5	-	-
	R18C	-	-	-	-	-	-	-	1.5	2.5	1.5
	R36R	-	-	-	-	-	-	-	-	-	-
	R18L	-	-	-	-	-	-	-	1.5	-	2.5
	R09	-	-	1.5	1.5	1.5	-	-	-	-	-
	R27	-	-	2.5	2.5	1.5	-	-	-	-	-
	R06	-	-	-	-	-	-	-	-	-	-
	R24	-	-	2.5	1.5	1.5	-	-	-	-	-

7.2.4. Arrival - Departure

When an arrival is followed by a departure, the dependency which arises at intersections is given as a percentage of the arrival runway occupancy time (AROT) which is presented in Table 7.4. The percentages are based on the location of the intersection with respect to the whole runway. Clearance can also be given to a departure when it is clear that the missed approach procedure is not necessary, because the arriving aircraft has landed. This completion time is taken to be 10 seconds in every case.

Table 7.4: Percentage of the AROT for aircraft departing after an arrival on EHAM

		Second RWY									
		R36L	R18R	R36C	R18C	R36R	R18L	R09	R27	R06	R24
First RWY	R36L	-	-	-	-	-	-	-	-	-	-
	R18R	-	-	-	-	-	-	-	-	-	-
	R36C	-	-	-	-	-	-	50	50	-	-
	R18C	-	-	-	-	-	-	50	50	-	-
	R36R	-	-	-	-	-	-	-	-	-	50
	R18L	-	-	-	-	-	-	-	-	-	-
	R09	-	-	-	-	-	-	-	-	-	-
	R27	-	-	-	-	-	30	-	-	-	-
	R06	-	-	-	-	-	-	-	-	-	-
	R24	-	-	-	-	-	30	-	-	-	-

7.3. Timetable

To further analyse the allocation of flights by the FRSM, a timetable is presented for the operating period for every runway end. For Scenario 1 some remarks can be made. When analysing *R06/R24* it is noted that there are four occurrences where the operating runway end is changed from *R24* to *R06*. While the predominant operation on *R24* are departures, the operations scheduled on *R06* are arrivals. The opposite direction operation separation requirement is large for a departure followed by an arrival (> 5 minutes), but the model finds this reduction in capacity worth the savings it provides. It can be clearly observed that *R18L* is the main runway to handle the departing demand. When investigating distances between pier and runway it is observed that the combination of pier-runway is shortest in most cases for *R18L*. Finally, if the departing demand is too high it can be seen that first *R09* and then *R36L* are used to handle these 'overflow' situations.

For Scenario 2 it can be noted that arriving aircraft are allocated to *R18R*, *R18C* and *R36R*. In the reference scenario *R24* is used solely for departing aircraft, but it can be noted that departures are scheduled on *R18L* as well. *R18L/R36R* is used in both directions and during a period of 90 minutes the operating order is switched multiple times. *R09/R27* is used as an overflow runway to handle demand if the other runways are in use.

Scenario 3 is a period where the mix between arrivals and departures is equal. For the 2 + 2 configuration in the reference scenario, *R18R* and *R18C* are used for arrivals and *R24* and *R18L* for departures. In the FRSM allocation it can be seen that this configuration is still somewhat present, but that a significant amount of flights is now scheduled on other runways as well. *R18R/R36L* and *R18L/R36R* are now used in both directions and there are four instances where *R06* is opened for arrivals as well. In this scenario the effect of the FRSM can be observed clearly. In the reference scenario the allocation of flights is strictly regulated to 2 runways per operation. The FRSM uses the whole airfield to accommodate the demand.

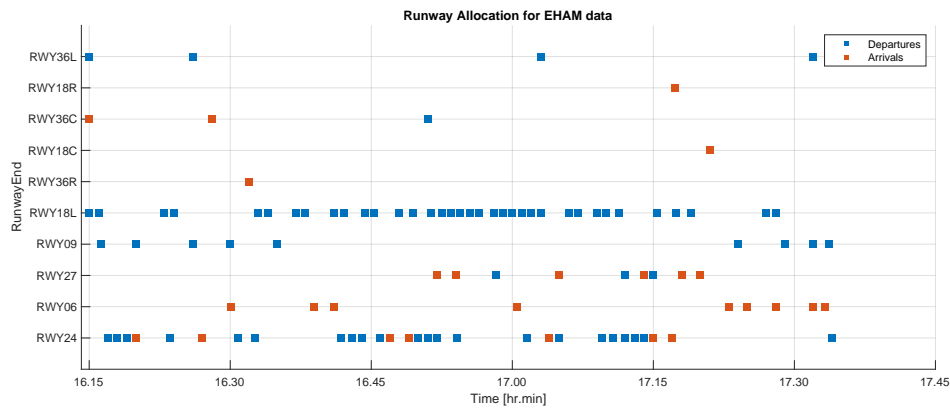


Figure 7.11: Runway Allocation in timetable for Scenario 1 with $\alpha = 0.4$

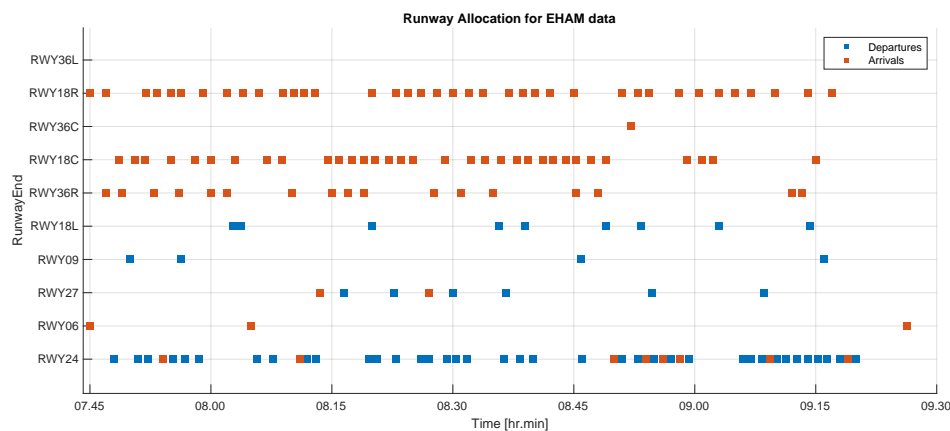


Figure 7.12: Runway Allocation in timetable for Scenario 2 with $\alpha = 0.2$

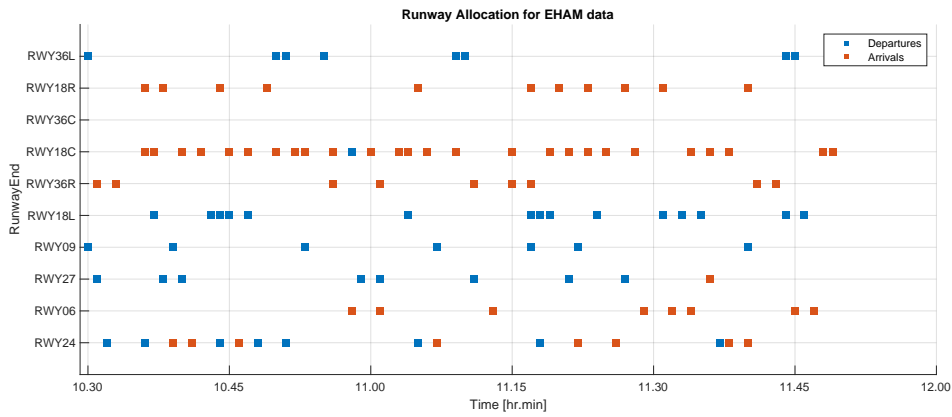


Figure 7.13: Runway Allocation in timetable for Scenario 3 with $\alpha = 0.65$

7.4. Delay

To investigate the delay distribution a histogram is created for every scenario. The width of each bar is 20 seconds, but delay is still continuous. The gradient of each histogram is as one would expect. Most flights are assigned no to little delay and only some flights have big delays. The biggest delay can be found in Scenario 2 where 1 flight is delayed for more than 400 seconds. This delay is most likely assigned due to the fact that assigning this flight to that runway would not violate any new gridpoints. The fact that separation requirements are stricter for arriving aircraft can be seen as well in the delay distribution as more flights are assigned longer delays.

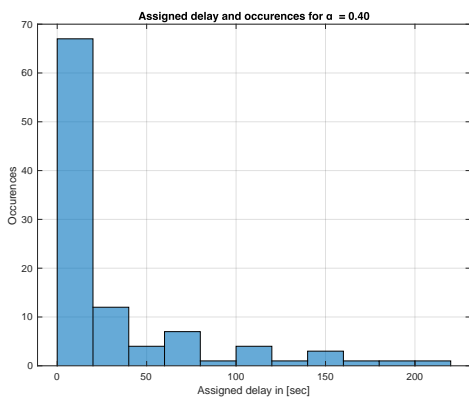


Figure 7.14: Assigned Delay for Scenario 1 with $\alpha = 0.4$

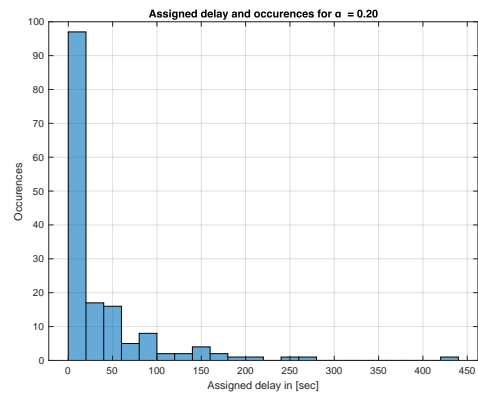


Figure 7.15: Assigned Delay for Scenario 2 with $\alpha = 0.2$

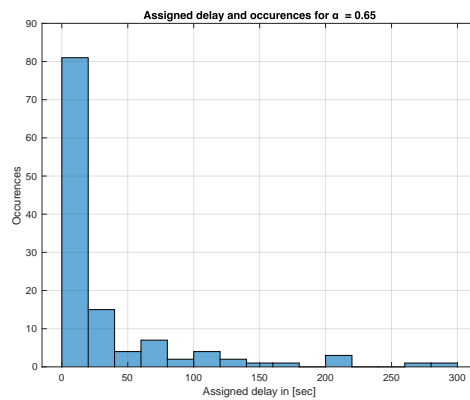
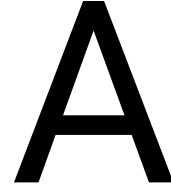


Figure 7.16: Assigned Delay for Scenario 3 with $\alpha = 0.65$

IV

Appendices



Amsterdam Airport Schiphol Data

This appendix provides an overview of the data used in the result analysis for Amsterdam Airport Schiphol. In Section A.1 an extract of the flight schedule is presented. For taxi operations the distances are presented in Section A.2. Finally, in Section A.3 the airborne distances are provided.

A.1. Flight Schedule

The flight schedule serves as the main source of information for the Flexible Runway Scheduling Model. The minimum required information for the flight schedule is shown in Table A.1. The weight classes are determined with the RECAT-EU scheme.

Table A.1: Part of the flight schedule for EHAM on August 8th, 2019. Used for analysis of scenario 3.

Scheduled Time	CallSign	Aircraft Type	Weight Class	Airline	Operation	O/D Data	SID/IAF	Pier
10:30:00	KL723	A332	UH	KLM	D	MUHA	BERGI	D
10:30:00	DL143	A333	UH	Delta Air Lines	D	KSEA	BERGI	D
10:31:00	KL598	B772	UH	KLM	A	FACT	RIVER	E
10:31:00	BE102	E175	LM	Flybe	D	EGBB	IDRID	D
10:32:00	KL945	E175	LM	KLM	D	EIDW	IDRID	D
10:33:00	AC824	B77W	UH	Air Canada	A	CYYZ	SUGOL	G
10:36:00	KL1126	B738	UM	KLM	A	EKCH	ARTIP	D
10:36:00	BA8451	E290	LM	British Airways	A	EGLC	SUGOL	D
10:36:00	AA221	B772	UH	American Airlines	D	KDFW	BERGI	G
10:37:00	KL1228	B738	UM	KLM	A	LFPG	RIVER	D
10:37:00	KL591	B77W	UH	KLM	D	FAOR	LEKKO	F
10:38:00	HV5132	B738	UM	Transavia	A	LEBL	RIVER	D
10:38:00	DL161	A333	UH	Delta Air Lines	D	KMSP	BERGI	D
10:39:00	KM394	A320	UM	Air Malta	A	LMML	ARTIP	B
10:39:00	BT610	B733	LM	airBaltic	D	EYVI	ANDIK	B
10:40:00	RO361	B738	UM	Tarom	A	LROP	ARTIP	D
10:40:00	KL1109	B739	UM	KLM	D	ESSA	ANDIK	C
10:41:00	DL76	B763	LH	Delta Air Lines	A	KTPA	SUGOL	D
10:42:00	AZ120	A319	UM	Alitalia	A	LIMC	RIVER	C
10:42:00	TS360	A332	UH	Air Transat	A	CYYZ	SUGOL	G
10:43:00	KL1583	E290	LM	KLM	D	LIPE	LEKKO	B
10:44:00	HV6820	B737	UM	Transavia	A	LJLJ	ARTIP	D
10:44:00	KL1823	B739	UM	KLM	D	EDDT	IVLUT	C
10:44:00	BE1272	E195	LM	Flybe	D	EGCC	IDRID	D
10:45:00	AA204	B763	LH	American Airlines	A	KPHL	SUGOL	D
10:45:00	KL571	B78X	UH	KLM	D	HTKJ	LEKKO	F
10:45:00	AF1341	A320	UM	Air France	D	LFPG	LEKKO	C
10:46:00	HV5672	B738	UM	Transavia	A	LEIB	ARTIP	C
10:47:00	DL74	A333	UH	Delta Air Lines	A	KATL	SUGOL	D
10:47:00	EJU7905	A320	UM	OpenSkies	D	LKPR	IVLUT	H
10:48:00	KL923	E195	LM	KLM	D	EGPE	IDRID	D
10:49:00	KL1792	E290	LM	KLM	A	EDDM	ARTIP	D
10:50:00	KL1954	E290	LM	KLM	A	LSZH	RIVER	B
10:50:00	SK822	B737	UM	Scandinavian	D	ENGM	ANDIK	C
10:51:00	DL135	A333	UH	Delta Air Lines	D	KDTW	BERGI	D
10:51:00	BA8496	E170	LM	British Airways	D	EGLC	IDRID	D
10:52:00	KL1868	E175	LM	KLM	A	EDDS	ARTIP	B
10:53:00	KL1754	E175	LM	KLM	A	EDDW	ARTIP	B
10:53:00	KL1711	E290	LM	KLM	D	LPPR	LEKKO	B
10:55:00	BT622	BCS3	UM	airBaltic	D	EETN	ANDIK	B

Scheduled Time	CallSign	Aircraft Type	Weight Class	Airline	Operation	O/D Data	SID/IAF	Pier
10:56:00	KL1516	E175	LM	KLM	A	EGSH	ARTIP	B
10:56:00	KL1142	E290	LM	KLM	A	ENGM	ARTIP	B
10:58:00	AF1030	CRJ7	LM	Air France	A	LFRN	RIVER	B
10:58:00	KL1050	E290	LM	KLM	A	EGGD	SUGOL	B
10:58:00	VY8301	A320	UM	Vueling	D	LEBL	LEKKO	D
10:59:00	DL49	B763	LH	Delta Air Lines	D	KJFK	BERGI	D
11:00:00	HV5764	B738	UM	Transavia	A	LEGE	RIVER	C
11:01:00	AZ108	A21N	UM	Alitalia	A	LIRF	RIVER	C
11:01:00	DL48	A333	UH	Delta Air Lines	A	KJFK	SUGOL	E
11:01:00	UA908	B763	LH	United Airlines	D	KORD	BERGI	D
11:03:00	KL1154	E175	LM	KLM	A	ESGG	ARTIP	B
11:04:00	KL1422	B738	UM	KLM	A	EGBB	SUGOL	D
11:04:00	VK6825	A21N	UM	FOO	D	LOWW	IVLUT	D
11:05:00	KL1342	E290	LM	KLM	A	EKBI	ARTIP	B
11:05:00	OR364	B788	UH	TUI fly	A	TNCC	SUGOL	G
11:05:00	KL735	B744	UH	KLM	D	TNCC	BERGI	F
11:06:00	A3624	A320	UM	Aegean Airlines	A	LGAV	ARTIP	B
11:07:00	KL1840	B738	UM	KLM	A	LOWW	ARTIP	C
11:07:00	D83539	B738	UM	Norwegian Air	D	EKCH	ANDIK	H
11:09:00	HV5472	B738	UM	Transavia	A	LEMH	RIVER	C
11:09:00	BA2759	A319	UM	British Airways	D	EGKK	IDRID	D
11:10:00	SK556	B738	UM	Scandinavian Airlines	D	ESSA	ANDIK	C
11:11:00	SV933	B77L	UH	Saudi Arabian Airlines	A	OENJ	ARTIP	F
11:11:00	SK552	A20N	UM	Scandinavian Airlines	D	EKCH	ANDIK	C
11:13:00	HV5462	B738	UM	Transavia	A	LIPX	RIVER	C
11:15:00	BA430	A21N	UM	British Airways	A	EGLL	SUGOL	D
11:15:00	KL1724	E290	LM	KLM	A	EBBR	RIVER	B
11:17:00	KL644	B744	UH	KLM	A	KJFK	SUGOL	F
11:17:00	KL1740	E175	LM	KLM	A	ELLX	RIVER	B
11:17:00	KL451	A332	UH	KLM	D	OMAA	IVLUT	F
11:17:00	FB462	B733	LM	Bulgaria Air	D	LBSF	IVLUT	D
11:18:00	UX1098	A332	UH	Air Europa	D	LEMD	LEKKO	C
11:18:00	LO266	B733	LM	Lot Polish Airlines	D	EPWA	IVLUT	C
11:18:00	JU361	A319	UM	Air Serbia	D	LYBE	IVLUT	D
11:18:00	KL1855	E290	LM	KLM	D	EDDL	IVLUT	B
11:19:00	KL1472	B737	UM	KLM	A	EGPF	SUGOL	D
11:19:00	LH2303	A320	UM	Lufthansa	D	EDDM	IVLUT	B
11:20:00	EJU7926	A320	UM	OpenSkies	A	LFMN	RIVER	H
11:21:00	KL954	E290	LM	KLM	A	EGNT	SUGOL	B
11:21:00	BE1532	DH8D	LM	Flybe	D	EGTE	IDRID	D
11:22:00	KL1330	E175	LM	KLM	A	EKYT	ARTIP	B
11:22:00	SQ323	A359	UH	Singapore Airlines	D	WSSS	ANDIK	G
11:22:00	UA71	B764	LH	United Airlines	D	KEWR	IDRID	D
11:22:00	BE1012	DH8D	LM	Flybe	D	EGHI	IDRID	D
11:23:00	EZY2157	A319	UM	EasyJet	A	EGGW	SUGOL	H
11:23:00	KL1414	E175	LM	KLM	A	LFLL	RIVER	B
11:24:00	KL421	A332	UH	KLM	D	OEDF	IVLUT	G
11:24:00	KL1975	B737	UM	KLM	D	LHBP	IVLUT	C
11:24:00	HV5953	B738	UM	Transavia	D	LPPT	LEKKO	C
11:25:00	KL1106	B738	UM	KLM	A	ESSA	ARTIP	C
11:25:00	KL1198	E175	LM	KLM	A	ENZV	ARTIP	B
11:26:00	KL1764	E290	LM	KLM	A	EDDF	ARTIP	B
11:27:00	KL792	B772	UH	KLM	A	SBGR	SUGOL	F
11:27:00	UA21	B772	UH	United Airlines	D	KIAH	BERGI	D
11:28:00	HV6918	B738	UM	Transavia	A	LIEO	RIVER	C
11:28:00	BA8452	E290	LM	British Airways	D	EGLC	IDRID	D
11:29:00	TK1961	A320	UM	Turkish Airlines	A	LTJF	ARTIP	D
11:31:00	PC1251	A20N	UM	Pegasus Airlines	A	LTJF	ARTIP	D
11:31:00	LH989	A20N	UM	Lufthansa	D	EDDF	IVLUT	B
11:32:00	KL1986	E175	LM	KLM	A	LFBS	RIVER	B
11:33:00	TK1952	B789	UH	Turkish Airlines	D	LTBA	IVLUT	G
11:34:00	EJU7988	A319	UM	OpenSkies	A	LIPX	RIVER	H
11:34:00	KL986	E290	LM	KLM	A	EGLC	SUGOL	D
11:35:00	KL539	A332	UH	KLM	D	HUEN	LEKKO	G
11:36:00	KK6725	A332	UH	Atlasglobal	A	LTBA	ARTIP	G
11:36:00	KL608	B789	UH	KLM	A	KSFO	SUGOL	E
11:37:00	KL713	B744	UH	KLM	D	SMJP	IDRID	F
11:38:00	KL1486	E175	LM	KLM	A	EGNJ	SUGOL	B
11:38:00	KL934	E290	LM	KLM	A	EIDW	SUGOL	B
11:40:00	KL696	B772	UH	KLM	A	CYZZ	SUGOL	F
11:40:00	HV1864	B738	UM	Transavia	A	LGMT	ARTIP	C
11:40:00	KL1693	B738	UM	KLM	D	LPPT	LEKKO	C
11:41:00	KL682	B772	UH	KLM	A	CVVR	SUGOL	D
11:43:00	KL758	B77W	UH	KLM	A	MPTO	SUGOL	F
11:44:00	KL1345	B737	UM	KLM	D	EKBI	ANDIK	C
11:44:00	KL1297	E290	LM	KLM	D	LFBD	LEKKO	B
11:44:00	KL1653	E175	LM	KLM	D	LIPZ	LEKKO	B
11:45:00	EZY6771	A319	UM	EasyJet	A	EGAA	SUGOL	H
11:45:00	RU428	B748	UH	AirBridgeCargo Airlines	D	UUEE	ANDIK	CARGO
11:46:00	KC904	A21N	UM	Air Astana	D	UATG	IVLUT	D
11:47:00	PS101	B739	UM	Ukraine Int. Airlines	A	UKBB	ARTIP	E
11:48:00	EJU7954	A320	UM	OpenSkies	A	LEPA	RIVER	H
11:49:00	EJU1353	A319	UM	OpenSkies	A	LSGG	RIVER	H

A.2. Taxi Distances EHAM

To model the taxi operations, distances are necessary from the pier to the runway and vice versa. Some assumptions are made for the determination of the taxi distances. First it is assumed that arriving aircraft are able to use the second taxi exit. As most runways have three exits, the middle exit will provide a reasonable average. Second, for some taxi operations multiple routes are possible and are determined by ATC. In this research the shortest taxi operation is chosen. Furthermore, some flights in the schedule are cargo flights. At AAS multiple cargo terminals are present and are dependent on the operator. As most cargo terminals are located east of R04/R22 the distance to this location is chosen as the average taxi distance. Further analysis of the taxi system shows that some routes can only be used in one way. Therefore, differences arise between the two taxi tables which are presented in Table A.2 and Table A.3.

Table A.2: Taxi-in distances at EHAM for operations from the runway to the pier. All values are expressed in meters. Runways without distances are not open for arrival.

Pier	Runway									
	R36L	R18R	R36C	R18C	R36R	R18L	R09	R27	R06	R24
B	-	8,237	5,194	3,338	2,030	-	-	3,083	855	2,258
C	-	8,577	5,531	3,705	1,776	-	-	2,790	771	2,543
D	-	7,337	5,067	4,690	1,184	-	-	2,213	1,796	3,548
E	-	6,371	4,023	3,232	1,658	-	-	874	2,897	4,685
F	-	5,643	3,352	2,599	2,026	-	-	926	3,321	4,677
G	-	5,335	3,059	2,255	2,364	-	-	1,317	3,714	4,353
H	-	5,473	3,182	2,409	2,921	-	-	1,799	4,194	4,521
CARGO	-	8,283	5,210	3,373	2,805	-	-	3,867	2,131	2,275

Table A.3: Taxi-out distances at EHAM for operations from the pier to the runway. All values are expressed in meters. Runways without distances are not open for departures.

Pier	Runway									
	R36L	R18R	R36C	R18C	R36R	R18L	R09	R27	R06	R24
B	7,656	-	2,614	5,413	-	3,342	3,788	3,956	-	1,530
C	8,020	-	2,906	5,719	-	2,930	4,126	3,587	-	1,158
D	8,884	-	3,825	5,632	-	2,133	3,423	2,757	-	901
E	6,233	-	3,712	4,741	-	1,543	2,475	2,668	-	1,775
F	5,320	-	3,185	3,612	-	1,905	1,855	3,105	-	2,191
G	4,942	-	3,027	3,317	-	2,231	1,481	3,453	-	2,547
H	4,940	-	2,991	3,499	-	2,725	1,337	3,947	-	3,025
CARGO	7,752	-	2,734	5,570	-	3,589	3,975	4,244	-	1,457

A.3. Flight Distances EHAM

To calculate the fuel burn during flight the distances from the IAF or towards the waypoint at the SID are determined as well. These distances are obtained through information in the Aeronautical Information Packages (AIP) provided by the local Air Navigation Service Provider. The difference in distances for incoming flights are smaller as it is assumed that from the IAF aircraft fly towards AAS first at indicator SPL and from there are sorted towards a runway.

Table A.4: Departure distances at EHAM for departing operations from the runway to the first waypoint indicator on the Standard Instrument Departure. All values are expressed in nautical miles.

SID	Runway									
	R36L	R18R	R36C	R18C	R36R	R18L	R09	R27	R06	R24
ANDIK	33.3	-	37.0	46.8	-	38.0	33.0	34.9	-	50.0
BERGI	26.3	-	31.7	42.2	-	48.4	31.0	37.3	-	42.2
IDRID	59.3	-	76.7	49.6	-	55.7	56.6	52.3	-	49.5
LEKKO	42.6	-	39.7	22.4	-	20.4	24.4	30.2	-	23.8
IVLUT	31.3	-	26.9	25.4	-	17.0	19.0	35.2	-	27.0

Table A.5: Arrival distances at EHAM for arriving operations from the Initial Approach Fix to the runway threshold. All values are expressed in nautical miles.

IAF	Runway									
	R36L	R18R	R36C	R18C	R36R	R18L	R09	R27	R06	R24
SUGOL	-	54.0	55.8	49.0	54.4	-	-	55.7	53.3	51.6
ARTIP	-	55.0	56.8	50.0	55.4	-	-	56.7	54.3	52.6
RIVER	-	57.0	58.8	52.0	57.4	-	-	58.7	56.3	54.6

B

Noise Grids and Runway Allocation

In this appendix an overview of additional noise grids and runway allocations are presented for each scenario. For every scenario the results are shown for different weight parameters and the reference scenario.

B.1. Noise Grid & Runway Allocation Scenario 1

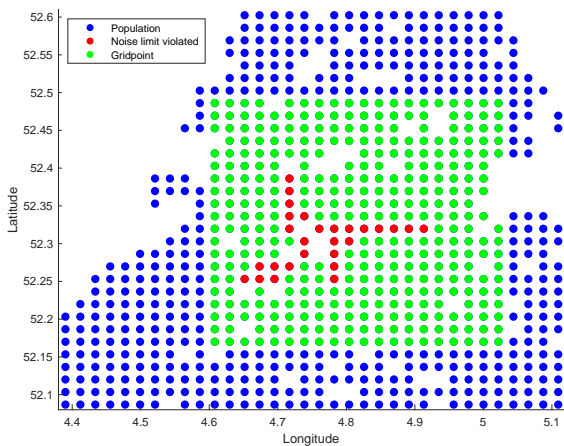


Figure B.1: Noise Grid Scenario 1: Noise optimized

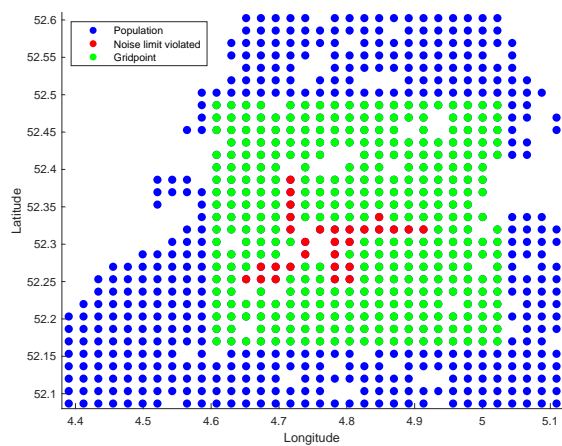


Figure B.2: Noise Grid Scenario 1: Multi-objective optimized

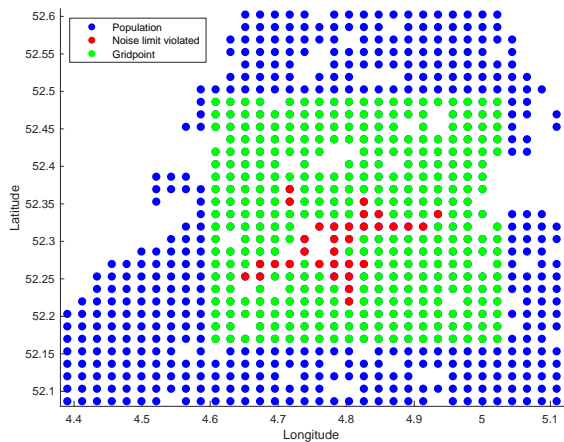


Figure B.3: Noise Grid Scenario 1: Fuel optimized

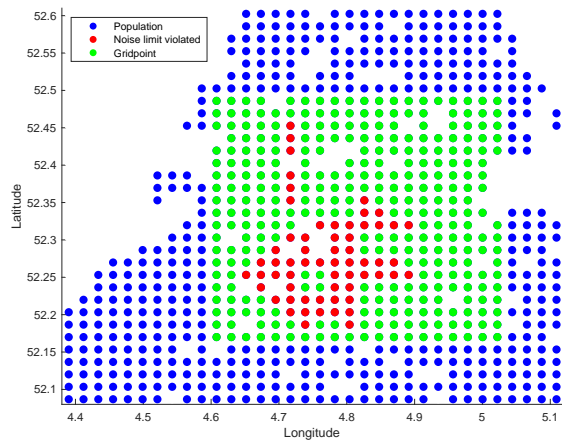


Figure B.4: Noise Grid Scenario 1: Reference Scenario

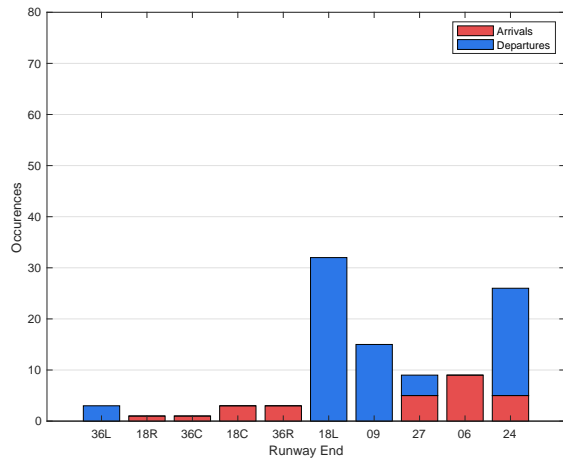


Figure B.5: Runway Allocation Scenario 1: Noise optimized

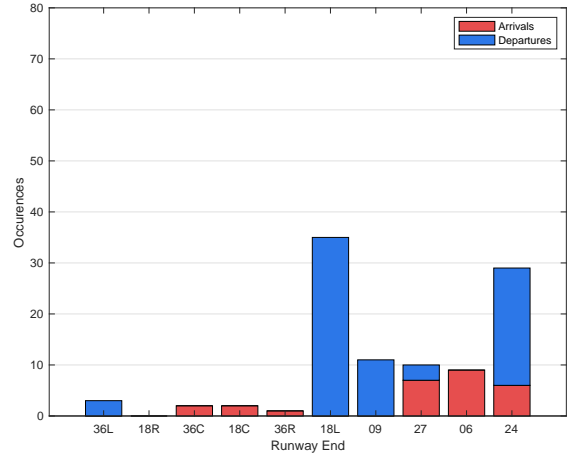


Figure B.6: Runway Allocation Scenario 1: Multi-objective optimized

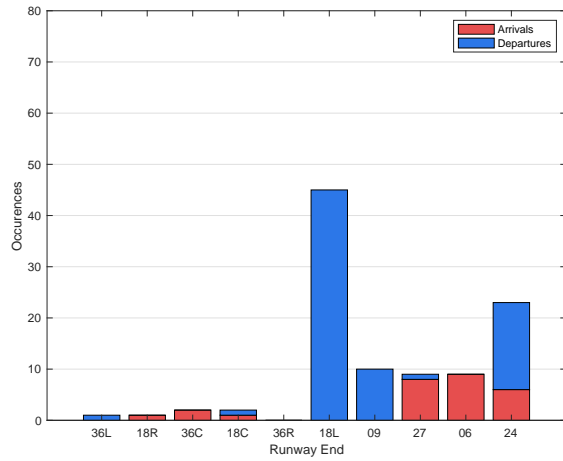


Figure B.7: Runway Allocation Scenario 1: Fuel optimized

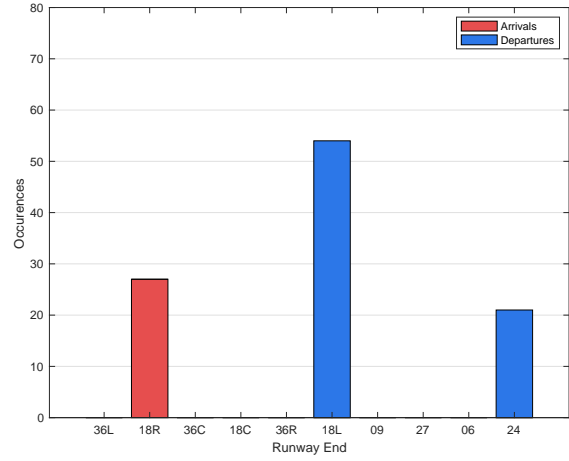


Figure B.8: Runway Allocation Scenario 1: Reference Scenario

B.2. Noise Grid & Runway Allocation Scenario 2

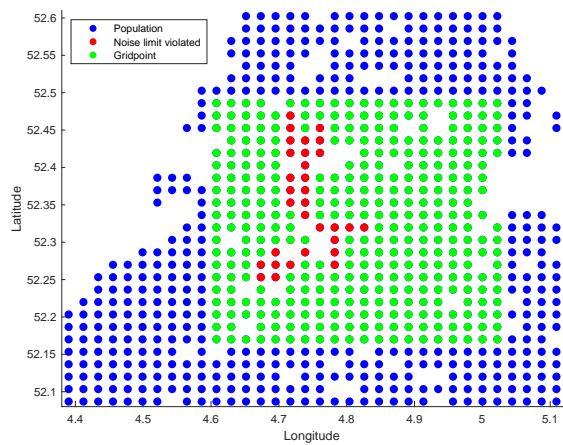


Figure B.9: Noise Grid Scenario 2: Noise optimized

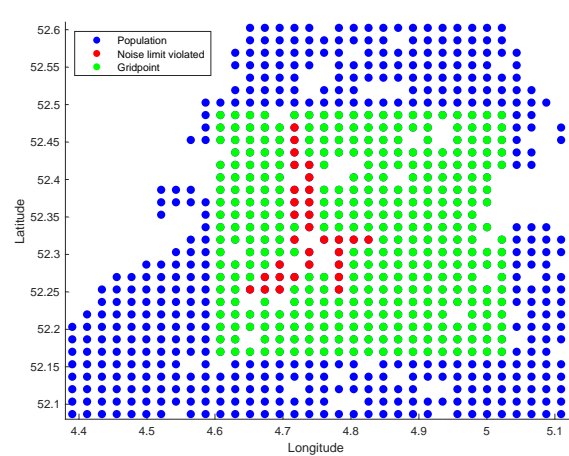


Figure B.10: Noise Grid Scenario 2: Multi-objective optimized

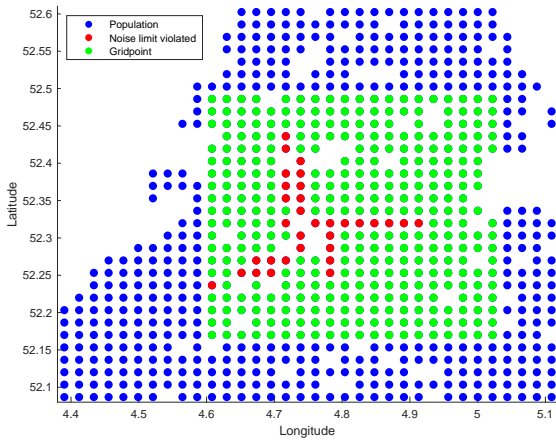


Figure B.11: Noise Grid Scenario 2: Fuel optimized

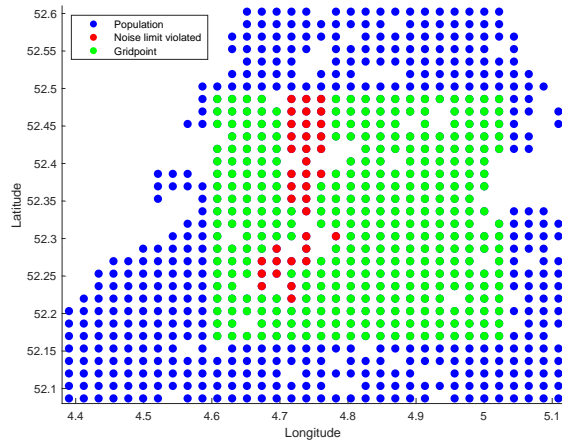


Figure B.12: Noise Grid Scenario 2: Reference Scenario

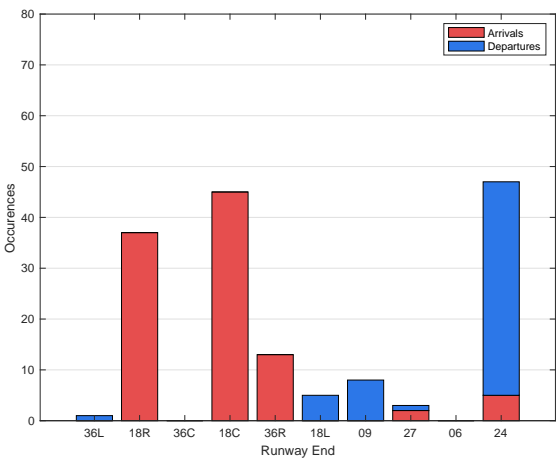


Figure B.13: Runway Allocation Scenario 2: Noise optimized

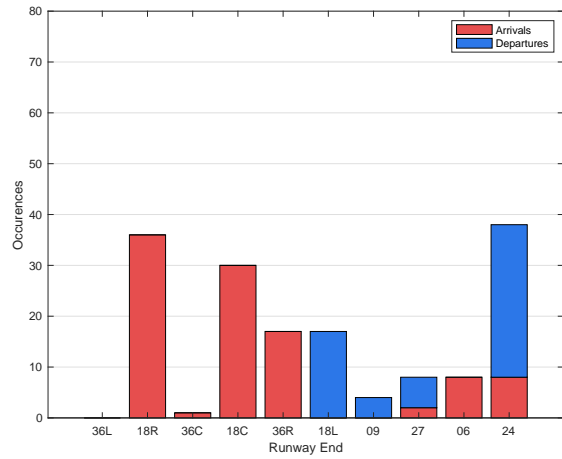


Figure B.14: Runway Allocation Scenario 2: Multi-objective optimized

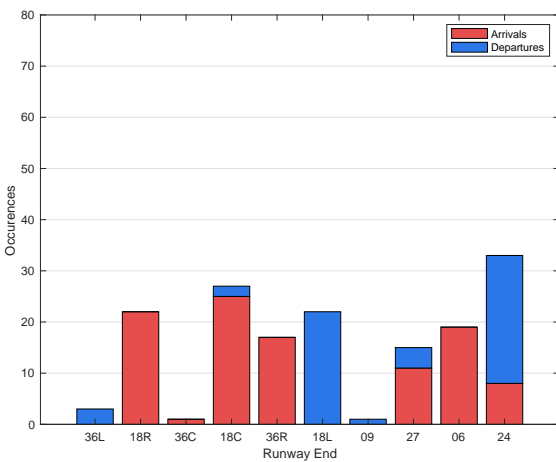


Figure B.15: Runway Allocation Scenario 2: Fuel optimized

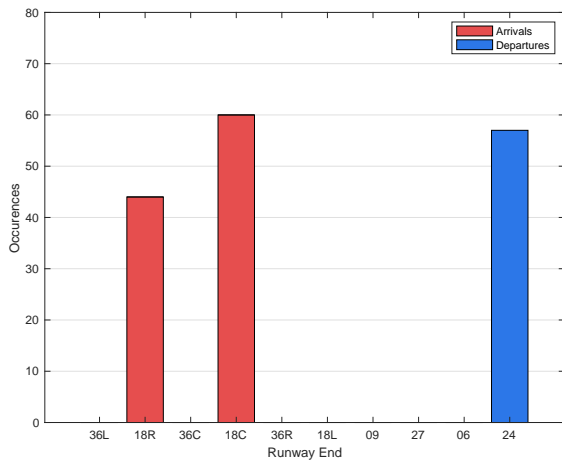


Figure B.16: Runway Allocation Scenario 2: Reference Scenario

B.3. Noise Grid & Runway Allocation Scenario 3

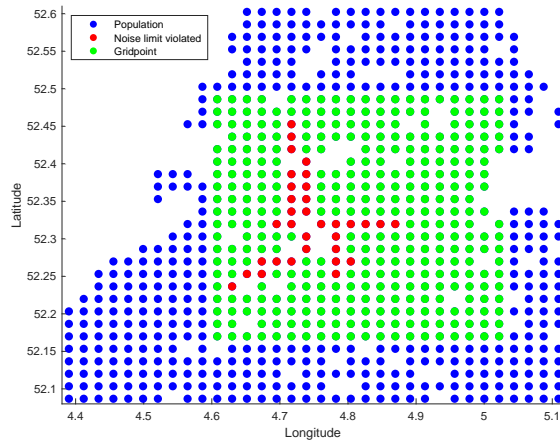


Figure B.17: Noise Grid Scenario 3: Noise optimized

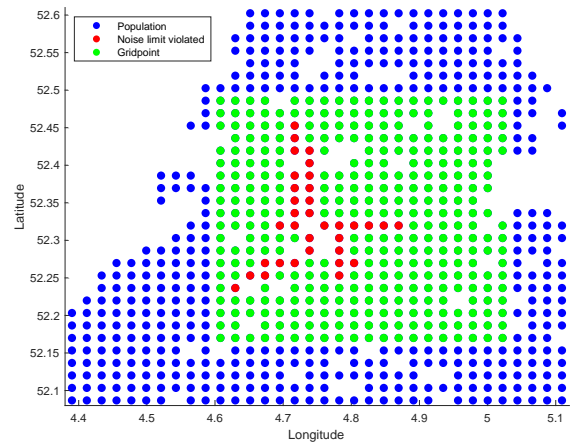


Figure B.18: Noise Grid Scenario 3: Multi-objective optimized

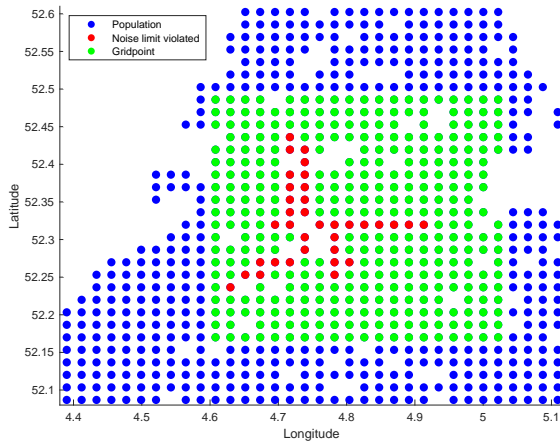


Figure B.19: Noise Grid Scenario 3: Fuel optimized

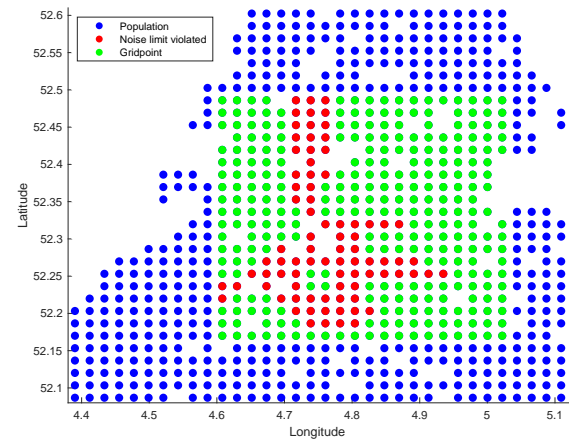


Figure B.20: Noise Grid Scenario 3: Reference Scenario

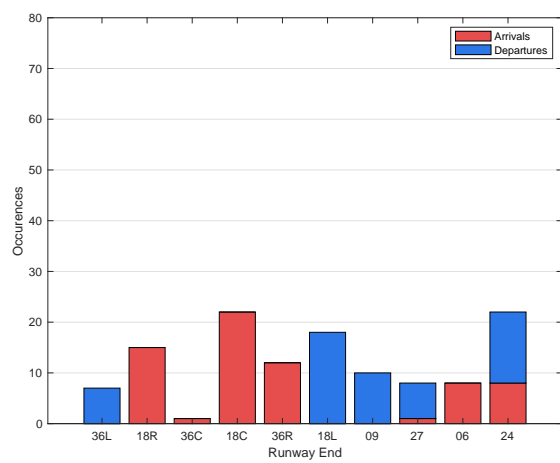


Figure B.21: Runway Allocation Scenario 3: Noise optimized

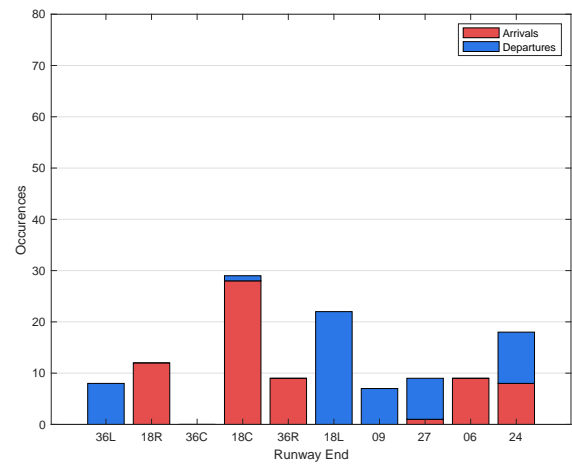


Figure B.22: Runway Allocation Scenario 3: Multi-objective optimized

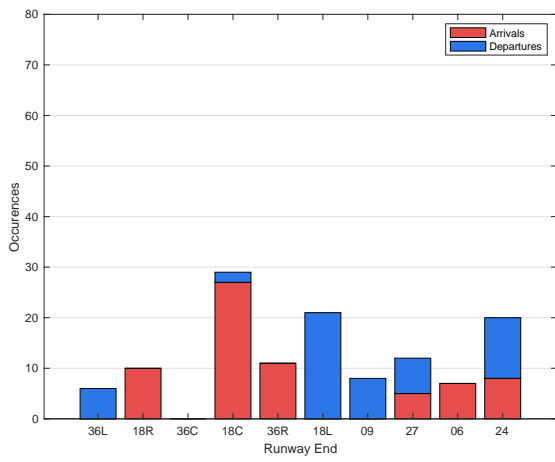


Figure B.23: Runway Allocation Scenario 3: Fuel optimized

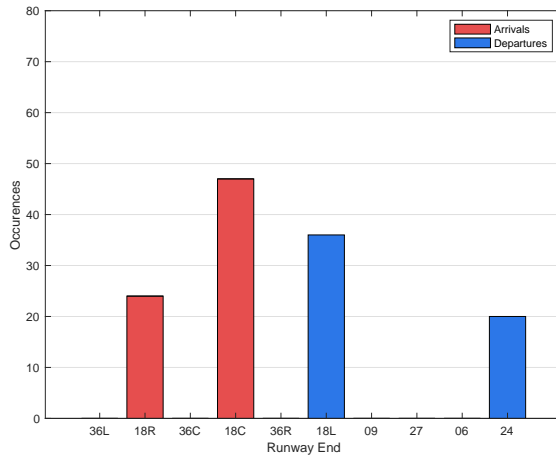


Figure B.24: Runway Allocation Scenario 3: Reference Scenario

Bibliography

- [1] A. Kim and M. Hansen. Validation of Runway Capacity Models. *Air Traffic Management Research and Development Seminar*, 2009.
- [2] A. Nuic and D. Poles and V. Mouillet. BADA: An advanced aircraft performance model for present and future ATM systems. *International Journal of Adaptive Control and Signal Processing*, 2010.
- [3] A.A. Trani, A.G. Hobeika et al. Runway Exit Designs for Capacity Improvement Demonstrations Phase II-Computer Model Development. Technical report, Virginia Polytechnic Institute and State University Center for Transportation Research, 1992.
- [4] A.F. El-Sayed and M.S. Emeara and M.A. El-Habet. Performance Analysis of High Bypass Ratio Turbofan Aeroengine. *International Journal of Development Research*, 06:8382 – 8398, 2016.
- [5] B. Boucsein and K. Christiaanse and E. Kasioumi and C. Salewski. The Noise Landscape. A Spatial Exploration of Airports and Cities. Technical report, NAI010 Publisher, 09 2017.
- [6] B. Mirkovic. Airfield modelling state of the art, 2010.
- [7] P. Belobaba, A. Odoni, and C. Barnhart. *The Global Airline Industry*. John Wiley & Sons, 2009.
- [8] Bewoners Aanspreekpunt Schiphol. 2019 Jaarrapportage. Technical report, BAS, 2020.
- [9] A. Blumstein. The Landing Capacity of a Runway. *Operations Research*, 7:752–763, 1959.
- [10] City of Atlanta, Department of Aviation. Master Plan - Executive Summary, 2015. URL https://www.atl.com/wp-content/uploads/2016/12/ATL_ExecSumm_2015_101415_Spreads.pdf.
- [11] D. Halperin. Environmental noise and sleep disturbances: A threat to health? *Sleep Science*, 7:209–212, 2014.
- [12] J.G. Delsen. Flexible Arrival and Departure Runway Allocation. Master’s thesis, Delft University of Technology, 2016.
- [13] D.G. Simons. *AE4431 - Aircraft Noise and Emissions*. TU Delft, 2019.
- [14] R. Doganis. *Flying Off Course - The Economics of International Airlines*. Routledge, 2002.
- [15] A.R. Odoni et al. Existing and Required Modeling Capabilities for Evaluating ATM Systems and Concepts. Technical report, International Center for Air Transportation MIT, 1997.
- [16] EUROCONTROL. Enhancing Airside Capacity, the Complete Guide, 2003. Edition 2.
- [17] EUROCONTROL. User Manual for The Base of Aircraft Data (BADA). Technical report, Eurocontrol Experimental Centre, 2004.
- [18] Federal Aviation Administration (FAA). Integrated Noise Model (INM) Version 7.0 Technical Manual. Technical report, FAA, 2008.
- [19] E.P. Gilbo. Airport Capacity: Representation, Estimation, Optimization. *IEEE Transactions on Control Systems Theory*, 1:144–154, 1993.
- [20] R.M. Harris. Models for Runway Capacity Analysis. Technical report, The MITRE Corporation, 1972.
- [21] S.L. Hockaday and A. Kanafani. Developments in Airport Capacity Analysis. *Transportation Research*, 8: 171 – 180, 1973.
- [22] International Civil Aviation Organization. Rules of the Air - Annex 2. Technical report, ICAO, 2005.

- [23] International Civil Aviation Organization. Doc 4444 - Procedures for Air Navigation Services - Air Traffic Management. Technical report, ICAO, 2016.
- [24] International Civil Aviation Organization. Annex 14 - Aerodromes - Volume I - Aerodromes Design and Operations. Technical report, ICAO, 07 2018.
- [25] International Civil Aviation Organization (ICAO). Procedures for Air Navigation Services Aircraft Operations (PANS-OPS) - Doc 8168 - Part I. Technical report, ICAO, 2006.
- [26] International Civil Aviation Organization (ICAO). ICAO Doc 9829, Guidance on the Balanced Approach to Aircraft Noise Management. Technical report, ICAO, 2011.
- [27] International Civil Aviation Organization (ICAO). ICAO's Policies on Charges for Airports and Air Navigation Services (Doc 9082). Technical report, ICAO, 2012.
- [28] International Civil Aviation Organization (ICAO). Annex 16 - Environmental Protection - Volume I - Aircraft Noise. Technical report, ICAO, 2017.
- [29] J.M. Hoekstra, J. Ellerbroek. AE4321-15 - Air Traffic Management, Lecture Slides, 2020. URL <https://brightspace.tudelft.nl/d21/1e/content/192007/Home>.
- [30] H. Khadilkar and H. Balakrishnan. Estimation of Aircraft Taxi-out Fuel Burn using Flight Data Recorder Archives. *AIAA Guidance, Navigation and Control Conference*, 2011.
- [31] L. Bertsch and D.G. Simons and M. Snellen. Aircraft Noise: The major sources ,modelling capabilities, and reduction possibilities. Technical report, German Aerospace Center & Delft University of Technology, 2015.
- [32] L.E. Mudd. Airport Capacity and Delay - Advisory Circular. Technical Report 150/5060-5, Federal Aviation Authority, 1983.
- [33] M. Bazargan and K. Fleming and P. Subramanian. A SIMULATION STUDY TO INVESTIGATE RUNWAY CAPACITY USING TAAM. *Winter Simulation Conference Proceedings*, 2002.
- [34] M.E. Koch and C.G. Roberts et al. runwaySimulator Validation Report. Technical report, MITRE Corporation, 2014.
- [35] Mordor Intelligence. JET FUEL MARKET - GROWTH, TRENDS, AND FORECAST (2020 - 2025). Technical report, Mordor Intelligence, 2020.
- [36] N. Pyrgiotis, K.M. Malone, A. Odoni. Modelling delay propagation within an airport network. *Transportation Research Part C*, 2013.
- [37] R. Neufville and A. Odoni. *Airport Systems: Planning, Design and Management*. McGraw-Hill Education, New York, second edition, 2013.
- [38] S. Pavlin. Runway Occupancy Time as Element of Runway Capacity. *Travel Planning Review*, 2006.
- [39] P.C. Roling. AE4446 - Airport Operations, Lecture Slides, 2020. URL <https://brightspace.tudelft.nl/d21/1e/content/192031/Home>.
- [40] P.V. Hyer. Demonstration of Land and Hold Short Technology at the Dallas-Fort Worth International Airport. Technical report, NASA, 2002.
- [41] R.A.A. Wijnen and W.E. Walker and J.H. Kwakkel. Decision support for airport strategic planning. *Transportation Planning and Technology*, 31:11–34, 2008.
- [42] J.P. Rodrigue. *The Geography of Transport Systems*. Routledge, 2020.
- [43] F. Rooseleer and V. Treve. European Wake Turbulence Categorisation and Separation Minima on Approach and Departure. Technical report, EUROCONTROL, 2015.
- [44] G. Ruijgrok. *Elements of Aviation Acoustics*. Delft University Press, Delft, 1993.

-
- [45] S. Heblj and R.A.A. Wijnen. Development of a Runway Allocation Optimisation Model for Airport Strategic Planning. *Transportation Planning and Technology*, 31, 2008.
- [46] M. Stamatopoulos. A decision support system for airport strategic planning. *Transportation Research Part C*, 12:91– 117, 2004.
- [47] W.J. Swedish. Upgraded FAA Airfield Capacity Model. Volume I Supplemental User's Guide. *The MITRE Corporation*, FAA-EM-81-1, Volume I and MTR-81W16, Volume I, 1981.
- [48] US DOT Volpe Center. Aviation Environmental Design Tool (AEDT). Technical report, FAA, 2014.
- [49] J. van der Klugt. Calculating capacity of dependent runway configurations. Master's thesis, Delft University of Technology, 2012.
- [50] S.A. van der Meijden. Improved Flexible Runway Use Modeling. Master's thesis, Delft University of Technology, 2017.
- [51] H.G. Visser and R.A.A. Wijnen. THE AIRPORT BUSINESS SUITE: A DECISION SUPPORT SYSTEM FOR AIRPORT STRATEGIC EXPLORATION. *AIAA*, 2003.
- [52] W. Horton. Air France-KLM Faces \$ 1 Billion Fuel Hedging Loss As Oil Price Falls Due To Coronavirus. *Forbes*, 2020.
- [53] World Health Organization (WHO). Night Noise Guidelines for Europe. Technical report, WHO, 2009.